# FUNDAMENTALS OF BACTERIA-BASED MOLECULAR COMMUNICATION FOR INTERNET OF BIO-NANOTHINGS

A Dissertation
Presented to
The Academic Faculty

By

Bige Deniz Unluturk

In Partial Fulfillment
of the Requirements for the Degree
Doctor of Philosophy in the
School of Electrical and Computer Engineering

Georgia Institute of Technology

August 2020

**FUNDAMENTALS OF BACTERIA-BASED MOLECULAR COMMUNICATION FOR INTERNET OF BIO-NANOTHINGS**

Approved by:


Dr. Ian F Akyildiz, Advisor
School of Electrical and Computer Engineering
*Georgia Institute of Technology*

Dr. A Fatih Sarioglu
School of Electrical and Computer Engineering
*Georgia Institute of Technology*

Dr. Raghupathy Sivakumar
School of Electrical and Computer Engineering
*Georgia Institute of Technology*

Dr. Chuanyi Ji
School of Electrical and Computer Engineering
*Georgia Institute of Technology*

Dr. Massimiliano Pierobon
Department of Computer Science and Engineering
*University of Nebraska-Lincoln*



Date Approved: June 18, 2020

*I dedicate this thesis,*

*To the loving memory of my father Ali Turgut Unluturk,*

*who planted seeds of curiosity in my mind, and love of science in my soul.*

*To my mother Hatice Unluturk, to my aunt Ayse Savus, to my husband Bircan Bugdayci,*

*for their endless love, support and encouragement.*

## ACKNOWLEDGEMENTS

I would like to express my heartiest thanks to Prof. Ian F. Akyildiz, who has been not only my Ph.D. advisor, but also a mentor and a second father for me. He has been there for me during the most difficult times of my life with his invaluable help and endless tolerance, as well as during the most joyful times of my life with his genuine support and encouragement. He is my north star in academic life, showing me the right way whenever I get lost and always there shining brightly as a role model, the epitome of the success arising from the combination of talent and hard-work. He is the star we all shoot for albeit won't be able to reach. The light of his gifted mind guided me on my research path and his passion for his job inspired me to work harder. He opened up the doors for me to pursue an incredible career I always dreamed of, the one that is changing my life completely, which I'm fully aware that would never realize without his guidance. For this and for countless lessons he taught me both in academic and personal life, I will be forever grateful to him.

I would also like to thank my committee members Dr. Raghupathy Sivakumar, Dr. Chuanyi Ji, Dr. Fatih Sarioglu, and Dr. Massimiliano Pierobon who kindly agreed to serve in my Ph.D. Defense Committee. Their invaluable feedback and continuous encouragement have helped me to take the final leap towards the completion of my Ph.D. journey.

My sincere and warm thanks go also to the whole Broadband Wireless Networking Laboratory family, to past and current members, Ph.D. students, Post-Docs, visitors, with whom I shared amazing memories throughout my years in lab and forged lifelong friendships. The United Nations in the lab opened up my mind to the world and I will never forget these amazing people with unique personalities.

Also, my sincere thanks go to all the people I worked with in the projects MoNaCo and INTRABIONETS. I would like to acknowledge the support of National Science Foundation through these projects, which made the completion of this thesis possible.

I'm also grateful to Dr. Sasitharan Balasubramaniam for hosting me in Finland and

Dr. Ilangko Balasingham for hosting me in Norway during my research stays and their contribution to my growth as a researcher.

I am very fortunate to be born to a very affectionate and supportive family who values education and knowledge above anything else. They ignited my interest in academia and research, and cleared my path to pursue my dreams. I want to thank my family, my mom Hatice Unluturk, my father Ali Turgut Unluturk, my aunt Ayse Savus for always putting me first in their life. Their love, caring and support are the source of my happiness. Words can not express how grateful I am for all their sacrifices that they have made for me throughout the years.

I express my most special thanks to Bircan Bugdayci, my beloved husband who stood by me in every step of the way. Understanding me the best as a PhD himself, Bircan has been my rock, my best friend, and the reason I could see the end of this long and difficult journey. He always motivated me to get out of my comfort zone and gave me full support to follow my dreams even if it meant for us to live in different continents for years. Even from the other side of the ocean, he always knows how to cheer me up, how to calm me down, and how to make me feel loved. He is my source of joy and happiness. My daily conversations with him on our research topics was a staple in my PhD journey. It was a way to organize my thoughts, and exchange ideas with this fellow smart engineer. He greatly contributed to my intellectual growth as a person and as a researcher. He is the best companion in life I could ever ask for with his unconditional love, endless support, brilliant mind, witty sense of humour and positivity. I am forever grateful for his love and support which gives me the strength and the purpose to go through life every day.

Lastly, I would like to thank my friends who made the world a better place for me. I would like to express my thanks to my friends and roommates Cansu Tetik and Ayse Selin Cakmak, my good friends Can Temel, Beren Semiz, Gozde Tutuncuoglu, Emre Gursoy, Nil Gurel, Sezen Yucel, Ozan Bicen, Sinan Hersek, Emre Yilmaz, Alper Yildirim, Ulkuhan Guler, Tevhide Ahmadov-Ozkaya.

## TABLE OF CONTENTS

## LIST OF TABLES

## LIST OF FIGURES

## SUMMARY

Today, thanks to synthetic biology, we can engineer living cells as biosensor devices and thanks to MEMS & nanotechnology, we can manufacture electronic devices at nanoscale. Molecular communication (MC), a novel communication technique where information transfer is based on exchange of molecules, emerges as a solution to establish communication among these natural and man-made biological and electronic devices at nanoscale. When complemented with existing wireless communications technologies, MC will enable a network of these devices, called Internet of Bio-NanoThings (IoBNT).

The focus of this PhD thesis is on the bacteria-based MC for IoBNT, where bacteria populations are considered both as devices generating MC signals and information carriers actively delivering molecules via chemotaxis. The objectives of the research presented in this thesis are to model and analyze bacteria-based MC from the point of communication engineering to provide solutions for the creation of artificial MC systems for IoBNT applications. First, a genetically engineered bacteria-based biotransceiver that can send and receive MC signals is designed. The principles of biological circuits for MC are illustrated. Second, the bacterial chemotaxis channels where bacteria actively carry information in its plasmid and move towards the nutrient gradient are modelled using Keller-Segel models. The impact of social behavior of cooperation, competition, and cheating among the microbial society is incorporated in the models. Third, three modulation schemes are proposed for the bacterial chemotaxis channels and their performance is compared in terms of probability or error. Fourth, to leverage natural bacteria-based MC in the body, Microbiome-Gut-Brain Axis is investigated as an infrastructure for IoBNT. Fifth, an IoBNT application for early detection of infections using bacteria-based MC concept is developed.

This research provides fundamental results that establish the use of bacteria for various MC functions, push the envelope towards the realization of MC networks by proposing design solutions, and developing specific applications of IoBNT for healthcare.

# CHAPTER 1
# INTRODUCTION

Over the last decade, the transformative concepts of information processing and propagation in the molecular domain have dramatically reshaped the frontiers of communication and networking research, with biomedicine as a natural application field [1].

The state-of-the-art diagnostics, monitoring, and therapy in clinical settings are limited by the imprecise nature of current methods and the use of devices that are either external, or when implanted, suffer from large size and poor biocompatibility. At the same time, we are at a critical crossroad in biomedical research in which our ability to miniaturize sensors and electronics is unprecedented, and our understanding of biological systems enables novel technologies to interface and manipulate cells and their biochemical realm.

As a result, nanotechnology and biotechnology-enabled wearable and implantable devices with ever increasing biocompatibility and operational autonomy are being developed. Thanks to synthetic biology, we can engineer living cells as biosensor devices and thanks to MEMS & nanotechnology, we can manufacture nanoscale electronic sensor and actuator devices, that are termed "Bio-NanoThings". These devices promise to pervasively, perpetually, and precisely sense, process, control, and exchange body health parameters in real time, and allow remote interrogation, which we classify under the paradigm of the Internet of Bio-NanoThings (IoBNT) [2]. This paradigm will enable accurate sensing and control of complex biological dynamics in the human body, and eventually be the basis of the next-generation biomedical solutions for unsolved clinical problems.

The IoBNT is envisioned to be a heterogeneous network of electronic and biological devices, deployed inside and outside of the body as shown in Fig. 1.1, communicating through different means, ranging from electromagnetic waves and coupling, electrical and mechanical stimulation, to Molecular Communication (MC) [1]. Electronic devices may

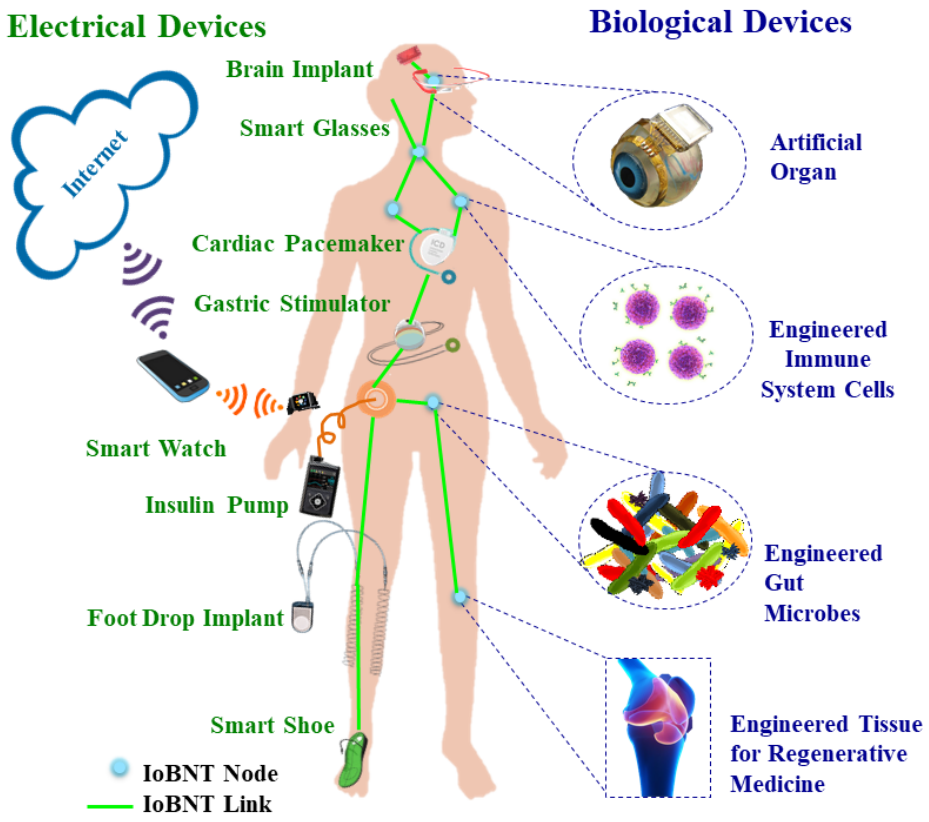


Figure 1.1: The Internet of Bio-NanoThings paradigm.

comprise implantable and wearable electronic devices such as brain implants, pacemakers, and smart watches, whereas biological devices may comprise manipulated natural cell and tissues or man-made synthetic ones such as engineered immune system cells, engineered gut microbes, and artificial cornea.

Due to their simple architecture, power and size limitations, BNTs can not perform complex tasks alone. To unleash the potential of BNTs, dense deployment of wirelessly networked BNTs is required. Various communication techniques have been suggested for realization of BNT networks such as nanomechanical, acoustic, and electromagnetic communication. These techniques are not favorable for use in the body since they suffer either from large size of antenna, poor propagation through tissues, or health hazard due to heating of tissues. Since molecular communication (MC) already exists in the body in various shaped and forms, it is the most promising approach, where information transfer occurs by

exchange of molecules. Even though MC already exists in nature in many scales such as communication inside the cells, between the cells, and between the animals/plants and it evolved over billion years [3], it has only recently been proposed as a solution for networking.

## 1.1 Background

### Internet of Bio-NanoThings

With the recent advances in electronics, it is now possible to fabricate smaller and cheaper devices with low power - high capacity communication capabilities, which are connected and are able to autonomously interact with each other forming a network of physical devices called, the Internet of Things (IoT). This concept is taken one more step ahead with novel studies in nanotechnology enabling nanoscale computing devices based on nanomaterials such as graphene and metametarials, called nanothings.

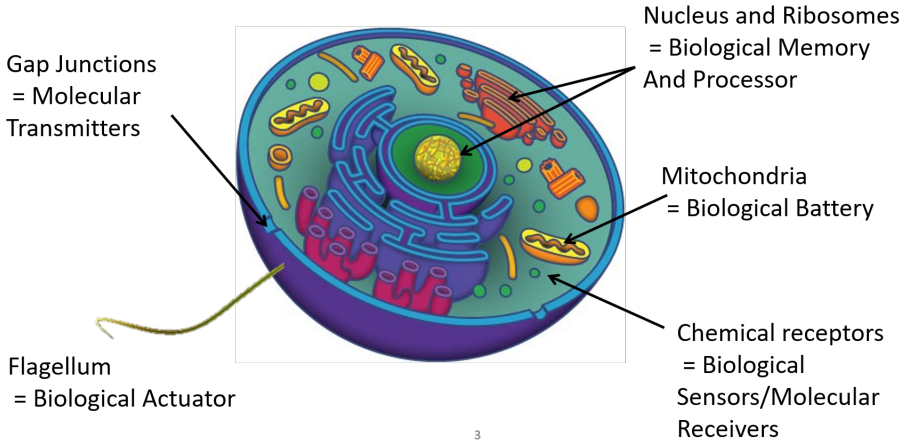


Figure 1.2: The conceptual illustration of a Bio-NanoThing.

First proposed in [4], the Internet of NanoThings is envisioned to be the basis for many future applications requiring very tiny, concealable, and non-intrusive things. However, these miniaturized electronic devices rely on electromagnetic communications, which suffer great attenuation through tissues and may have detrimental effects on health when used

in biomedical applications. To overcome these problems, a novel paradigm, called the Internet of Bio-NanoThings (BNTs), is proposed in [5] combining synthetic biology and nanotechnology in order to engineer biological embedded computing devices. An analogy can be drawn between an IoT device and a biological cell both capable of sensing, actuation, information processing and communication as shown in Fig. 1.2. By modifying the DNA of biological cells, it is possible to engineer a cell-based Bio-NanoThing capable of executing instructions embedded in its DNA, biochemical processing of sensed information, transformation of chemical energy, and transfer of information through exchange of molecules.

The IoBNT will enable a plethora of applications especially in biomedical field such as i) intra-body sensing and actuation, where BNTs deployed in human body would sense, process, control body health parameters and transmit this data to external healthcare provider over the Internet as shown in Fig. 1.3, ii) intra-body connectivity control, where BNTs would detect and repair any impairment in the natural communication mechanisms within the body connecting organs and tissues to each other such as nervous system, iii) environmental monitoring and control, where BNTs would collaboratively sense the quality of air or water, report the sensed data over the Internet and eliminate source of pollution upon command [5].

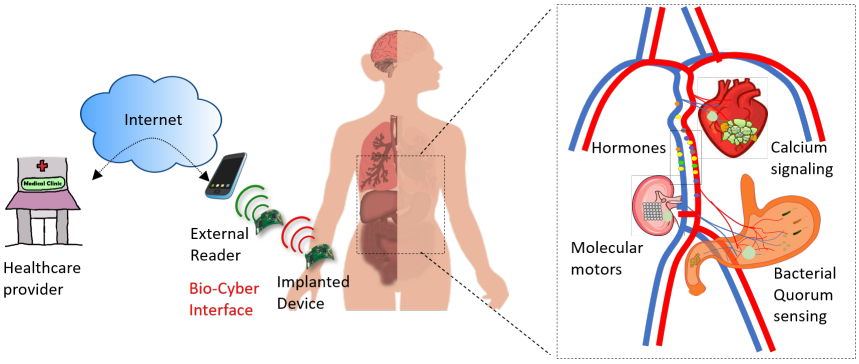


Figure 1.3: The conceptual illustration of Internet of Bio-NanoThings.

As promising as it is, realizing the IoBNT concept requires tackling many challenges

especially in communications and networking such as developing novel communication techniques among BNTs based on molecule exchange, termed Molecular Communication (MC), networking in biochemical domain, and developing an interface from biochemical domain to the electrical domain of the Internet.

**Molecular Communication**

Molecular Communication is a bio-inspired approach studying inherent communication mechanisms between biological entities with the aim of utilizing them to form biocompatible nanocommunication networks [6, 7]. In nature, cells exchange information based on the synthesis, emission, propagation, and reception of molecules at various scales enabling cells' interactions and coordination to regulate vital functions of individual cells or multi-cellular tissues and organisms [8]. For example, bacteria exchange signals among each other whose concentration increases as a function of bacterial cell density and alters behaviour of the population accordingly, which is called quorum sensing [9]. In MC, information can be modulated into chemical characteristics of molecular signals such as molecule concentration, type, and arrival time through biochemical reactions. The propagation medium that modulated signals propagate from the transmitter to the receiver serves as a basis for classification of MC techniques such as diffusion-based MC [10, 11], flow-based MC over microfluidic channels [12, 13], active transport using molecular motors within a cell [14], calcium signalling within tissues [15], fluorescence energy transfer among fluorescent proteins [16]. An example MC channel is illustrated in Fig. 1.4.

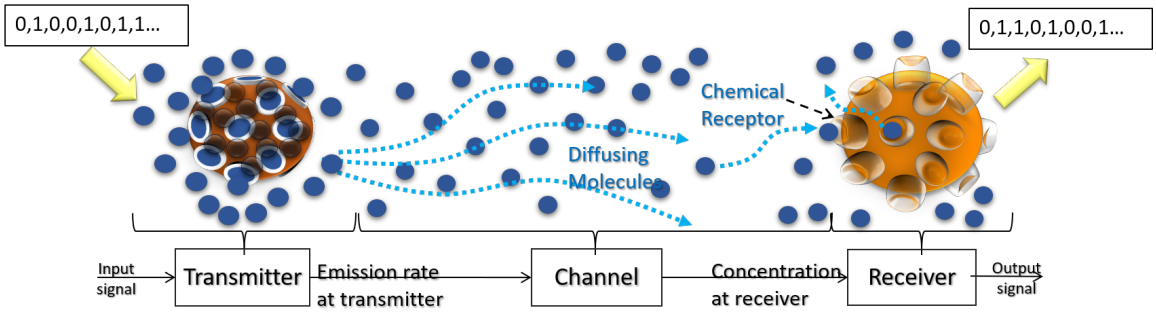


Figure 1.4: Overview of Molecular Communication Channel

## 1.2 Research Objectives

In MC, the transmitter sends a message encoded on the concentration, type or timing of molecules that are then propagated through the medium to the receiver via diffusion or convection. Since this new channel is drastically different than traditional radio frequency channels, the longstanding definitions of signal, noise, information capacity, and energy need to be revisited. Besides the characterization of signal propagation in the channel, MC requires the design of unprecedented devices capable of transmitting and receiving MC signals that can release, sense, store, harvest and re-use molecules. This motivates us to study bacteria as biological devices that inherently communicate with each other through molecules. The programmability of bacteria with genetic engineering and the observability of their behavior provide us the ability to examine and model the natural bacteria communication, and mimic it to create artificial MC systems.

In the literature, various MC techniques encoding information on time of arrival, number and type of molecules, and considering different biological phenomena such as neural transmission, calcium signalling, chemotaxis of bacteria, active transport using molecular motors, and ion channels for signal propagation are proposed. A detailed overview is given in Chapter 2. Most of these studies focus on modeling the propagation of molecules in the medium, under the categories of random walk, drifted random walk, and active transport, as well as developing modulation, detection, routing, and addressing schemes on top of these channels.

Often times, researchers only take into account the behavior of molecules in a homogeneous propagation medium such as a liquid or gas described by the Fokker-Planck equation [17] and calculate the channel capacity given the stochastic propagation of molecules. However, especially for IoBNT applications in the body, propagation medium is not always a homogeneous liquid/gas but it is also full of living cells both generating and/or responding to MC signals and also actively carrying MC signals.

The focus of this PhD thesis is on the modeling and analysis of bacterial cells and their behavior to reflect the effects of living cells on the performance of MC channels. The objective of this thesis is to establish the fundamentals of bacteria-based molecular communication where bacteria populations are considered as both MC devices and MC information carriers. The research objectives addressed in this PhD thesis, and the proposed solutions are summarized in the following.

The first research objective is to design a biotransceiver capable of processing signals in molecular form and sending & receiving MC signals. For this purpose, genetically engineered bacteria-based biotransceivers are investigated for transmission of information between bacteria populations, where bacteria can generate and respond to the molecular signals. A biochemical model of biological circuits is presented, and both analog and digital signaling are studied. The challenges in connecting basic biological circuits to build these blocks are revealed. A biotransceiver architecture is introduced that combines sensing, transmitting, receiving and processing blocks. Furthermore, biological circuit design framework is proposed for transmission of signals with M-ary pulse amplitude modulation.

The second objective is to model and analyze bacterial chemotaxis channels where bacteria are considered as information carriers. In bacterial nanonetworks, bacteria carry information encoded plasmid DNA from the transmitter to the receiver by chemotaxis, i.e., the movement of bacteria in the medium towards chemical attractants. Keller-Segel models has been applied to describe the motion of bacteria populations as travelling waves to derive closed form solutions for bacterial population density at the receiver, delay, and attenuation. Furthermore, since in natural environments, bacteria coexist in multiple populations of similar and different species, complex communities are formed with social interactions that include cooperation and cheating, as well as competition. These social interactions are incorporated into the Keller-Segel model and their effects on delay, attenuation, and data rate are investigated.

The third objective also targets bacterial chemotaxis channels where bacteria are con-

sidered information carriers. A previously proposed model for molecular communication is using bacteria as information carriers between transmitters and receivers. This approach has suggested encoding information into the plasmids inserted into the bacteria which leads to extra overhead for the receivers to decode and analyze the plasmids to obtain the encoded information. Another scheme, which is proposed in this thesis, is to determine the digital information transmitted based on the quantity of bacteria emitted. While this scheme has its simplicity, the major drawback is the low data rate resulting from the long propagation of the bacteria. To improve the performance, several modulation schemes, namely, Binary Density Modulation, M-ary Density Modulation, and Distributed Receivers Modulation are proposed. Their performance is analyzed in terms of probability of error as well as the achievable rate for varying quantity of bacteria transmitted, distances, and time slot length.

The fourth objective is to investigate bacteria-based MC inside the body towards an IoBNT application aiming to interconnect wearable and implantable devices through the natural communication channels of the body. Especially the focus is on Microbiome-Gut-Brain Axis (MGBA), composed of the gut microbial community, the gut tissues, the enteric nervous system and investigate the utilization of the MGBA as an IoBNT communication network infrastructure to transmit and receive information generated by and/or directed to electronic and biological devices. A framework to develop a network infrastructure on top of the biological processes underlying the MGBA, and the intercommunications among its components is proposed. To this end, a methodology that comprises both analytical and experimental efforts is presented. The analytical effort builds on top of neuroscience and bioinformatics to abstract and model with reliable mathematical expressions the propagation of device-sourced information through biological tissues utilized as communication channels. The experimental effort is based on the design of a unique integrated network probe device composed of a hub connected to an ensemble of electrical and molecular stimulation and sensing interfaces.

The fifth objective is to utilize bacteria-based MC concept for an IoBNT healthcare

application called PANACEA and to design an end-to-end IoBNT system for the first time in literature. The architecture of PANACEA is tailored to focus on diagnosis and therapy of infectious diseases. In PANACEA, to detect the communication within the cells of the body to deduce infection level, a submilimeter implantable bio-electronic device, a Bio-NanoThing, is proposed. BNT can transmit the detected infection data remotely to a wearable hub/gateway outside of the body. The hub can use mobile devices and the backbone network such as Internet or cellular systems to reach the healthcare providers who can remotely control the BNTs. An intra-body MC channel through tissues is modeled using diffusion in porous medium principles and an infection scenario is simulated to quantify the detection time through PANACEA.

### 1.3 Organization of the Thesis

The rest of this thesis is organized as follows. An overview of existing body of work on the study of MC and IoBNT is given in Chapter 2. In Chapter 3, a biotransceiver architecture using genetically engineered bacteria has been proposed and analyzed as a MC device capable of sending and receiving MC signals. In Chapter 4, travelling wave channel models are presented for bacteria considered as messengers actively carrying messages via chemotaxis and the impact of social behavior of bacteria on this communication channel is analyzed. In Chapter 5, a novel modulation scheme for bacterial chemotaxis channel studied in the previous chapter is proposed and compared to other modulation schemes in terms of probability of error. In Chapter 6, an application scenario of bacteria-based MC for IoBNT is presented where microbiome-gut-brain-axis is proposed as an intra-body communication infrastructure. In Chapter 7, another IoBNT application scenario focusing on the early detection of infections is presented and analyzed. In Chapter 8, the research contributions are summarized and future research avenues are discussed. Finally, the publications resulted from the research presented in this PhD thesis are listed.

# CHAPTER 2
# PREVIOUS WORK

This chapter of the thesis contains a review of the literature for the research on IoBNT and MC. This review is organized as follows. In Section 2.1, Internet of NanoThings paradigm is discussed. In Section 2.2, the state-of-the-art molecular communication techniques are presented. In Section 2.3, the recent advances in the synthetic biology used to engineer cells as bio-nanothings are provided.

## 2.1 Internet of NanoThings

With the recent advances in bioMEMS, many implantable micro-devices are devised for wireless intrabody sensor networks. However, these devices suffer intrusive deployment, limited lifetime, large sizes, limited external communication, and biocompatibility issues leading to imprecise diagnostics and therapy. A novel bio-inspired direction called Internet of Bio-Nanothings (IoBNT) first proposed in [5] is envisioned as a key technology to overcome these problems by developing and integrating nanoscale, bioelectronic components and engineered biological cells, namely, Bio-Nano Things, to sense and control biological processes in real time. IoBNT stems from synthetic biology and molecular communication(MC) allowing the engineering of biological cells to acquire sensing, actuation, and communication functionalities for biocompatible intrabody applications.

The Internet of Things (IoT) defines a cyber physical paradigm, where all types of real-world physical elements (sensors, actuators, personal electronic devices, or home appliances, among others) are connected, and are able to autonomously interact with each other. This new form of seamless connectivity is the enabler for many applications such as machine to machine communication, real time monitoring of industrial processes, smart cities, smart grids for energy management, intelligent transportation, environmental monitoring,

infrastructure management, medical and healthcare systems, building and home automation, and large scale deployments. The Internet of Things became a focus for research and development in the last 15 years. A large amount of investments for Internet of Things was and is still being made by government agencies and industry worldwide. Recently, the concept of IoT has been revised in light of novel research advances made in the field of nanotechnology and communication engineering, which enable the development of networks of embedded computing devices, based on nanomaterials such as graphene or metamaterials, having scales ranging from one to a few hundred nanometers, called nanothings. The Internet of NanoThings (IoNT), introduced for the first time in [4], is proposed as the basis of numerous future applications, such as in the military, healthcare, and security fields, where the nanothings, thanks to their limited size, can be easily concealed, implanted, and scattered in the environment, where they can cooperatively perform sensing, actuation, processing, and networking. While nanothings can push the engineering of devices and systems to unprecedented environments and scales, similarly to other devices, they have an artificial nature, since they are based on synthesized materials, electronic circuits, and interact through electromagnetic (EM) communications [5]. These characteristics can be detrimental for some application environments, such as inside the body or in natural ecosystems, where the deployment of nanothings and their EM radiation could result in unwanted effects on health or pollution. Therefore, to incorporate IoNT to biomedical applications, a novel concept Internet of Bio-NanoThings is introduced. IoBNT envisioned to be a heterogeneous network of electronic devices and engineered cells, communicating by electromagnetic waves, and coupling, and by molecular communication, respectively. Therefore, IoBNT can directly interact with the cells enabling more accurate sensing and eventually control complicated biological dynamics of the human body.

## 2.2 Molecular Communication

Molecular communication relies on chemical signals as information carriers which are released from the transmitter in forms of molecules or lipid vesicles into an aqueous or gaseous environment. Then, these chemical signals propagate in the environment and arrive to the receiver where they are detected by corresponding receptors or sensors in order to extract the information encoded on them. There has been an extensive research effort on the MC in recent years which is extensively compiled in [18].

Molecular communication techniques are often categorized with respect to propagation medium and the associated molecules. The most basic MC technique is diffusion-based free-space MC where molecules are propagating in a liquid environment by diffusion only. An end-to-end physical model for diffusion based MC is proposed in [19] where the effects of noise and the memory are not taken into consideration. All three processes, namely, the transmission, the propagation, and the reception are modeled deterministically to analyze the delay and attenuation of this system. Later, the effects of noise is incorporated to this model in [10], where the noise is characterized as particle sampling and particle counting noises. A stochastic model for MC is presented where MC processes now are analyzed with statistical models. In [20], the noise is associated with the ligand-receptor binding on the receiver side to capture the random perturbations in the chemical processes of the reception. A closed form solution is provided to represent this noise effect.

Based on the models of the channel and the noise discussed above, the information capacity of a diffusion-based free-space MC system is investigated in [11]. The capacity is expressed in closed-form taking into account the two main characteristics of the channel, i.e., the noise and the memory. The derived expression depends on diffusion constant, the distance between the transmitter and the receiver, and the bandwidth of the transmitted signal. Numerical results show that for a distance range of tenth of a micrometer, a few kilobits per second capacity can be reached. Another study on the capacity of diffu-

sion based channels is [21], where a deterministic capacity expression for point-to-point, broadcast, and multiple-access molecular channels is derived. This study also reveals that the noise in diffusion-based MC is input depending unlike traditional Gaussian white noise models used in electro-magnetic communication.

The diffusion-based MC is often used as the gold standard when comparing MC techniques since it captures the general idea of MC very well. However, diffusion-based models are not realistic since they consider an unlimited medium where molecules can propagate in any direction freely. To address this issue, flow-based MC over microfluidic channels is proposed in [13]. A system theoretic model is derived for molecular transport over microfluidic channels composed of basic building blocks of linear channels, turning channels, bifurcations and combinations. Then, the end-to-end noise and memory of this channel is investigated in [22] where the noise is modeled as an additive white Gaussian noise and the memory is described as interdiffusion among transmitted molecular signals. Building upon these models, the interference of transmitters to each others signals and the capacity is studied in [23]. For MC over microfluidic channels, the capacity is found to be bounded by 1 bit/per channel use with a single interferer where the capacity decays by a factor of N incase of N interferers.

Another MC technique concentrates on the utilization of bacteria as information carriers, which we term as **bacterial nanonetworks** [24]. This is based on a number of bacterial properties that includes the ability to move following a chemical gradient, i.e., bacterial chemotaxis, and ability to hold DNA plasmids that store encoded information as well as mechanisms to transfer them within the population, i.e., conjugation. In bacterial nanonetworks, messenger bacteria pick up information encoded in DNA plasmids from the source using the conjugation process, move actively in the environment following a chemical gradient released from the destination and delivers the information to the destination. Therefore the reliability of this channel depends on the number of bacteria reaching to the receiver. In [24], a simulation model is developed to study the channel capacity in bacterial

nanonetworks. In both of these studies, bacteria is considered to move following run-and-tumble cycles as in our work, however, the motion is not analytically modeled. [25] only simulates the propagation channel but does not calculate any other communication metric whereas [24] does not consider the loss due to random motion of bacteria but incorporates it as a term in delay. These studies approach the problem by considering that there is no other bacteria in the environment than the messengers. The objective of our studies is to investigate the social behavior of bacterial nanonetworks where populations of bacteria interact with each other and the incorporation of it into the design of artificial bacterial nanonetworks.

The common vulnerability of all of these techniques is their limited range. The longest achievable range by these techniques reaches only millimeters with bacterial networks. To extend this range up to hundreds of meters, we consider pheromone channel. Pheromones are used for alarming and potential mating within a species, and for attracting or repelling other species [26]. By exchanging different pheromone signals, the members of a species share information messages necessary for the survival and organization of the group. Using pheromone channel for long range MC is first proposed in [7]. Then in [27], a very simple propagation model is described without taking into account the peculiarities of pheromone channels. Our objective is to lay down a solid channel model for one of the long range MC techniques, i.e., pheromone communication between plants, on top of which communication devices and model will be built.

## 2.3 Synthetic Biology

Most of the studies in the literature investigating MC mainly focus on the channel in which molecular concentration signals propagate and the channel effects on the communication performance. To realize MC networks, it is imperative to develop methods to generate these molecular signals for transmission and to interpret them after reception. This motivates us to study bacteria populations as nanomachines which inherently communicate with each

other through molecules. To program the bacteria, molecular biologists modify the genetic code, i.e., the DNA of bacteria plasmid (Fig. 3.1), such that they can control the activity of the genes [28, 29]. Thus, the **gene expression**, i.e., the production of the proteins coded by those genes, can be controlled externally via changing the environmental conditions, i.e., the stimuli, which is called **gene regulation** [30]. A **biological circuit** provides signal transduction based on the modified gene sequences, the stimuli, and the proteins coded by the genes. Biological circuits can be engineered using various techniques intervening in different stages of the gene expression such as transcriptional regulation [31], translational regulation [32] or spatial and temporal compartmentalization [33]. In our work, we consider the transcriptional regulation, i.e., controlling the synthesis of mRNA from DNA by inserting promoters before genes, which is one of the most studied regulation techniques [34]. More complex biological circuits can be built by combining all the above techniques. Although there are several different biological circuit parts implemented in bacteria, e.g., logic gates [33], toggle switches [35], and concentration filters [36], there are several challenges in combining these parts for a more complex circuit such as orthogonality, timing and delay, and modularity.

# CHAPTER 3

# GENETICALLY ENGINEERED BACTERIA BASED BIOTRANSCEIVER

## 3.1 Motivation and Related Work

Most of the studies in the literature investigating MC mainly focus on the channel in which molecular concentration signals propagate and the channel effects on the communication performance. To realize MC networks, it is imperative to develop methods to generate these molecular signals for transmission and to interpret them after reception. This motivates us to study bacteria populations as nanomachines which inherently communicate with each other through molecules.

The objective of this chapter of the thesis is to design a biotransceiver hardware as a communication device for MC nanonetworks by using genetically engineered bacteria populations. The proposed biotransceiver is capable of sensing, processing, transmitting, and receiving. To program the bacteria, molecular biologists modify the genetic code, i.e., the DNA of bacteria plasmid (Fig. 3.1), such that they can control the activity of the genes [28, 29]. Thus, the **gene expression**, i.e., the production of the proteins coded by those genes, can be controlled externally via changing the environmental conditions, i.e., the stimuli, which is called **gene regulation** [30]. A **biological circuit** provides signal transduction based on the modified gene sequences, the stimuli, and the proteins coded by the genes.

Biological circuits can be engineered using various techniques intervening in different stages of the gene expression such as transcriptional regulation [31], translational regulation [32] or spatial and temporal compartmentalization [33]. In our work, we consider the transcriptional regulation, i.e., controlling the synthesis of mRNA from DNA by inserting promoters before genes, which is one of the most studied regulation techniques [34]. More

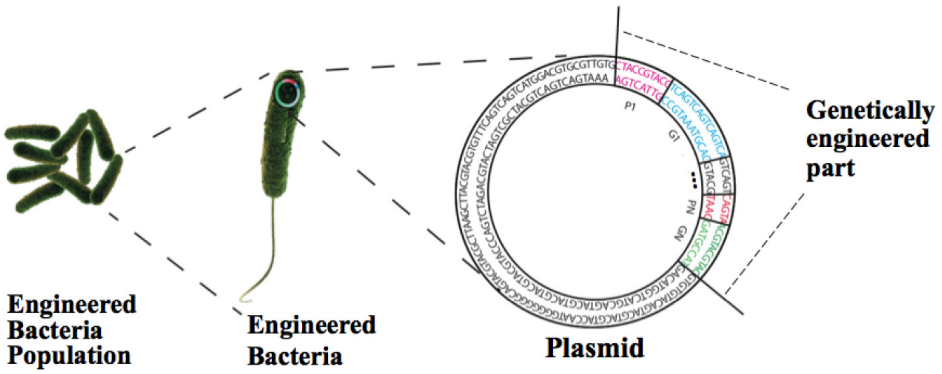


Figure 3.1: Genetically engineered bacteria population produced by inserting genes to the plasmids of bacterial cells.

complex biological circuits can be built by combining all the above techniques.

Although there are several different biological circuit parts implemented in bacteria, e.g., logic gates [33], toggle switches [35], and concentration filters [36], there are several challenges in combining these parts for a more complex circuit as follows:

- **Orthogonality:** When a biological circuit containing multiple parts is implemented on the plasmid of a bacteria, all parts operate in the same cell environment simultaneously. If these parts include similar genes or proteins, there will be interference. Thus, to isolate each part from one another, a biological circuit design should consider using orthogonal elements, i.e., a molecule used in one biological circuit part should not interact with the rest of the biological circuit. This challenge prevents the recurrent use of the same circuit parts and modularity.

- **Timing and Delay:** Since each biological circuit part has a different delay, synchronizing the signals in the circuit is challenging. Besides, the gene expression process takes very long time, usually in the order of hours, which causes huge delays in biological circuits. Hence, concatenation of multiple biological circuit parts poses a severe limit on the information processing speed.

Considering these challenges, we present a concrete design for a complete nanomachine

using MC for the first time in the literature. Furthermore, we lay down the principles of biological circuits from the view of electrical engineering for other scientists who may use them as a tool in their own nanomachine designs. Our work can be extended to form more complex biotransceivers or nanomachines by incorporating more detailed gene regulation techniques and stochastic properties of gene regulation.

The salient features of our work can be listed as:

1. *An overview of biochemical analysis of biological circuits:* We present a mathematical model for gene regulation by using reaction-rate equations (RRE) which include Hill functions. Then, we analyze biological circuits for analog and digital operations by approximating Hill functions as a linear and a step function, respectively. We present how biological circuit parts can be interconnected to form more complex circuits.

2. *Novel biotransceiver architecture:* Since the biological circuits have very limited capabilities, the complex architecture of electromagnetic transceivers cannot be adopted. Taking into account the peculiarities of biological circuits, a novel biotransceiver architecture with sensing, transmitting, processing and receiving blocks is presented.

3. *Biotransceiver design:* Biological circuits are designed for each block of the biotransceiver. The rates of different steps of gene regulation process are adjusted to equalize the delay of parallel paths and to ensure the timely delivery of signals to the next stages. The output signals of each part are designed such that the amplitudes of these signals stays in the defined range ensuring analog or digital operation of the consecutive circuit according to Hill function approximations.

The rest of this chapter is organized as follows. In Sec. 3.2, we review the principles of gene regulation, and we present a basic biological circuit. Section 3.3 analyzes a basic biological circuit unit and Section 3.4 explains different gene-promoter configurations which will be used to connect the basic units together. In Sec. 3.5, we propose a general

transceiver architecture for genetically engineered bacteria based transceivers. Then, biological circuit designs for each block are provided in Section 3.6. Numerical results are presented in Section 3.7. Finally we conclude our study in Sec. 3.8.

## 3.2 Biochemical Model for Biological Circuits

To incorporate biological circuits into MC, the underlying biological phenomena of gene regulation in bacteria must be understood first. To regulate the expression of a gene, i.e., to control the production of the protein coded by that gene, an external stimuli is applied to the environment where the genetically engineered bacteria live. The external stimuli can be created by adding reactive molecules in the environment or by changing the environmental conditions such as light, pH, oxygen level [30]. According to the amount of the external stimuli, bacterial cell adjusts the production rate of the protein coded by the gene. In MC, the information can be encoded in the concentration, type, or arrival time of the molecules. Here, we assume that the information is encoded in the concentration of the molecules, and we investigate the gene regulation dynamics for the application of molecular concentration signals as stimuli to biological circuits.

Changes in bacterial gene expression are often mediated by the regulator sites on DNA called **promoter**. The promoter sites can bind to the molecules called **transcription factors** which control the expression level of the genes coded in DNA after the corresponding promoter site. The basic unit is composed of a gene and its corresponding promoter specially designed to bind and respond to a transcription factor, which acts as an **activator** enhancing the protein production or **repressor** inhibiting the protein production as illustrated in Fig. 3.2. The produced protein as the output of this basic unit might act as a transcription factor for another.

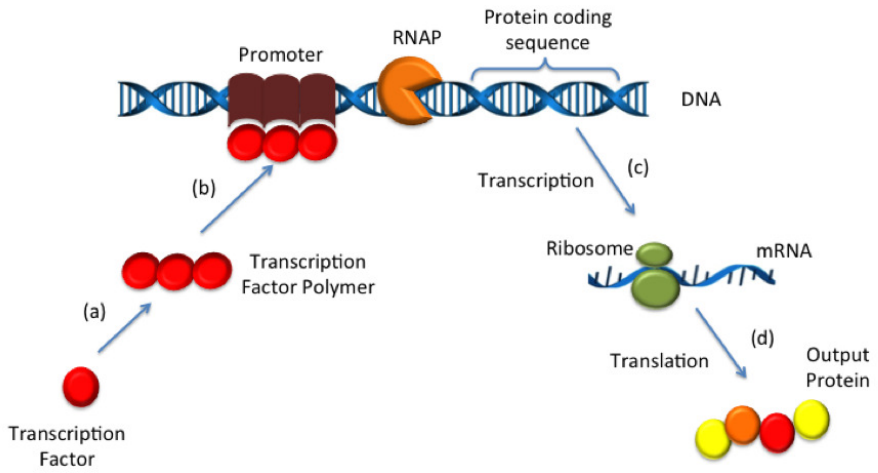


Figure 3.2: Gene regulation processes. (a) The transcription factor (TF) forms a polymer. (b) TF binds to the promoter helping RNAP to separate DNA. (c) DNA is transcripted into mRNA. (d) Ribosomes read the mRNA and produce the protein.

### 3.2.1 Chemical Kinetic Model of Gene Regulation

The regulation of a gene constitutes of multiple steps, namely, polymerization, promoter binding, transcription, translation and natural decay illustrated in Fig. 3.2 [37]. In this subsection, each step is explained in detail and the governing chemical reaction for each step is provided.

1. *Polymerization*: Usually, the transcription factor added to the medium as the input signal cannot bind the promoter directly. Multiple molecules of the transcription factor bind to each other to take an active form which is suitable for binding. The combination process of $n$ molecules of transcription factor denoted with $X$ is called *polymerization*. When $n$ increases, the cooperativity of that transcription factor increases and the system becomes more robust to the abrupt changes of $X$. The polymerization reaction can be characterized as

$$nX \underset{k_{p0}}{\overset{k_p}{\rightleftharpoons}} X_n. \tag{3.1}$$

where $k_p$ is the rate of forward polymerization reaction, and $k_{p0}$ is the rate of the

reverse reaction.

2. *Transcription factor-promoter binding*: The polymer of $X$ binds to the promoter $P$ on DNA next to its corresponding gene forming a complex $C$. After this binding, the promoter is activated and RNA polymerase denoted by $RNAP$ sticks to the promoter. The binding reaction is

$$X_n + P \underset{k_{b0}}{\overset{k_b}{\rightleftharpoons}} C, \tag{3.2}$$

where $k_b$ is the rate of forward binding reaction, and $k_{b0}$ is the rate of the reverse reaction.

3. *Transcription*: If the transcription factor is an activator then the chemical affinity of the promoter and $RNAP$ increases which means that $RNAP$ binds to the promoter more easily resulting in a boost in $mRNA$ production rate. If the transcription factor is a repressor, then the chemical affinity decreases, so the $mRNA$ production rate. This step is called *transcription* since the information about the protein coded on DNA is copied to $mRNA$. The $mRNA$ production from the unactivated promoter, i.e., $P$, corresponding to the basal level of protein production is described as

$$P + RNAP \xrightarrow{\alpha_0} P + RNAP + mRNA, \tag{3.3}$$

where $\alpha_0$ is the basal $mRNA$ production rate. The $mRNA$ production from the activated promoter, i.e., C, is described as

$$C + RNAP \xrightarrow{\alpha_1} C + RNAP + mRNA, \tag{3.4}$$

where $\alpha_1$ is the regulated $mRNA$ production rate.

4. *Translation*: Ribosomes in the cell bind to the $mRNA$ produced in the transcrip-

tion step and read the information on $mRNA$ about the number, the order, and the type of the aminoacids forming the output protein $Y$. Starting from one end of the $mRNA$, ribosomes composed of rRNAs form a chain of aminoacids which will fold and take its final form as the output protein. As the sequence of bases in $mRNA$ are interpreted as the chain of aminoacids, this step is called the *translation* which is described by

$$mRNA + rRNA \xrightarrow{k_t} mRNA + rRNA + Y, \tag{3.5}$$

where the transcription rate is given as $k_t$.

5. *Natural Decay*: All the proteins are degraded by the enzymes in cell after they complete their lifetime. This *natural decay* is described by

$$mRNA \xrightarrow{\gamma_M} \emptyset, \tag{3.6}$$

$$Y \xrightarrow{\gamma_Y} \emptyset, \tag{3.7}$$

$$X \xrightarrow{\gamma_X} \emptyset, \tag{3.8}$$

$$X_n \xrightarrow{\gamma_{X_n}} \emptyset, \tag{3.9}$$

where decay occurs for $i^{th}$ species with rate $\gamma_i$.

### 3.2.2 Reaction-Rate Equation Model of Gene Regulation

Chemical processes in gene regulation consist of discrete and stochastic components and exhibit a very noisy behavior. When the number of molecules of each specie is large, the change in concentrations can be accurately calculated by the law of mass action using RRE [38]. Since in this work we are considering a population of bacteria containing thousands

of bacterium, the number of molecules can be approximated by a continuous molecular concentration and the chemical processes can be approximated by an RRE model, which gives the mean of the stochastic molecular signals. This approach is widely adopted in MC literature based on genetically engineered nanomachines and it is experimentally verified in [39, 30]. The use of RRE model simplifies the analysis, where the effects of the number of cells and the spatial distribution of cells are implicitly captured in the reaction rates. The incorporation of these effects into the model as additional parameters is beyond the scope of this study.

In our model, we consider that the differences between each individual bacteria are assumed to be averaged out such that we observe the mean response of the population [38]. Furthermore, the diffusion of the molecules into bacterium and out of bacterium are not taken into consideration, since the diffusion takes places very rapidly compared to translation and transcription processes [40]. Besides, it is considered that the environment contains plenty of oxygen and nutrients such that the bacterial population density is maintained, and the bacteria have enough energy to express the regulated genes. Also, it is assumed that the biofilms formed by bacteria are weak and they do not limit the diffusion of molecules.

The derivation of RRE from the chemical reactions using the law of mass action is explained in the Appendix. Using this method, we converted the chemical reactions of gene regulation (3.1)-(3.6) into the reaction-rate equations (3.10)-(3.15). Accordingly the rate of change of the input signal, i.e., the transcription factor, $X$, is given by

$$\frac{dX}{dt} = k_{p0} X_n - n k_p X^n - \gamma_X X, \tag{3.10}$$

which is obtained by reactions (3.1) and (3.6).

The rate of change of the transcription factor polymer is

$$\frac{d(X_n)}{dt} = k_p X^n + k_{b0} C - k_b X_n P - \gamma_{X_n} X_n, \tag{3.11}$$

which is obtained based on reactions (3.1), (3.2) and (3.6).

The rate of change of the free promoter $P$ is

$$\frac{dP}{dt} = k_{b0}C - k_b X_n P, \tag{3.12}$$

whereas the rate of change of the bound promoter $C$ is

$$\frac{dC}{dt} = k_b X_n P - k_{b0}C, \tag{3.13}$$

which are obtained by reaction (3.2).

The rate of change of $mRNA$ is obtained from reactions (3.3) and (3.4) as

$$\frac{d(mRNA)}{dt} = \alpha_0 P + \alpha_1 C - \gamma_M mRNA. \tag{3.14}$$

Finally, the rate of change of the output protein $Y$ found from reaction (3.5) is

$$\frac{dY}{dt} = k_t(mRNA)(rRNA) - \gamma_Y Y. \tag{3.15}$$

The output protein concentration, $Y$, can be determined by solving the ordinary differential equation (ODE) set (3.10-3.15). However when there are multiple transcription factor-gene pairs, multiple coupled sets of ODE's should be considered which is difficult to solve analytically. In Section 3.3, methods for simplifying this ODE set are introduced.

### 3.3 Analysis of Regulated Gene Expression

RRE models capture the dynamical nature of biological processes. However, these models are not easy to analyze when the complexity of the biological circuit increases [41]. Here, we simplify (3.10)-(3.15) by using three approaches, namely, elimination of irrelevant species, time-scale differences, and Michaelis-Menten approximation [30].

The model in (3.10)-(3.15) captures also the concentration of intermediate species like transcription factor-promoter complexes and RNAP which are not the essential points of interests. Thus, it is important to simplify the model by removing these irrelevant species [30]. To do so, time scale differences between the fast reaction of promoter binding (3.2) and the slow reactions of translation (3.5) and transcription (3.3,3.4) are exploited. We consider that the fast reactions are in steady-state. Thus, we assume that there is not a significant change in the concentrations of $X$ and $X_n$. Then, we combine the equations (3.10)-(3.13) as

$$\frac{dC}{dt} = k_b P X^n - k_{b0} C, \tag{3.16a}$$

$$\frac{dP}{dt} = -\frac{dC}{dt}. \tag{3.16b}$$

Due to the conservation of mass principle, the total amount of free or bound promoter sites is constant, i.e., $P + C = P_T$. Setting the equations for C and P at quasi steady-state, i.e., $dC/dt \approx 0$, we obtain

$$C = P_T \frac{X^n}{\theta_X^n + X^n}, \tag{3.17a}$$

$$P = P_T \frac{\theta_X^n}{\theta_X^n + X^n}, \tag{3.17b}$$

with $\theta_X = (k_b/k_{b0})^n$. The amount of mRNA molecules depends both on the concentration of promoter sites bound to an activator or repressor, and on the amount of free promoters. Since the production of mRNA depends linearly on $P$ and $C$, mRNA decays at a constant rate $\gamma_M$.

If the transcription factor is an activator, the contribution of $C$ to $mRNA$ production is much larger than that of $P$, which is represented by $\alpha_1 >> \alpha_0$. Substituting the quasi-

steady state expressions for $C$ and $P$ in (3.17) into (3.14) yields:

$$\frac{d(mRNA)}{dt} = \kappa_0 + \kappa_1 \frac{X^n}{\theta_X^n + X^n} - \gamma_M(mRNA), \tag{3.18}$$

where $\kappa_0 = \alpha_0 P_T$ and $\kappa_1 = (\alpha_1 - \alpha_0)P_T$.

If the transcription factor is a repressor, the contribution of $C$ to $mRNA$ production is much smaller than that of $P$, i.e., $\alpha_1 << \alpha_0$. In this case, (3.14) becomes

$$\frac{d(mRNA)}{dt} = \kappa_0 + \kappa_1 \frac{\theta^n}{\theta_X^n + X^n} - \gamma_M(mRNA), \tag{3.19}$$

where $\kappa_0 = \alpha_1 P_T$ and $\kappa_1 = (\alpha_0 - \alpha_1)P_T$. In both cases, the parameter $\kappa_0$, which is much less than $\kappa_1$, denotes a residual or basal activity considered to be $0$.

The next step is translation, shown with the following equation derived from (3.15) in the abundance of rRNA

$$\frac{dY}{dt} = k_t(mRNA) - \gamma_Y Y. \tag{3.20}$$

So the simplified set of equations is

$$\begin{aligned} \frac{d(mRNA)}{dt} &= \kappa_1 f^{\pm}(\theta_X, X, n) - \gamma_M(mRNA), \\ \frac{dY}{dt} &= k_t(mRNA) - \gamma_Y Y, \end{aligned} \tag{3.21}$$

where $\kappa_1 = (\alpha_1 - \alpha_0)P_T$. The expression $f^{\pm}(\theta_X, X, n)$ is called Hill function. For the activator case, Hill function becomes $f^{+}(\theta_X, X, n) = X^n/(\theta_X^n + X^n)$ while for the repressor case, $f^{-}(\theta_X, X, n) = \theta_X^n/(\theta_X^n + X^n)$. For gene regulatory networks, the exponent $n$ is considered to be large $(n >= 2)$ according to the experimental data [42]. For large $n$, the parameter $\theta_X$ has therefore a special meaning: it is a threshold value below which there is practically no activity and above which activity is (almost) maximum. In the limit as $n$ tends to infinity, the Hill function becomes a step function.

Similar to electrical circuits, we can define analog and digital operation for biological

circuits too [43]. In this study, we differentiate these two operation modes according to the operation region of Hill function.

### 3.3.1 Analog Interpretation of Biological Circuits

For analog operation, we consider that the input concentration falls down to the interval where the Hill function acts almost as a linear function [44]. Assuming an oscillatory input $X = \theta_X + X_0 cos(2\pi f_0 t)$, we approximate the Hill function as $f^+(\theta_X, X, n) = 1/2 + \frac{n}{4\theta_X}(X - \theta_X)$ calculated by Taylor's expansion for $X_0 \ll \theta_X$. By applying Fourier transform to (3.21), the transfer function of an activator can be found as

$$H(j\omega) = \frac{\kappa_1 k_t n}{4\theta_X (j\omega + \gamma_M)(j\omega + \gamma_Y)}. \tag{3.22}$$

The transfer function of an activator expressed in (3.22) shows low-pass characteristics. Since mRNA decays much faster than the protein ($\gamma_M \gg \gamma_Y$), for frequencies higher than $\gamma_Y$, $H(j\omega)$ decreases rapidly [45]. The analog operation of a basic biological circuit unit illustrated in Fig. 3.2 can be seen in Fig. 3.3 where an input concentration signal with multiple frequencies is applied. We observe that the higher frequencies are suppressed by the biological circuit due to the low-pass characteristics of the biological circuit.

Since the repressor shows the same frequency domain characteristics, we conclude that the basic biological circuit units can follow input signals up to critical frequency, $f_c = \gamma_Y / 2\pi$, which settles an upper limit for the operation frequency of biological circuits. For the linear approximation of Hill function, the biological activator circuit resembles a transistor which operates as an amplifier biased with a DC voltage [45].

### 3.3.2 Digital Interpretation of Biological Circuits

In electrical circuits, transistors are also used as digital switches. To obtain a switch from biological circuits, it is considered that for the high cooperativity $n$, the Hill function be-

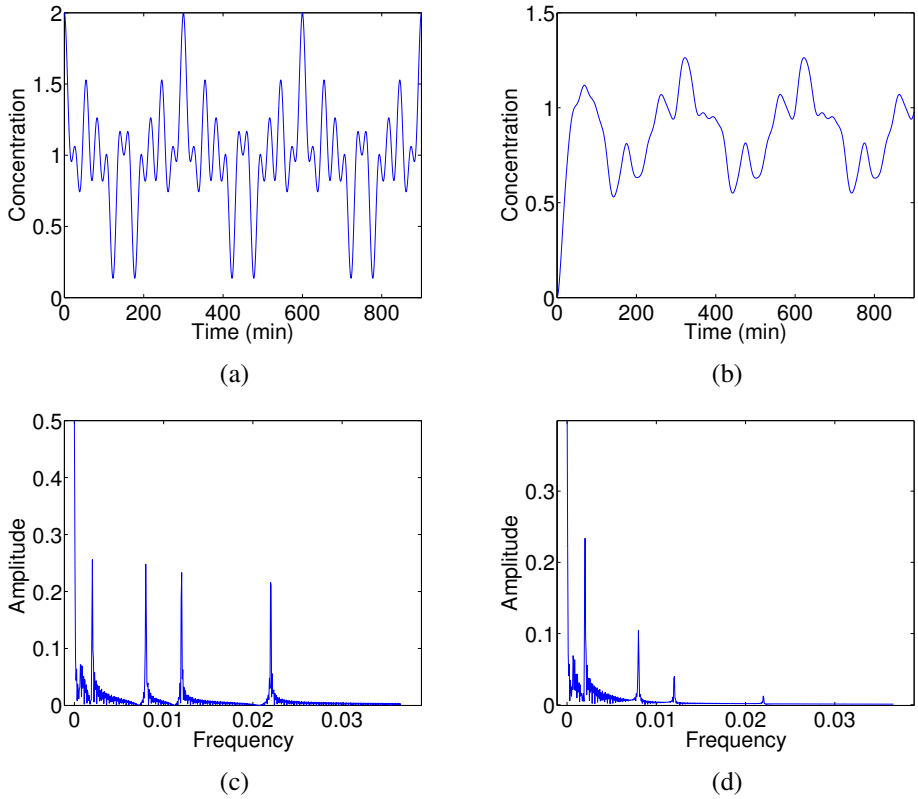


Figure 3.3: Analog operation of the basic biological circuit unit. (a) Applied input signal, i.e., the concentration of the transcription factor X is presented which is composed of the mixing of three different frequencies 0.005, 0.007 and 0.01 Hz. (b) The output signal, i.e., the concentration of the protein Y is presented, which is smoother than the input signal. (c) The frequency spectrum of the input signal. (d) The frequency spectrum of the output signal whose higher frequencies are suppressed.

comes a step function [28]. For an activator, it is assumed that $mRNA$ production is zero below the threshold $\theta_X$, and mRNA production is maximum above the threshold $\theta_X$. It is expressed as $f(\theta_X, X, n) = I(X > \theta_X)$ for an activator and $f(\theta_X, X, n) = I(X < \theta_X)$ for a repressor, where $I$ denotes the unit step function. The step function approximation of the Hill function may not fully describe the transient response of a biological circuit but it describes the state information of the circuit effectively [46]. For digital operation, the input is defined as the molecular concentration signal alternating between the levels '0' and '$N_c$' $\mu mol/V$ representing '0' and '1' bit according to the message. An input concentration signal $x(t)$ to an activator behaving like a switch is assumed to be a pulse of amplitude

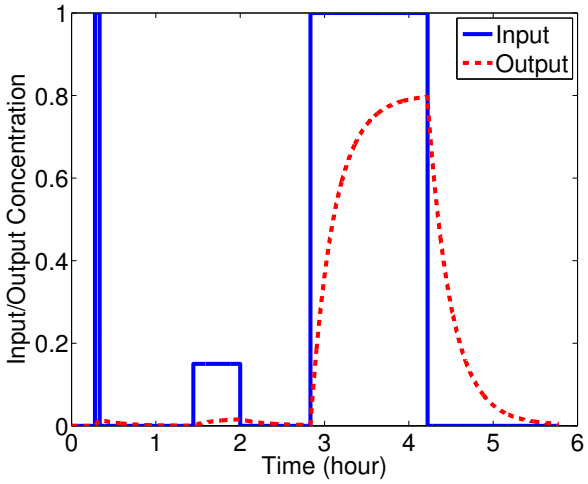


Figure 3.4: Operation of the basic biological circuit unit. The output is produced when a high enough input concentration is applied during a long enough time.

$N_c$ and width $T$, i.e., $x(t) = N_c$ for $t < T$ and $x(t) = 0$ for $t > T$. The output protein concentration $y(t)$ can be calculated as $y(t) = Y_{st}(1 - e^{-\gamma_y t})$ by solving the differential equation system in (3.21) where $Y_{st} = \kappa_1 k_t/(\gamma_y \gamma_M)$ and the delay is $\tau_d = ln(2)/\gamma_y$.

For the given input, the maximum value of the output depends on the duration of the input, $T$. When the input pulse finishes, the protein production stops and the output concentration starts to decrease due to natural decay. Thus, the maximum value that $y(t)$ can reach is its concentration at $t = T$ which is $y_{max} = Y_{st}(1 - e^{-\gamma_Y T})$. Then, the decaying output concentration after $t > T$ is expressed as $y(t) = Y_{st}(1 - e^{-\gamma_Y T})e^{(-\gamma_Y (t-T))}$.

The output concentration $y(t)$ decays exponentially. Even though it will take long time to totally vanish because of exponential decay, $y(t)$ will be significantly reduced after $\tau_y = 1/\gamma_Y$. The digital operation of the basic biological circuit unit can be seen in Fig. 3.4 where in order to obtain digital pulses as outputs, the input molecule concentration should be long enough and should have high enough amplitude.

Up to now, we considered a basic biological circuit unit comprising only a single promoter and a single gene. By combining these units we can build more complex circuits.

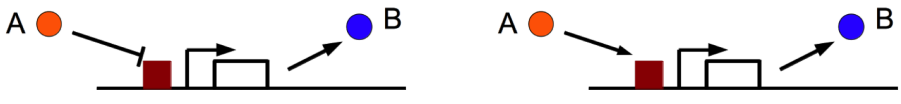


(a) (b)

Figure 3.5: SISO Configuration. (a) The transcription factor A binds to the promoter activating the production of the molecule B. (b) The transcription factor A binds to the promoter and stops the production of B.

## 3.4 Interconnecting Basic Biological Circuit Units

To build functional circuits we need to connect the basic units together using three different configurations, namely, single input single output (SISO), multiple input single output(MISO), single input multiple output (SIMO) [28]. Using these configurations, an input signal can be fed to different paths and signals coming from different paths can be merged.

### 3.4.1 Single Input Single Output Configuration

In SISO configuration, there is a single input transcription factor controlling the concentration of a single output protein. The activating characteristic is shown by an arrow in Fig. 3.5 (a) while the repressing characteristic is shown by a flat-end arrow in Fig. 3.5 (b). In both figures, squares represent promoters, rectangles represent genes, where A is the input transcription factor and B is the output protein produced from that gene.

### 3.4.2 Multiple Input Single Output Configuration

In this configuration illustrated in Fig. 3.6, a single gene is controlled by two activator transcription factors A and C which may activate the gene either collaboratively or additively. If they work collaboratively, both of the transcription factors need to be present to activate the gene and the mRNA production rate $\kappa_1 f(\theta_X, X, n)$ in (3.21) is replaced by $\kappa_{AC} f(\theta_A, A, n) f(\theta_C, C, n)$. If they work additively, either of the transcription factors may activate the gene independently and the total mRNA production rate is the sum of the contributions of the two transcription factors. The total mRNA production rate in this case is

expressed as $\kappa_A f(\theta_A, A, n) + \kappa_C f(\theta_C, C, n)$. When one or both of the transcription fac-

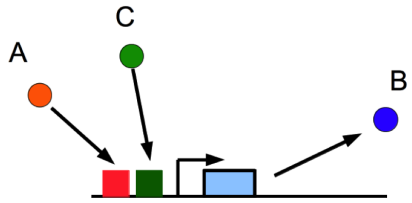


Figure 3.6: Multiple Input Single Output Configuration

tors are repressors, the functions $f(\theta_A, A, n)$ and $f(\theta_C, C, n)$ are replaced by the repressor Hill functions. This configuration serves for merging two signals coming from different sources.

### 3.4.3 Single Input Multiple Output Configuration

In this configuration illustrated in Fig. 3.7, a promoter is controlling two different genes producing proteins B and C simultaneously with the same rate. By using multiple outputs, two molecular concentrations representing the same signal are obtained, where one may be used for monitoring while the other is propagated to the latter parts of the circuit.

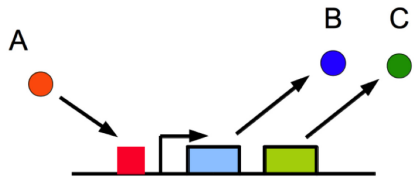


Figure 3.7: SIMO Configuration. The transcription factor A binds to the promoter producing the proteins B and C proportionally.

## 3.5 Biotransceiver Architecture

A transceiver for MC should be capable of sensing the environment, receiving signals from other MC devices, processing the received and sensed information and finally transmitting

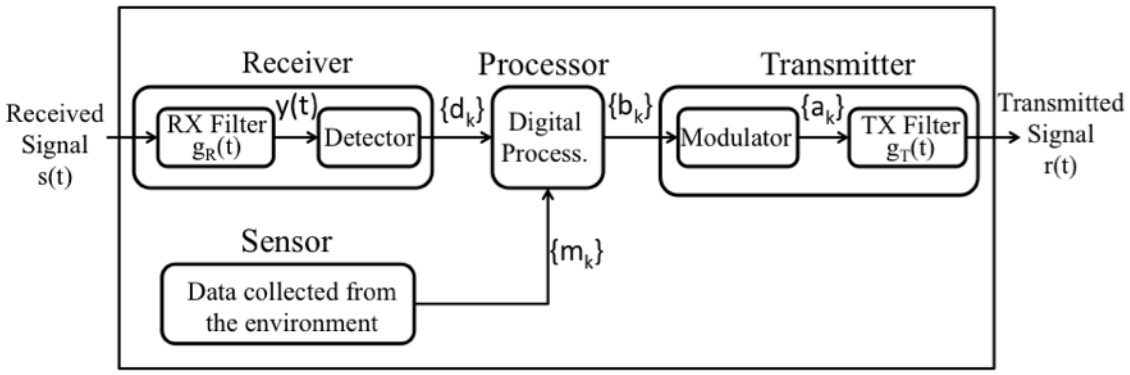


Figure 3.8: Transceiver architecture for MC illustrating the connections between its functional blocks.

the processed information as molecular signals. To this end, we propose the architecture illustrated in Fig. 3.8.

In our transceiver architecture, we adopt a baseband pulse transmission scheme where the molecular signals are subject to channel effects and noise. For the sake of simplicity we adopt a coded modulation scheme. The transmitter modulates the bit sequence $\{b_k\}$ received from the processor block and generates the symbol sequence $\{a_k\}$. Then, the transmit filter $g_T(t)$ generates a pulse according to the symbol $\{a_k\}$ and produces the transmitted signal $r(t)$. All types of MC channels such as diffusion-based, flow-based or walkway-based distort the transmitted signal $r(t)$ and add noise. To reconstruct the original signal from the distorted signal $s(t)$, a receiver filter followed by a detector is used which regenerates the intended bit sequence $\{d_k\}$ from $y(t)$. The sensor block of the architecture collects data from the environment and generates a bit sequence $\{m_k\}$. Then, the processor block merges the information generated in the sensor block $\{m_k\}$ with the information coming from the other nanomachines $\{d_k\}$ and produce an output bit sequence $\{b_k\}$ to be transmitted.

The link between two different bacteria populations can be constructed only if the transmitted signal of one population is using the same type of molecule that the other bacteria population is intended to receive. If all biotransceivers transmit different types

of molecules, the identity of the biotransceiver will be inferred from the molecule type which solves the addressing problem and also it will avoid self-interference. However, this will require the production of different types of biotranceivers which is not that easy from the biological point of view. Furthermore, scalability problems may arise when creating a nanonetwork with a large number of biotransceivers. Otherwise, if all biotransceivers transmit the same type of molecule, the production of biotransceivers will be relatively easy despite the fact that it will cause inter-user interference, addressing and medium access control problems. In our work, we focus on the physical layer, these challenges about the link layer will be addressed in future research.

## 3.6 Biological Circuit Design for a Biotransceiver

Exploiting the mathematical abstraction provided in Section 3.2 and 3.3, and the interconnections defined in Section 3.4, we design representative biological circuits for each block of the biotransceiver architecture introduced in Section 3.5 for baseband pulse amplitude modulation.

### 3.6.1 Transmitter

The function of the transmitter is the generation of molecular concentration signals $r(t)$ according to the data to be transmitted represented by the bit sequence $\{b_k\}$. It consists of a modulator which creates symbols $\{a_k\}$ from the bit sequence $\{b_k\}$ and a transmission filter $g_T(t)$. The transmitted signal at the output of the transmitter can be expressed as

$$s(t) = \sum_{k=0}^{\infty} a_k g_T(t - kT), \tag{3.23}$$

where $T$ is the bit duration.

*Modulator*

In MC literature, there are numerous modulation techniques such as concentration shift keying, frequency shift keying, pulse position modulation, and molecular shift keying. Since MC channels are often very slow [11], they do not support utilization of high frequency carriers. The most suitable modulations techniques are On-Off Keying (OOK) and M-ary amplitude modulation, where the information is encoded on the amplitude of baseband MC signal.

For this design, we adopt M-ary amplitude modulation. Converting the consecutive bits into different amplitude levels representing the symbols, requires many parallel biological circuits. Here we consider a M-ary modulation scheme with M=4. Since a concentration cannot be negative, all symbols are positive and equally distant to each other assigned as follows:

$$\{a_k\} = \begin{cases} 4A_0, & \text{if } (b_k, b_{k-1}) = (1,0) \\ 3A_0, & \text{if } (b_k, b_{k-1}) = (1,1) \\ 2A_0, & \text{if } (b_k, b_{k-1}) = (0,1) \\ A_0, & \text{if } (b_k, b_{k-1}) = (0,0) \end{cases} \tag{3.24}$$

where the Gray coding is used to minimize the error.

To implement this M-ary modulator, we propose the circuit in Fig. 3.9 where the concentration of the protein $X_1$ is the input of the modulator representing bit sequence $\{b_k\}$ and the concentration of the protein $X_3$ is the output representing symbol sequence $\{a_k\}$. Here we assume that the circuit in Fig. 3.9 operates as a digital circuit as described in Section 3.3.2.

The basic unit composed of $P_1$ and $G_1$ pair serves as a unit delay element. When $k = i$, $X_2$ represents the previous input $b_{i-1}$ where $X_1$ represents the input $b_i$. In all the four branches depicted in Fig. 3.9, the previous input is compared with the current input and each branch is activated only for one of the possible input sequences $\{(1,1),(0,0),(1,0),(0,1)\}$, respectively from the top to the bottom, respectively.

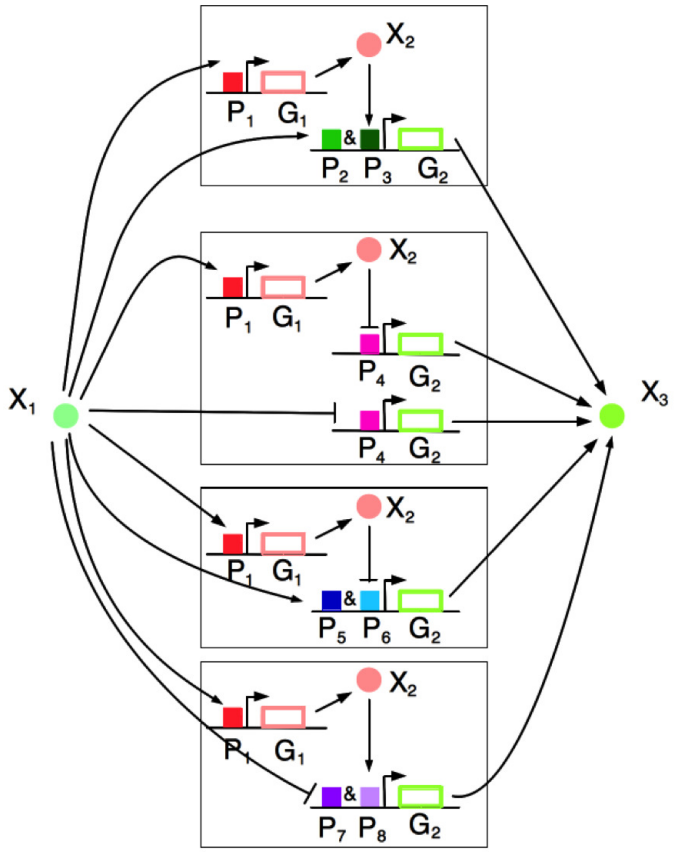


Figure 3.9: M-ary modulator biological circuit. The input protein $X_1$ represents digital bits which are translated into M concentration levels in the output protein $X_3$.

When activated, each branch produces the same output molecule but with different rates $\kappa_1^i$ which provides different amplitude levels as symbols. In ideal case, $\{a_k\}$ is composed of impulses. However, in the practical biological circuits, according to Section 3.3.2, $\{a_k\}$ corresponds to consecutive pulses $p^i(t)$ of the form

$$p^i(t) = \begin{cases} \frac{\kappa_1^i k_t}{\gamma_{X_3}\gamma_M}(1 - e^{-\tau t}), & \text{if } t < T_b \\ \frac{\kappa_1^i k_t}{\gamma_{X_3}\gamma_M} e^{-\tau T_b} e^{-(t-T_b)}, & \text{if } t \geq T_b \end{cases} \tag{3.25}$$

where $i \in \{P_2\&P_3, P_4, P_5\&P_6, P_7\&P_8\}$ and the continuous signal $a(t)$ is expressed as $a(t) = \sum_{k=-\infty}^{\infty} p^i(t - kT)$. Thus, we can map $\{a_k\}$ to $\kappa_1^i k_t/(\gamma_{X_3}\gamma_M)$. Since $k_t, \gamma_{X_3}, \gamma_M$ are the same for all branches, we can find $\kappa_1^i$ as follows $\kappa_1^{P_2\&P_3} = 3\kappa_{1o}, \kappa_1^{P_4} = \kappa_{1o}, \kappa_1^{P_5\&P_6} = 4\kappa_{1o}, \kappa_1^{P_7\&P_8} = 2\kappa_{1o}$.

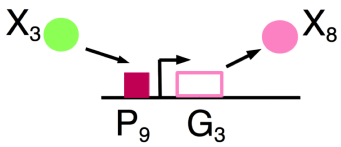


Figure 3.10: Transmit filter biological circuit operates in analog mode and shapes the modulator output $X_3$ into $X_8$.

Here, as the color coding in Fig. 3.9 indicates, each branch is using different promoters to establish the orthogonality. Since the delay of a basic biological circuits unit depends only on the decay rate of the output protein as specified in Section 3.3.2, even though the four branches include different promoters, they have the same delay $t_d = ln(2)/\gamma_{X_3}$. So for all four branches, the total delay is $t_d^{mod} = ln(2)/\gamma_{X_2} + ln(2)/\gamma_{X_3}$.

*Transmit Filter*

The symbols $\{a_k\}$ are fed to the transmit filter $g_T(t)$ which generates a rectangular pulse for each symbol ideally. In this study, we consider a simple low-pass transmit filter which corresponds to the activator configuration depicted in Fig. 3.10 used in the analog operation mode described in Section 3.3.1. Using the equation (3.22), the transfer function of $\hat{g}_T(t)$ can be expressed as

$$\hat{G}_T(j\omega) = \frac{\kappa_1^{P_9} k_t n}{4\theta_{X_3}(j\omega + \gamma_M)(j\omega + \gamma_{X_2})}, \tag{3.26}$$

where the output of the transmit filter, i.e., the output of the transmitter block is $y(t) = a(t) * \hat{g}_T(t)$. Note that since the modulator block is not ideal, the actual transmit filter $g_T(t)$ is expressed as $g_T(t) = p(t) * \hat{g}_T(t)$. To guarantee that the transmit filter operates always in the analog mode, the concentration of input $X_3$, i.e, the modulated signal $a(t)$ must be in the linear range of the Hill function, thus $\theta_{X_2} - \frac{2\theta_{X_2}}{n} < a(t) < \theta_{X_2} + \frac{2\theta_{X_2}}{n}$ should hold.

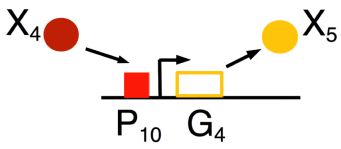


Figure 3.11: Sensory biological circuit reports the changes in $X_4$ to the processor by producing the protein $X_5$.

### 3.6.2 Sensor

Biological circuits can sense a variety of environmental conditions such as light, temperature, and presence of food or poison. When there is a change in the environmental conditions, the rate that the promoters activate the genes changes resulting in a change in the concentration of proteins.

A basic sensory block can be composed of a single activator circuit operating in digital mode. When the stimuli is above a threshold, the output protein concentration will go to high level while the stimuli is below the threshold, the output concentration will drop to 0. By this sensor design, an on-off sensor or a hypothesis testing sensor can be build. An example circuit is shown in Fig. 7.3. The sensor design can be extended to more sensitive sensors with higher precision, by combining several of these 1 bit sensors.

The bit sequence $m_k$ represents the output of the sensor block and corresponds to the concentration of $X_5$. The concentration of $X_4$ is denoted by $d(t)$ and $m_k$ is

$$m_k = \begin{cases} C_0, & \text{if } d(t) > \theta_{X_4} \\ 0, & \text{if } d(t) < \theta_{X_4} \end{cases} . \tag{3.27}$$

### 3.6.3 Processor

The processor considered in this study is composed of logic gates and memory elements demonstrated to be implementable by synthetic biology studies [47].

*Logic Gates*

Recently biologists have implemented all the logic gates in bacteria. Although complex logic gates such as NAND, NOR can also be constructed by biological circuits, only NOT, AND and OR gates are described in this work.

**NOT:** A NOT gate is a repressor circuit which produces molecule B when it is not stimulated. When the transcription factor A is present, the promoter is repressed so the gene becomes deactivated and molecule B production stops.

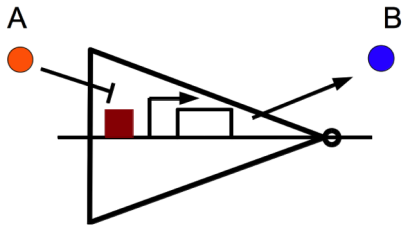


Figure 3.12: NOT gate composed of a repressing biological circuit where B is the logical inverse of A.

**AND:** By the means of the MISO configuration described in Section 3.4.2, an AND gate can be constructed using only a single basic biological circuit unit. The gene is activated only when both of the transcription factors are present.

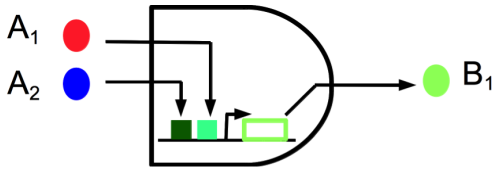


Figure 3.13: AND gate including two promoters which activate the gene collaboratively. $B_1$ is the logical 'AND' of $A_1$ and $A_2$.

**OR:** The OR gate constitutes of two basic biological circuit units that produce the same output molecule. When one or both of the inputs are present, the output protein is produced.

Since there is no isolation between biological circuit units, designing a circuit with multiple logic gates requires choosing orthogonal, i.e., noninteracting promoters and genes

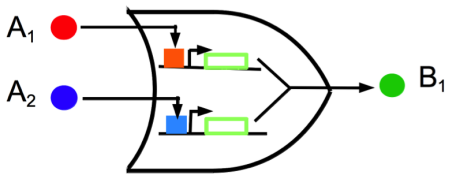


Figure 3.14: OR gate composed of two parallel circuits which activate the same gene independently. $B_1$ is the logical 'OR' of $A_1$ and $A_2$.

for each gate. This orthogonality problem prevents the multiple use of the same gate. On the contrary, in electrical circuits, it is favorable to use the same gate for the whole design due to transistor fabrication simplicity.

*Memory*

Memory in biological circuits is achieved by a toggle switch which includes two promoters which are effected by two inducers [35]. One of the two inducers sets the switch into one of the stable states, and the other sets it to the other stable state. Then, the toggle switch holds the state even the inducers are drawn back.

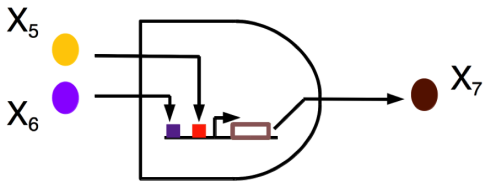


Figure 3.15: Processor circuit having two promoters binding to inputs $X_5$ and $X_6$ which are both required to activate the gene producing $X_7$. This block acts as an AND gate.

In this study, an AND gate, combining the sensor data with the received data is used as the processor as shown in Fig. 3.15. For example, the sensor measures the food level. When the food level is above the threshold, the sensor gives a high output which allow the processor to transfer the received data to the transmitter block. Thus, the bacterium relays a message only if there is food.

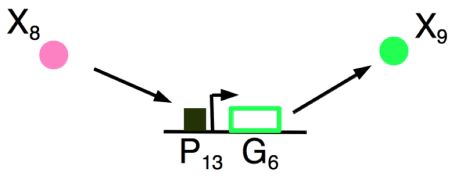


Figure 3.16: Receive filter biological circuit operating in analog mode which filters the received signal $X_8$ and outputs $X_9$.

### 3.6.4 Receiver

This block identifies the incoming molecular signal, measure its amplitude and convert the information encoded in the amplitude of the molecular signal to digital bits. For amplitude-based modulation techniques, concentration band detector circuits [48] can be used to identify different amplitude levels. The received signal $s(t)$ is first passed through a receive filter $g_R(t)$ and $y(t)$ is obtained. Then, the detector determines the intended bits by thresholding $y(t)$.

*Receive Filter*

In classical communication the receive filter is used to shape the pulse for optimal detection in the presence of channel noise. The optimal filter is the matched filter when the noise in the channel is additive white noise. However, with biological circuits it is not easy to create the matched filter. Thus, a low-pass filter illustrated in Fig. 3.16 is used as the receive filter to lower complexity of the receiver yet reducing noise. Using the equation (3.22), the transfer function of $g_R(t)$ can be expressed as

$$G_R(j\omega) = \frac{\kappa_1^{P_{13}} k_t n}{4\theta_{X_8}(j\omega + \gamma_M)(j\omega + \gamma_{X_9})}, \tag{3.28}$$

where the output of the receive filter is $y(t) = s(t) * g_R(t)$. Note that to avoid self-interference, the molecules used for $r(t)$ and $s(t)$ are different.

*Detector*

In classical communication the output of the receive filter is sampled and applied to a threshold detector. In this study, since sampling with biological circuits is not feasible, we will directly apply thresholding to the filtered received signal $y(t)$. In order to do so, four parallel branches of biological circuits are designed as seen in Fig. 3.17 using activator circuits in digital mode where the promoter of each branch has a different activation threshold. If $y(t)$ is above that threshold that branch is activated and produce the output molecule representing the bit sequences $\{m_k\}$.

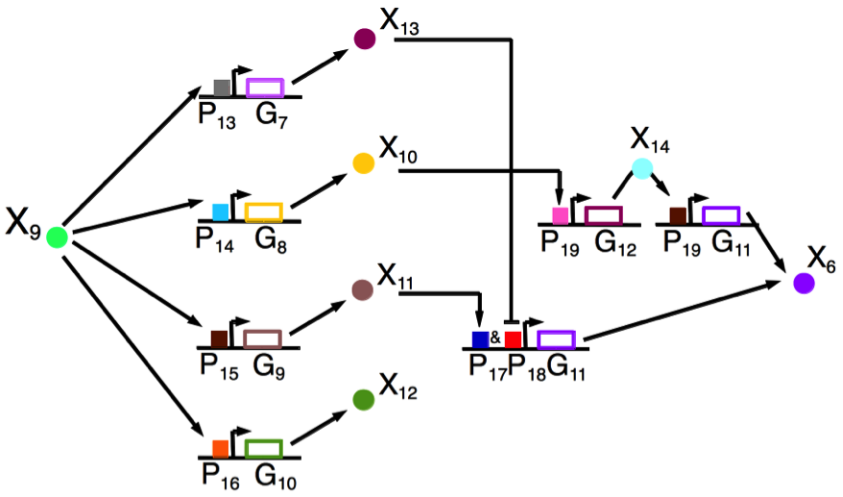


Figure 3.17: Detector circuit compares the filtered received signal $X_9$ with the activation thresholds of the four branches' promoters on the left-hand side to detect which M-ary amplitude level was transmitted. Then, the right-hand side generates the bit sequence according to the detector concentrations.

Remembering (3.24) and assuming each symbol is equally likely, detection thresholds of each branch expressed as $\theta_{P_{13}} = 3.5A_0, \theta_{P_{14}} = 2.5A_0, \theta_{P_{15}} = 1.5A_0, \theta_{P_{16}} = 0.5A_0$.

The proteins $X_9, X_{10}, X_{11}, X_{12}$ are produced for the following intended bit sequences

$$\begin{aligned} X_9 &\rightarrow \{(1,0)\} \\ X_{10} &\rightarrow \{(1,0),(1,1)\} \\ X_{11} &\rightarrow \{(1,0),(1,1),(0,1)\} \\ X_{12} &\rightarrow \{(1,0),(1,1),(0,1),(0,0)\} \end{aligned} \tag{3.29}$$

from which we can deduce how to generate $\{m_k\}$ according to the these proteins. For the first bit of $\{m_k\}$, it is enough to check $X_9$ and $X_{11}$. If they are both present than they activate the gene $G_{11}$ which produces a pulse representing the first 1 bit of the sequence. Then, for the second bit, it is enough to check $X_{10}$. If it is present, then the gene $G_{12}$ is activated. To adjust the timing of the second bit, we include an intermediary stage after $G_{12}$ such that it is expressed as the second bit after the expression of the first bit.

### 3.7 Numerical Results

In this section, we investigate the operation of the biotransceiver proposed in Section 3.6. The analytical expressions in time domain given in Section 3.3 and 3.6 are evaluated.

In this study, E. Coli is assumed to be the host bacteria for the biological circuits since the genetic manipulation of E. Coli is well-studied in synthetic biology literature. The evaluation parameters are taken from the literature and scaled up or down in the same order. The promoter activity is $\kappa_1 = 10$ [49], translation rate is $k_t = 150\ \mathrm{h}^{-1}$ [38], protein decay rate is $\gamma_Y = 4.15\ \mathrm{h}^{-1}$ [50], mRNA decay rate $\gamma_M = 10.05\ \mathrm{h}^{-1}$ [50], and bit duration $T_b = 30$ min. For simplicity we assumed that decay rates and translation rates for every promoter-gene pair are equal which in turn equalize the delay of each basic unit. Also, in the rest of this section, the molecular concentration signals presented are all normalized such that the maximum concentration of a pulse representing bit 1 is $1\ \mu\mathrm{M}$.

Using libraries of genetic parts such as BioBricks [51], promoter-gene pairs which have

parameters in the order of the designed values can be found. Then, to tune the parameters, three different techniques may be used [29]. The first one is the iterative rational design where the performance is experimentally evaluated at each step and the system design is modified until a specific performance requirement is met. The second technique is creating variants of the same circuits with different elements such as different promoters and testing all the variants until a suitable one is found. The third technique is the directed evolution which is based on mutation and selection. By using these techniques, the genetic circuit components used in the abstract circuit design can be mapped to actual promoter-gene pairs.

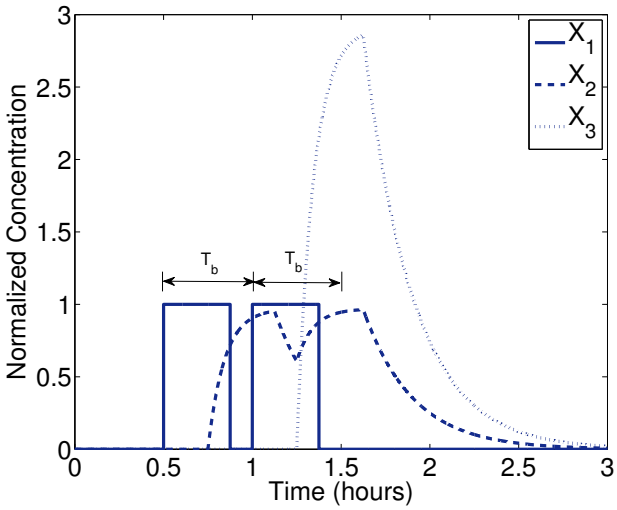


Figure 3.18: Concentration of the input bits $X_1$, intermediary signal $X_2$, and the output M-ary modulated signal.

### 3.7.1 Transmitter

Let us consider that there are two biotransceivers A and B. Assume that the processor of A generates a bit sequence $b_k$ of two consecutive bits with perfectly rectangular digital pulses that A encodes and sends to B. Assuming that the bit duration is $T_b$ and the line code is return-to-zero, the input $X_1$ and the output $X_3$ of the modulator described in Fig. 3.9 are considered for two consecutive bits '11'. In Fig. 3.18, it is observed that the symbol

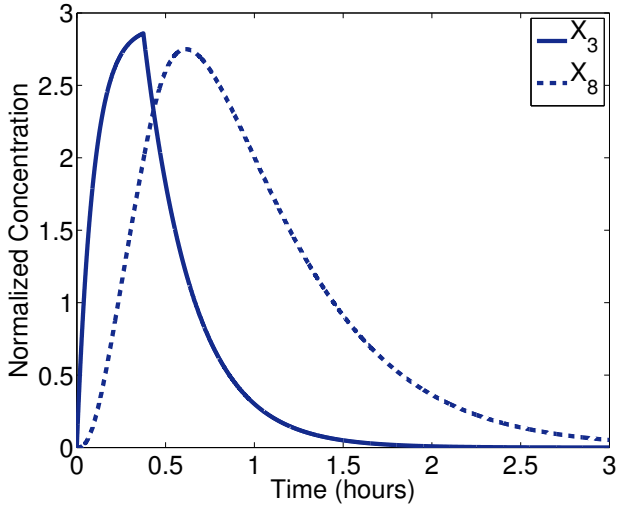


Figure 3.19: Concentration of the input $X_3$ and the output $X_8$ of the transmitter filter which shapes the transmitted signal.

'3' is generated by the modulator according to (3.24). Note that the concentration signal representing the symbol peaks after the second bit finishes which indicates the delay which is approximately equal to the bit duration of 30 min.

After the symbols are generated the transmitter filter shapes the pulse as shown in Fig. 3.19. Here, $X_3$, is the input signal representing the symbol level and $X_8$ is the output of the transmitter, i.e., the signal put into the channel $r(t)$.

### 3.7.2 Receiver

The signal $r(t)$ propagates through a diffusion based channel and it is distorted by the channel noise assumed to be an Additive White Gaussian with zero mean and $0.05$ $\mu$M variance [22]. In Fig. 3.20, both the signal given to the channel, $r(t)$, and the distorted signal, $s(t)$, are shown. Furthermore, the output of the receive filter $y(t)$ shown in Fig. 3.20 compensates for the attenuation in the channel and filters the noise.

The filtered received signal $y(t)$ is measured by the detector described in Fig. 3.17 which selects the symbol $'3'$. Then, it generates the corresponding bit sequence '11', i.e., the original information sent by the transceiver A, as shown in Fig. 3.21. Note that the

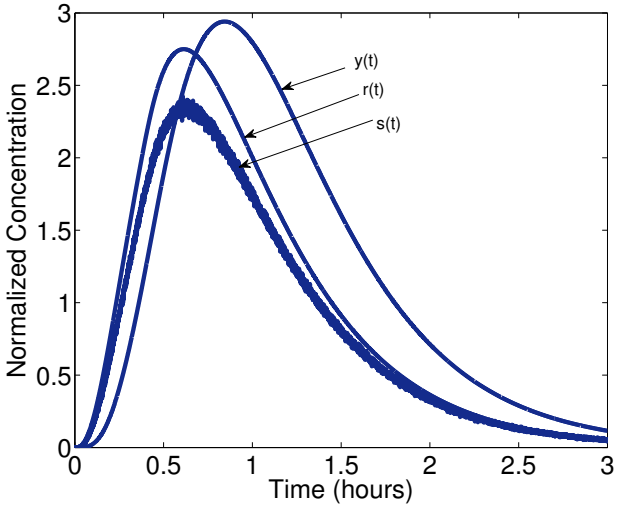


Figure 3.20: Concentration of the transmitted signal r(t), the received signal with noise s(t), and the filtered signal y(t).

generated bits do not have perfectly rectangular shapes but the existence of two different peaks indicates the generation of two consecutive '1' bits.

## 3.8 Conclusion

In this chapter of the PhD thesis, a biotransceiver design for MC using genetically engineered bacteria is presented. First, the operation principles of biological circuits are modeled with RRE and both the digital and analog interpretations of biological circuits are provided. Then, the interconnections of basic biological circuits are defined. Using this mathematical framework, a biotransceiver architecture tailored for MC environment is proposed. The biological circuit designs for every block of the proposed biotransceiver are presented. Numerical results show that biotransceivers have long delays and very low operation speeds. However, they can operate in parallel within the small cell volume. Therefore, genetically engineered bacteria can achieve a very high computational density in terms of the number of operations per time per volume [52]. Furthermore, since the human body already contains billions of bacteria, usage of genetically engineered bacteria as nanocommunication devices inside human body will reduce biocompatibility problems.

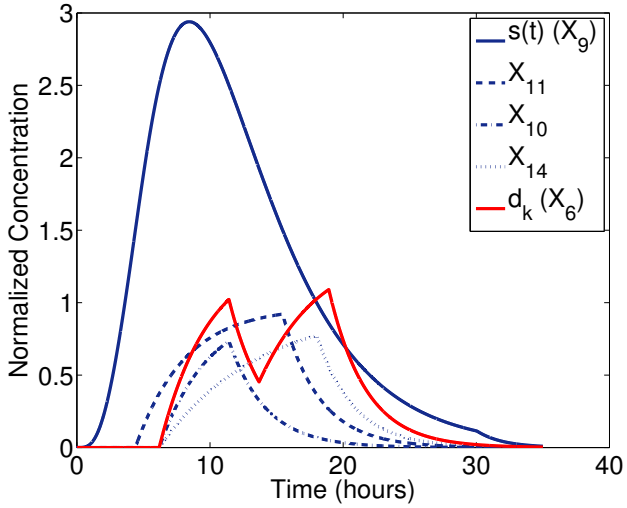


Figure 3.21: The filtered signal s(t) and the signal representing the generated digital bits $d_k$ by the detector.

Thus, genetically engineered bacteria is a perfect candidate for biomedical applications of nanocommunication networks such as diagnosis and treatment of lethal diseases, health monitoring, drug delivery, bio-hybrid implants.

# CHAPTER 4
# TRAVELLING WAVE CHANNEL MODELS AND IMPACT OF SOCIAL BEHAVIOR FOR BACTERIAL CHEMOTAXIS CHANNEL

## 4.1 Motivation and Related Work

In this chapter of the PhD thesis, we concentrate on a specific type of MC where bacteria are utilized as information carriers, which we term as **bacterial nanonetworks** [24], in contrast to 3 where bacteria are utilized as MC devices. This is based on a number of bacterial properties that includes the ability to move following a chemical gradient, i.e., bacterial chemotaxis, and ability to hold DNA plasmids that store encoded information as well as mechanisms to transfer them within the population, i.e., conjugation. Chemotaxis and conjugation play crucial roles for the survival of the bacteria. By chemotaxis, bacteria sense the gradient of molecules in the environment and bias its motion towards the attractants and away from the repellents to find more suitable environment for themselves [53]. Besides moving, bacteria also respond and adapt to its environment by exchanging DNA plasmids among them by conjugation such as plasmids containing genes for antibiotic resistance [54].

In bacterial nanonetworks, messenger bacteria pick up information encoded in DNA plasmids from the source using the conjugation process, move actively in the environment following a chemical gradient released from the destination and delivers the information to the destination as illustrated in Fig 4.1. Therefore the reliability of this channel depends on the number of bacteria reaching to the receiver. The programmability by genetic engineering and the widespread availability of bacteria who can survive in many diverse and harsh environmental conditions make bacteria a promising information carrier for MC. Furthermore, the possibility of encoding thousands of bits into a single DNA plasmid provides a

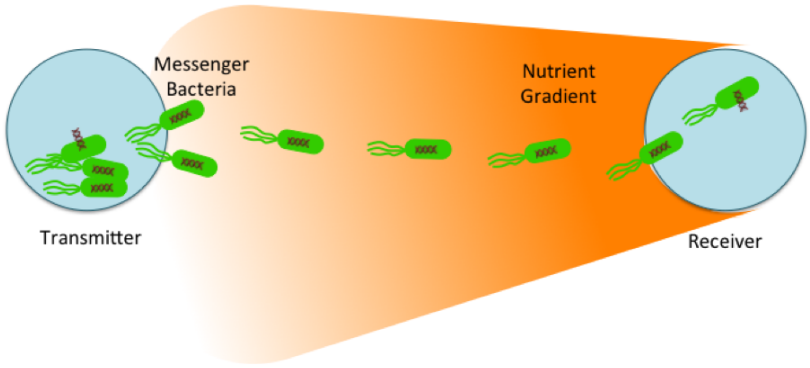


(a)

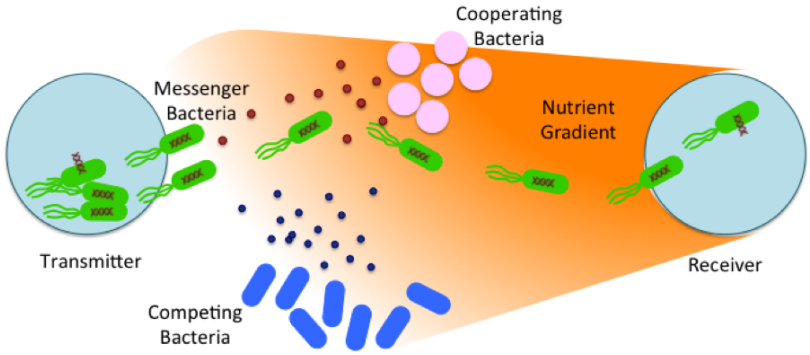


(b)

Figure 4.1: (a) Bacterial communication in ideal environment. (b) Bacterial communication in realistic environment.

potential for fast delivery of a huge amount of information between MC nodes and make bacterial nanonetworks stand out among other MC techniques [24].

Researchers have studied bacteria as an information carrier for MC in [27, 55, 24, 56, 57] which analyze the communication performance of the channel in terms of end-to-end delay, reliability as well as capacity. These studies approach the problem by considering that there is no other bacteria in the environment than the messengers. However, in nature bacteria always are present within microbiomes consisting of several different populations engaging in social behavior with one another [58]. The objective of this study is to investigate the social behavior of bacterial nanonetworks where populations of bacteria interact with each other and the incorporation of it into the design of artificial bacterial nanonetworks.

Bacteria have a highly complex form of community structure that is maintained by different types of social interactions such as competition, cooperation, and cheating leading to formation of biofilms, production of antibiotics, bacteria-host interactions, production of infectious diseases, and developmental processes such as sporulation [58, 59, 60, 61]. Cooperative behavior manifests in many forms such as hierarchical organization, cooperative sensing, foraging and collective learning. However, during the cooperative process, certain bacteria can switch to selfish behavior in which they do not contribute to the production of public goods but benefit from the ones produced by others. If the ratio of cheaters increases to a critical level, this may even lead to the collapse of the community. On the other hand, competition occurs when bacteria fight for the limited nutrient sources by inhibiting other populations' reach to the resources [62]. In order to evaluate the performance of a bacterial nanonetwork, the social interactions among bacteria and their impact on the information transmission must be investigated. Since all these interactions affect the number of messenger bacteria reaching the receiver, the communication performance of the bacterial nanonetworks will be affected. In our study, we present a realistic environment for MC utilizing bacteria as information carrier where we consider both cooperative and competitive social interactions, and analyze their effects on the communication channel performance, as illustrated in Fig. 4.1. In particular, we analyze the effects of social interactions between the populations, and how this affects the bacterial propagation, which in turn affects the communication channel.

We can summarize the main contributions of this chapter as follows:

- For the first time in literature, we study the bacteria nanonetwork channel on the population level utilizing *Keller-Segel* model and traveling wave solutions to investigate the propagation of bacteria carrying information.
- For the abundant nutrient case where the diffusion of the chemoattractant is strong and the consumption by bacteria is negligible, we identify the chemotactic response

to the nutrient gradient and derive closed form solutions for bacterial density at the receiver, as well as the delay and the attenuation of the bacterial channel.

- We investigate the impact of social behavior on the chemotactic response of the bacteria, and analyze the effects of cooperation, competition and cheating on the delay, attenuation and data rate of the channel.

The rest of this chapter is organized as follows. In Section 4.2, we present the Keller-Segel model for bacterial propagation and we derive the bacterial density, as well as the delay and attenuation of the bacterial nanonetwork channel. In Section 4.3, the data rate in bacterial nanonetworks is calculated from the bacterial density. Then, in Section 4.4, we analyze the social behavior of bacteria, where we characterize the effects on their chemotactic response and derive the delay and attenuation when the population faces cooperation or competition. The numerical results are given in Section 4.5 and the chapter is concluded in Section 4.6.

## 4.2 Traveling Wave Model of Bacterial Chemotaxis

### 4.2.1 General Bacterial Chemotaxis Model

Chemotaxis is the movement of the bacteria in response to chemical changes in the environment to relocate towards favorable environments. This behavior is observed in many bacterial species such as *E. coli*, *Salmonella enterica*, *Pseudomonas aeruginosa* which possess flagella [63]. In this study, we give a generic propagation model applicable to all motile chemotactic bacteria populations.

Bacterial chemotaxis is studied both at the single-cell level [64] as well as the population level [65] to reveal the causes and mechanisms of the motility process. One approach is using the Keller-Segel model, which presents a system of two coupled differential equations that describes the aggregation of motile bacteria under the influence of diffusing chemoattractants. Besides being the most adopted model for chemotaxis, we chose to use this model

due to its intuitive simplicity, analytical tractability and the ability to estimate the behavior of bacterial populations accurately [66].

The general form for the Keller-Segel model is expressed as [67]

$$\frac{\partial n(r,t)}{\partial t} = \nabla(\mu(n,S)\nabla n - n\chi(S)\nabla S) + f(n), \tag{4.1a}$$

$$\frac{\partial S(r,t)}{\partial t} = D_S \triangle(S) + g(n,S) - h(n,S), \tag{4.1b}$$

where $n(r,t)$ denotes bacterial cell density, $S(r,t)$ denotes chemoattractant concentration, $\mu$ is the random motility coefficient of the cells, $\chi(S)$ is the chemotactic sensitivity, $D_S$ is the diffusion coefficient of chemical attractants, $g(n,S)$ is the production rate of chemoattractant, $h(n,S)$ is the degradation rate of the chemoattractant, and $f(n)$ represents the additional growth term capturing the reproduction of bacteria. Furthermore, $t$ denotes time and $r$ is the distance to the origin where the messenger bacterial population is inoculated initially.

In the literature, each term in (4.1) takes different forms depending on the properties of the bacterial population and the culture environment. An extensive overview can be found in [65]. The random motility coefficient, i.e., $\mu(n,S)$ in (4.1) assumed to be a constant $\mu$, accounts for the random, unbiased motion of a bacterial cell [66]. The chemotactic sensitivity, $\chi(S)$, is the response of a bacterium to the chemoattractant gradient which is modeled as $\chi(S) = \chi_0/S$, which accounts for the saturation of the bacterium response when the attractant concentration is high.

The growth term, $f(n)$, represents the increase in the bacterial cell density arising from the replication process. This term may be neglected when the time-scale of the bacteria movement are considered to be faster than the replication process [68] which is the case in our study since we consider that the time frame in which the bacteria will reach the receiver is significantly less than the reproduction time. For time intervals larger than the replication time of the bacteria, a population control mechanism can be used by genetically engineer-

ing the bacteria [69] which maintain a stable population without growth by programmed cell death [70]. Therefore, we can assume that the messenger bacteria population under consideration has no growth.

The chemoattractant $S$ defined in the Keller-Segel model in (4.1), may represent either a nutrient source or a cell-to-cell signaling molecule attracting other bacteria. In this study, we set the chemoattractant to be a chemical gradient emitted from a nutrient source, e.g., glucose, and is co-located with the receiver nanomachine. Furthermore, we consider that the bacteria does not produce any nutrient, i.e., $g(n, S) = 0$, and decay of the nutrient is at a fixed rate, i.e. $h(n, S) = h_0 n + kS$.

The Keller-Segel model in (4.1) provides a nonlinear set of partial differential equations which is not easy to solve analytically for most cases due to the coupling between the two equations. To decouple the equations, we consider the case where the diffusion of the attractant is strong ($D_S$ large) and its consumption by bacteria is negligible ($h_0 \to 0$). In the next section, we investigate the solutions for (4.1) in the strong attractant diffusion case.

### 4.2.2 Traveling Wave Solutions for Strong Attractant Diffusion

We consider the asymptotic case for the Keller-Segel model, where the diffusion of the chemoattractant is strong ($D_S$ is large) compared to its consumption, i.e, bacteria do not change the attractant concentration while sensing the attractant gradient [71]. It is considered that the attractant in this case is the nutrient whose concentration is given as $S(r, t)$. Also, we assume that the nutrient source which is co-located with the receiver generates nutrients at a constant rate to establish a steady-state nutrient concentration in the environment. Since the consumption by bacteria does not affect the nutrient concentration profile, we consider that $h_0 = 0$ which makes the diffusion equation for the nutrient density, $S(r, t)$, independent of the bacterial density, $n(r, t)$.

The equations in (4.1) become

$$\frac{\partial n(r,t)}{\partial t} = \frac{\partial}{\partial r}\left(\mu\frac{\partial n}{\partial r}\right) - \frac{\partial}{\partial r}\left(n\chi(S)\frac{\partial S}{\partial r}\right), \tag{4.2a}$$

$$\frac{\partial S(r,t)}{\partial t} = \frac{\partial}{\partial r}\left(D_S\frac{\partial S}{\partial r}\right) - kS. \tag{4.2b}$$

The boundary conditions are defined as

$$\mu\frac{\partial n}{\partial r} - \chi n\frac{\partial S}{\partial r} = 0, (r \to \pm\infty) \tag{4.3}$$

$$S = 0, (r \to \pm\infty) \tag{4.4}$$

where the initial conditions are defined as:

$$n(r,0) = g(r), \quad t = 0. \tag{4.5}$$

Then, we can easily solve for the concentration of the nutrients $S(r,t)$ considering a continuous release from the receiver considered as a point source co-located with the receiver at $r_r$ establishing a steady-state expressed as

$$S(r,t) = S_0 e^{-\left(\frac{|r-r_r|}{\rho}\right)}, \tag{4.6}$$

where $S_0$ is the nutrient release rate from source and $\rho = \sqrt{D_S/k}$ is the exponential mean distance depending on the diffusion coefficient $D_S$ and decay rate $k$. For distances larger than $\rho$, the nutrient concentration drops below to $1/e$ of its initial concentration. Since now the nutrient density is known, the response of the bacteria to this density needs to be determined.

To find the bacterial density $n(r,t)$, we define the chemotactic response $\gamma(r)$ as

$$\gamma(r) = \chi(S)\frac{\partial S}{\partial r}, \tag{4.7}$$

which leads to a constant value for the strong attractant diffusion case due to the cancellation of the $r$ dependent terms in the expression of nutrient density $S(r,t)$ found in 4.6 and the definition of chemotactic sensitivity, $\chi(S) = \chi_0/S$.

Let's assume that the diffusion of species is weak compared to the chemotaxis so that we can use the method of multiple scales to solve the problem analytically [71]. Considering the constant $\gamma$, now we look for a solution to (4.2) in the traveling wave form expressed as

$$n = \phi(r - \gamma t, t), \tag{4.8}$$

where $\phi(x,t)$ is the solution for $\gamma \to 0$.

We consider that the bacteria population is inoculated into the environment at a single point which corresponds to an initial bacterial density expressed as $g(r) = N_0\delta(r)$ where $N_0$ is the total number of bacteria in the inoculated population. Then, the bacterial density $n(r,t)$ is expressed in the traveling wave form as

$$n(r,t) = \frac{N_0}{\sqrt{4\pi\mu_0 t}} exp\left(-\frac{(r-\gamma t)^2}{4\mu_0 t}\right), \tag{4.9}$$

where $\gamma = \chi_0/\rho$ is the wave speed.

### 4.2.3 Delay and Attenuation

In the bacterial channel, when the transmitter has a message to send, it instantaneously releases messenger bacteria that contains the information encoded into the plasmid, with a cell density $N_0$ at time $t = 0$. We consider that the transmitter is located at $r = 0$. The release of the bacteria into the channel from the transmitter sets the initial condition of the bacterial cell density for (4.2).

The propagation of the message is defined as the movement of bacteria released from the transmitter towards the receiver governed by the equations in (4.2). When a threshold number of bacteria reach the receiver, the message is considered to be delivered. Hence,

we are interested in the density of bacteria at the receiver $n(r,t)|_{r=r_r}$, where $r_r$ is the receiver location. Because of the slow nature of diffusion and chemotaxis, not all the bacteria released from the transmitter will reach the receiver. Also, it requires a significant amount of time for a threshold number of bacteria to reach the receiver and successfully deliver the information. Therefore, we are interested in finding the delay and attenuation characteristics of the channel.

The delay of the channel, $\tau_d$, is defined as the time required for the bacteria to reach the receiver, i.e., the time that the traveling wave solution for the bacterial cell density reaches its peak, and can be evaluated as:

$$\tau_d = \{t | \max_t \ n(r_r, t)\}. \tag{4.10}$$

By using the expression in (4.9), $\tau_d$ is expressed as

$$\tau_d = \frac{r_r}{\gamma}. \tag{4.11}$$

The attenuation of the channel, $\Gamma$, is defined as the ratio of the total number of released cells by the transmitter to the peak bacterial density of the traveling wave at the receiver, which can be represented as

$$\Gamma = \frac{n(r_t, t)|_{t=0}}{n(r_r, t)|_{t=\tau_d}}. \tag{4.12}$$

By substituting $\tau_d$ in (4.12), the attenuation can be expressed as

$$\Gamma = \sqrt{4\pi\mu_0(r_r/\gamma)}. \tag{4.13}$$

### 4.3 Data Rate in Bacterial Nanonetworks

In the previous section we derived the bacterial density at the receiver as well as the delay and attenuation in bacterial nanonetworks. Since the information is encoded on the bacte-

rial density, any change in it directly effects the data rate of the network. In this section, we derive the maximum data rate for binary transmission with ON-OFF keying.

We consider that the transmitter releases bacteria with intervals of bit period $T_s$, where $N_0$ bacteria are released to transmit bit $1$ and no bacterium is released to transmit bit $0$. The released bacteria follow the traveling wave model described in Section 4.2.2. To detect the maximum density of the incoming bacterial density wave, the receiver samples the bacterial density at $\tau_d$ and decides whether bit $0$ or $1$ was sent.

$T_s$ corresponds to the separation between two consecutive pulses distinguishable from each other. When $T_s$ increases, the information transmitted in unit time becomes lower. To maximize the data rate, $T_s$ should be minimal. To find the minimum separation $T_s$, we look for the effects of the previously transmitted pulses on the current pulse. Since the attenuation in the channel significantly increases with time, we assume that only the immediate previous pulse interfere with the current pulse. We choose $T_s$ such that the tail of the bacterial density of the previous pulse, does not exceed 10% of the maximum bacterial density of the current pulse, i.e., $n_p(r_r, \tau_d + T_s) = 0.1 n_c(r_r, \tau_d)$. Therefore the corresponding maximum data rate for this binary transmission can be expressed as

$$R = \frac{1}{T_s}. \tag{4.14}$$

## 4.4 Social Behavior Analysis for Bacterial Channel

In the nature, bacteria form communities which frequently contain multiple populations [60]. The survival of the bacterial community relies on its complex community structure as well as the coordination between multiple populations. To adapt to the environmental conditions which sometimes become harsh for bacteria to live in such as starvation, extreme temperatures, hazardous chemicals [72], bacterial populations interact through cell-to-cell communication.

There are many types of social interactions that is associated with bacteria such as co-

operation, competition and cheating [61]. A good example that exhibits dynamic social interaction between the bacteria happens during fluctuations of nutrient resources. Bacteria may assist and support each other to discover nutrient sources or act selfishly and block other species from reaching the scarce resources. In the following subsections, we investigate how this social behavior affect the performance of the bacterial channel. The two basic social interaction, namely, cooperation and competition, are chosen to be studied in this chapter.

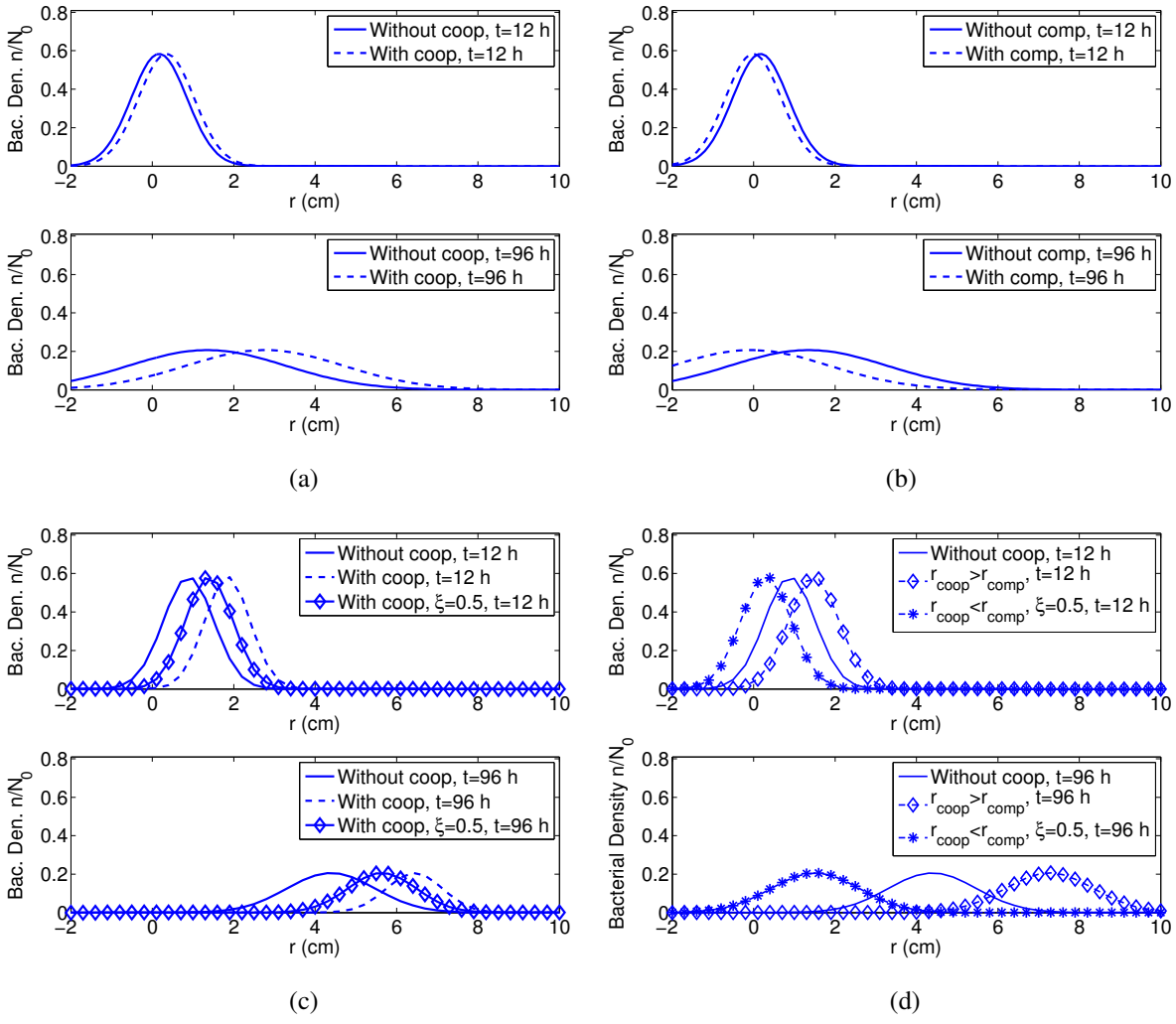


Figure 4.2: (a) Bacterial density against distance in presence of a cooperative population. (b) Bacterial density against distance in presence of a competitive population. (c) Bacterial density against distance in presence of a cooperative population with cheaters. (d) Bacterial density for against distance in presence of cooperative and competitive populations.

### 4.4.1 Impact of Cooperation on Chemotaxis

The cooperative process is achieved when the bacteria cooperate through cell-to-cell signaling. This signaling process is used to attract other bacteria towards them when they are closer to nutrient sources as illustrated in Fig. 4.1-b [59]. In the bacterial nanonetwork scenario, we assume to have two populations. The first population is defined to be the messenger population with the encoded DNA plasmids, while the second cooperating population that is closer to nutrient sources will emit chemoattractant molecules to attract the first population.

To incorporate the effects of cooperation into our model, first we define bacterial cell density of the first population as $n_1(r,t)$ and the bacterial cell density of the second population as $n_2(r,t)$. Also, we denote the concentration of the attractant emitted by the second population as $Q(r,t)$. Then, by rewriting the first equation of (4.1) for the first population we obtain

$$\frac{\partial n_1(r,t)}{\partial t} = \nabla(\mu \nabla n_1 - n_1 \chi_1(S) \nabla S - n_1 \chi_2(Q) \nabla Q), \tag{4.15}$$

where $\chi(S)$ is the chemotactic sensitivity of the first population to $S$ whereas $\chi_Q(Q)$ is the chemotactic sensitivity of the first population to $Q$. The nutrient density $S$ is expressed as in (4.6).

The bacterial cell density for the second population is written similarly as

$$\frac{\partial n_2(r,t)}{\partial t} = \nabla(\mu \nabla n_2 - n_2 \chi(S) \nabla S). \tag{4.16}$$

We consider that the second population consists of non-motile bacteria hence its bacterial cell density has established a steady-state profile centered at $r_{coop}$ expressed as

$$Q(r) = Q_0 e^{-\left(\frac{|r - r_{coop}|}{\rho_{coop}}\right)}, \tag{4.17}$$

where $Q_0$ is the release rate of the attractant molecule.

Furthermore, we assume that this steady-state profile gives rise to a chemotactic response found as

$$\gamma + \gamma_Q = \chi(S)\frac{\partial S}{\partial r} + \chi_Q(Q)\frac{\partial Q}{\partial r}, \tag{4.18}$$

which is similar to (4.7) where $\gamma$ belongs to the case without any social behavior. Let's define $\gamma_{coop} = \gamma + \gamma_Q$ where $\gamma_Q = \chi_Q/\rho_{coop}$. According to (4.9), $\gamma$ represents the speed of the traveling wave. Hence, when cooperation takes place, the speed of the traveling case increases by $\gamma_Q$ representing the attraction effect of the cooperating population. Moreover, since the wave is arriving to the receiver sooner, it has less time to diffuse which leads to lower attenuation.

Following a similar derivation to (4.9) in Section 4.2, we obtain the bacterial cell density for the first population as

$$n_1(r,t) = \frac{1}{\sqrt{4\pi\mu_0 t}} exp\left(-\frac{(r-\gamma_{coop}t)^2}{4\mu_0 t}\right), \tag{4.19}$$

where basically we replaced $\gamma$ with $\gamma_{coop}$. The bacterial density profile with and without cooperation is illustrated in Fig. 4.2-a which shows that with cooperation the bacterial density waves move faster.

Then, the delay of the system in the presence of cooperators can be expressed as

$$\tau_d^{coop} = \frac{r_r}{\gamma_{coop}}, \tag{4.20}$$

whereas the attenuation is expressed as

$$\Gamma^{coop} = \sqrt{4\pi\mu_0(r_r/\gamma_{coop})}. \tag{4.21}$$

Even though cooperation benefits both populations, eventually there will be individuals in each population who will breakdown the cooperation by pursuing their own interests [73], and these are called "*cheaters*". The cheaters will avoid the cost of producing coop-

eration molecules while still benefiting from the cooperation. When the ratio of cheaters to cooperators increases significantly, cheaters will dominate the population and the cooperation between the two populations will be disrupted [61]. To reflect the impact of cheaters, the cooperative chemotactic response $\gamma_{coop}(r)$ can be refined by the cheater frequency $\xi$, which is defined as the ratio of the number of cheaters in the cooperative population to the total number of bacteria in the cooperative population. Then, the chemotactic term in (4.15) becomes $(1-\xi)n_1\chi_2(Q)\nabla Q$. $\xi = 0$ represents the case where there is no cheating while $\xi = 1$ represents the case where all cooperative bacteria became cheaters and disrupted the cooperation totally.

### 4.4.2 Impact of Competition on Chemotaxis

When the nutrient sources are scarce, bacteria populations which are spatially close to each other compete by releasing repellent chemicals to keep the others away from the nutrient sources as shown in Fig. 4.1-b [72]. The repellents only affect the other bacterial populations if they are from the same species or if they are genetically close so that the competitors identify and respond to the repellents.

Now, let's consider that we have two sibling populations where the first population is the messenger population and the second population is the competitor of the first one which was already in the environment before the release of the messenger population. The bacterial density of the messenger population is expressed as

$$\frac{\partial n_1}{\partial t} = \nabla(\mu\nabla n_1 - n_1\chi(S)\nabla S + n_1\chi_P(P)\nabla P), \tag{4.22}$$

where $\chi(S)$ is the chemotactic sensitivity for the attractant $S$, while $\chi_P(P)$ is the chemotactic sensitivity for the repellent $P$. Note that, since $P$ is a repellent, the sign in front of the second term of the right hand side is negative. The nutrient density $S$ is expressed as in (4.6).

We consider that the second population consists of non-motile bacteria and its bacterial cell density has also established a steady-state profile centered at $r_{comp}$. Similar to the attractant concentration in the cooperation case in (4.17), the repellent concentration $P(x,t)$ is expressed as follows

$$P(r) = P_0 e^{-\left(\frac{|r-r_{comp}|}{\rho_{comp}}\right)}, \tag{4.23}$$

where $P_0$ is the release rate of the repellent molecules and $D_P$ is the diffusion coefficient for the repellents.

Then, the chemotactic response in case of competition is found as $\gamma_{comp} = \gamma - \gamma_P$, which is similar to (4.18). Note that there is a negative sign representing the repellent gradient that makes the bacteria move away from the poisonous source. Then, the chemotactic response to $P$ is found by $\gamma_P = \chi_P/\rho_{comp}$. Since $\gamma_{comp}$ represents the speed of the traveling wave, we can conclude that according to the strength of competition, the speed of the traveling wave is decreasing accordingly. Since the traveling wave is slower, the bacteria will arrive to the receiver later and will diffuse more into the environment, leading to higher attenuation.

Similar to (4.19), we obtain the bacterial cell density for the messenger population in case of competition as

$$n_1(r,t) = \frac{1}{\sqrt{4\pi\mu_0 t}} exp\left(-\frac{(r-\gamma_{comp}t)^2}{4\mu_0 t}\right), \tag{4.24}$$

where basically we replaced $\gamma_{coop}$ with $\gamma_{comp}$. Fig. 4.2-b illustrates the slow moving bacterial density that results from the competition process.

The delay of the system in the presence of competitors can be expressed as

$$\tau_d^{comp} = \frac{r_r}{\gamma_{comp}}, \tag{4.25}$$

while the attenuation is expressed as

$$\Gamma^{comp} = \sqrt{4\pi\mu_0(r_r/\gamma_{comp})}. \tag{4.26}$$

### 4.4.3 The Impact of Joint Cooperation and Competition

Often bacteria live in microbiomes where there are multiple populations cohabiting the environment. When messenger bacteria is assumed to live in such an environment, there may be multiple populations that they interact with cooperatively or competitively. Each population will effect the propagation of the messenger bacteria in different strengths according to its distance to the messenger population and the diffusion properties of the chemoattractant/chemorepellent it releases. To combine the effects of every population present in the environment we can modify the bacterial density expression as follows

$$\begin{aligned}\frac{\partial n_1}{\partial t} &= \nabla(\mu\nabla n_1 - n_1\chi(S)\nabla S \\ &\quad - n_1\sum_{i=1}^{N_{coop}}\chi_{2,i}(Q_i)\nabla Q_i + n_1\sum_{i=1}^{N_{comp}}\chi_{P,i}(P_i)\nabla P_i),\end{aligned} \tag{4.27}$$

where $N_{coop}$ is the number of cooperating populations, $N_{comp}$ is the number of competing populations, $\chi_{2,i}$ is the corresponding chemotactical sensitivity of $i^{th}$ population, $\chi_{P,i}$ is the corresponding chemotactical sensitivity of $i^{th}$ population, $Q_i$ is the density of the $i^{th}$ cooperative population, and $P_i$ is the density of the $i^{th}$ competitive population.

Following similar derivations to Section 4.4.1 and 4.4.2, the bacterial cell density for the joint cooperation-competition case with multiple populations can be expressed as

$$n_1(r,t) = \frac{1}{\sqrt{4\pi\mu_0 t}}exp\left(-\frac{(r-\gamma_j t)^2}{4\mu_0 t}\right), \tag{4.28}$$

where $\gamma_j = \gamma + \sum_{i=1}^{N_{coop}}\gamma_{Q_i} - \sum_{i=1}^{N_{comp}}\gamma_{P_i}$.

By substituting $\gamma$ in the expression of delay given in (4.11) and the attenuation expres-

sion given in (4.13) by $\gamma_j$, the delay of the system for joint case is found by

$$\tau_d^j = \frac{r_r}{\gamma_j}, \tag{4.29}$$

while the attenuation is found by

$$\Gamma^j = \sqrt{4\pi\mu_0(r_r/\gamma_j)}. \tag{4.30}$$

Fig. 4.2-d illustrates the bacterial density under the effects of both cooperation and competition.

## 4.5 Numerical Results

In this section, the analytical results obtained for the performance of bacterial nanonetwork channel as they undergo social interactions are numerically evaluated. First, we study the case of cooperation and investigate the delay and attenuation of the channel for various transmitter-receiver distances. Then, we conduct a similar study for the case of competition. For the numerical evaluations, *E. coli* is chosen to be the bacterial species for the messenger, cooperator and competitor populations due to the abundance of experimental studies on the interactions of E.coli populations. The parameter values are taken from [74] which studies the bacterial density of *E. coli* bacteria subject to multiple attractant/repellents environments, and from [75] for chemotactic coefficients. The random motility coefficient of bacteria is set at $\mu_0 = 1.5 \times 10^{-5}\mathrm{cm}^2/\mathrm{s}$. The chemotactic sensitivity coefficient $\chi_0$ for the nutrient is taken as $\chi_0 = 4.1 \times 10^{-4}\mathrm{cm}^2/\mathrm{s}$ and the chemotactic sensitivity for cooperation and competition molecules are taken as $\chi_Q = \chi_P = 1.5 \times 10^{-5}\mathrm{cm}^2/\mathrm{s}$. The initial bacterial density is taken as $10^8$ cells/mL and the length of the observation chamber is considered to be $4$ cm as in [75]. The transmitter is located in the middle of the chamber and the receiver's location is varied from $0.01 - 0.05$ cm which limits the maximum transmitter-receiver distance to $0.05$ cm.

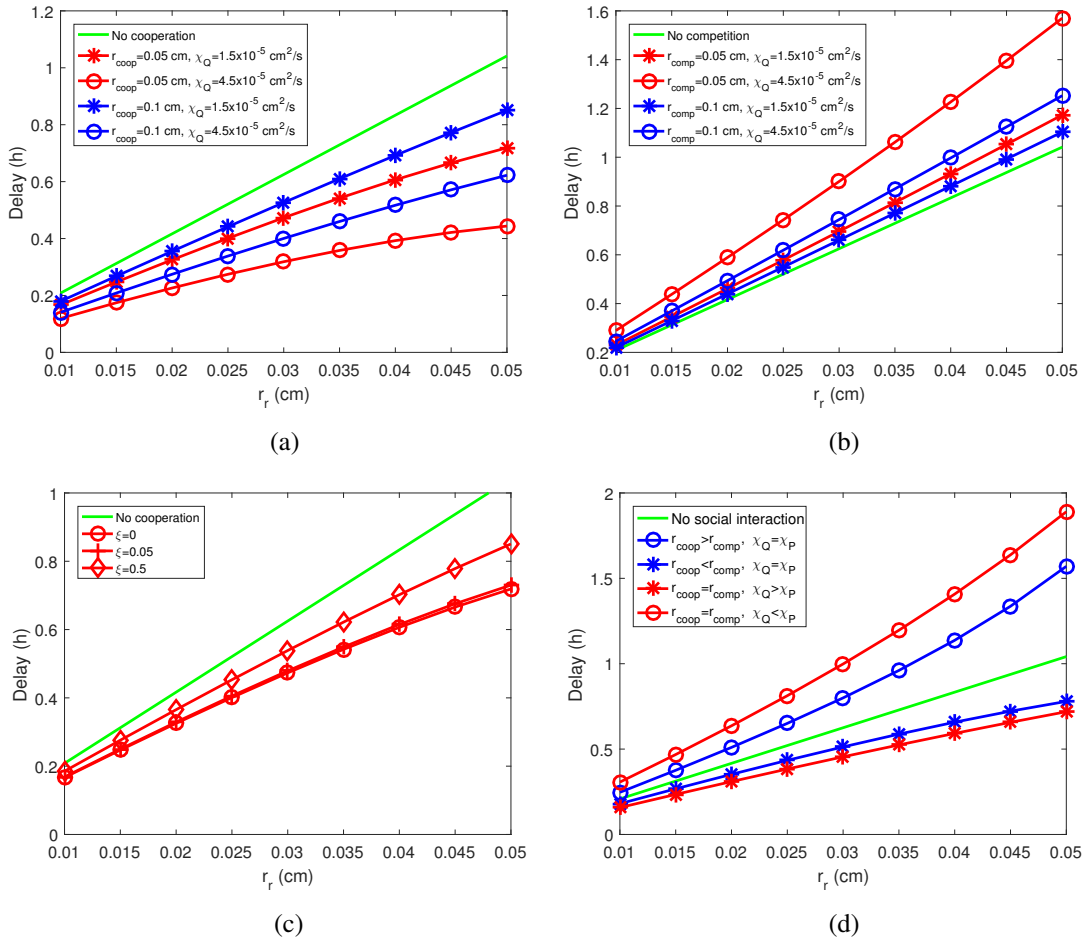


Figure 4.3: Delay of the channel against the transmitter-receiver distance for (a) Cooperation. (b) Competition. (c) Cooperation with cheating. (d) Joint cooperation and competition.

### 4.5.1 Impact of Cooperation

*Delay of The Channel*

In Fig. 4.3-a, the impact of cooperation on the delay of the bacterial channel is illustrated. We evaluated the channel delay for $r_{coop} = 0.05$ cm and $0.1$ cm and for $\chi_Q = 1.5 \times 10^{-5}$ cm$^2$/s and $4.5 \times 10^{-5}$cm$^2$/s. It is observed that cooperation reduces the delay of the channel significantly in all cases. It is also observed that with decreasing $r_{coop}$ the delay is decreasing. These results can be attributed to the closeness of the transmitter to the cooperative population producing attractants with a steeper gradient. Due to the steeper

gradient, the messenger bacteria are drawn faster towards the receiver based on (4.18). Furthermore, it is observed that the higher the chemotactic sensitivity $\chi_Q$, the smaller is the delay. This follows from the fact that the messenger bacteria are more sensitive to cooperative molecules with higher $\chi_Q$ which increases the strength of the chemotactic response, which in turn increasing the speed of the bacterial density wave according to (4.18). Note that a small increase in $r_{coop}$ causes larger deviation in delay than an increase in $\chi_Q$ due to the fact that while $\chi_Q$ is directly proportional to delay, $r_{coop}$ has a more complex effect. Firstly, with smaller $r_{coop}$, the cooperative population gets closer to the receiver, i.e., the nutrient source which increases their energy to use for cooperation. Secondly, due to smaller distances between the cooperative population and the messenger population, the molecule exchange gets easier.

In Fig. 4.3-c, the impact of cheating on delay is illustrated where $\mu_0 = 1.5\times10^{-5}\mathrm{cm}^2/\mathrm{s}$, $r_{coop} = 0.05$ cm, $\chi_Q = 4.5 \times 10^{-5}$ $\mathrm{cm}^2/\mathrm{s}$. Since cheating occurs when some of the bacteria in the population stop cooperating, it deteriorates the positive effect of cooperation. When the cheating frequency, $\xi$, is $0.05$, i.e. there are only $5\%$ cheaters, the delay is almost overlapping with the case without cheating, i.e., $\xi = 0$. However, when the cheating frequency rises to $0.5$, the delay increases since $10\%$ of the population is not involved in the production of cooperative molecules reducing the positive effect of cooperation.

*Attenuation of The Channel*

In Fig. 4.4-a, the impact of the cooperation on the attenuation of the channel is investigated. We evaluated the attenuation for $r_{coop} = 0.05$ cm and $0.1$ cm and for $\chi_Q = 1.5 \times 10^{-5}$ $\mathrm{cm}^2/\mathrm{s}$ and $4.5 \times 10^{-5}\mathrm{cm}^2/\mathrm{s}$ to reveal the effect of these two factors defining the strength of the cooperation. It is observed that when the cooperative population is closer, i.e. $r_{coop}$ is short, the attenuation is improved. As $r_{coop}$ decreases, the attraction between the messenger bacteria and the cooperative bacteria increases yielding a faster bacterial density wave. Since according to (4.9), the amplitude of the bacterial density is time-dependent,

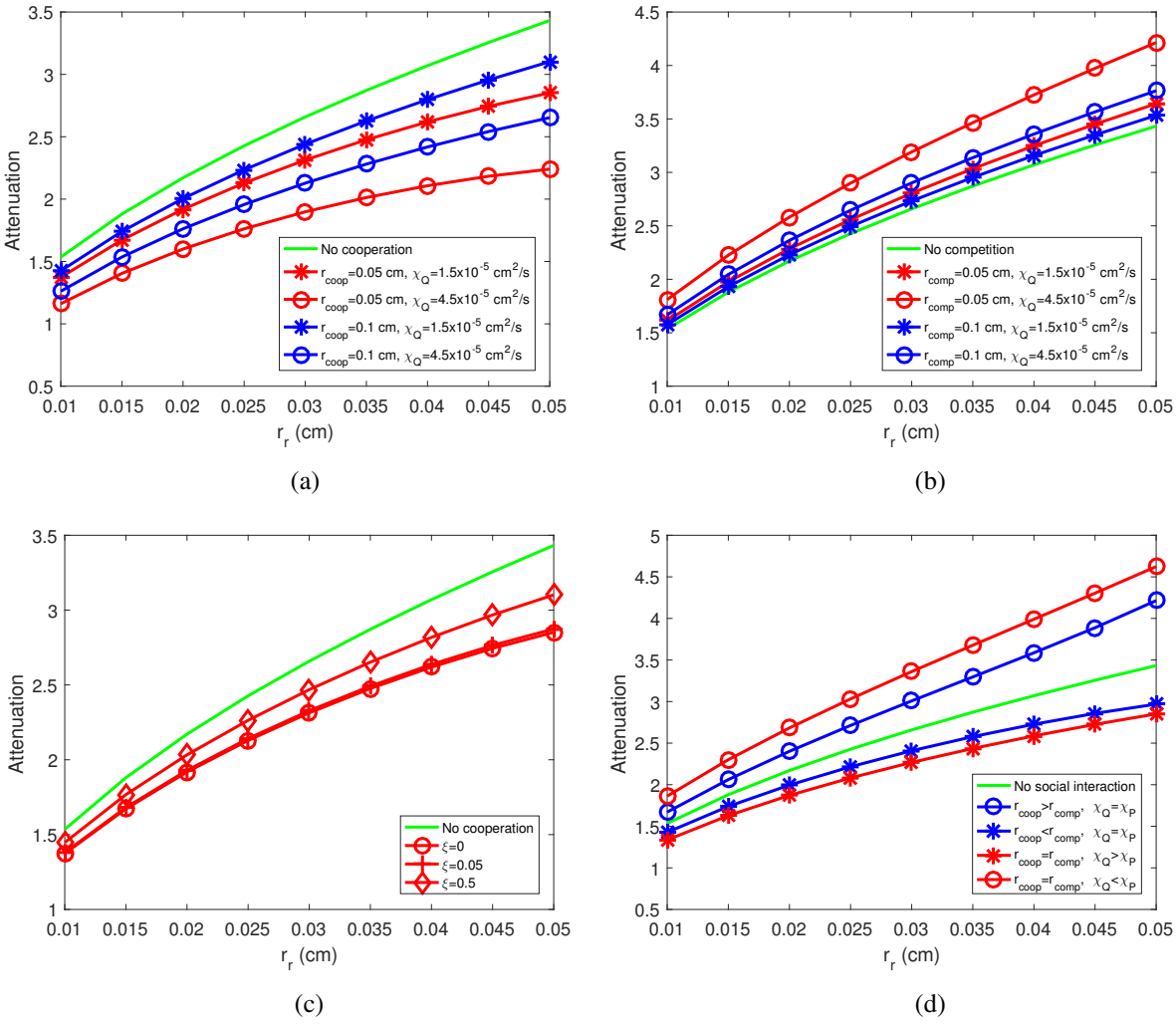


Figure 4.4: Attenuation of the channel against the transmitter-receiver distance for (a) Cooperation. (b) Competition. (c) Cooperation with cheating. (d) Joint cooperation and competition.

faster moving bacterial waves are less attenuated. Similarly, for higher chemotactic sensitivities $\chi_Q$, the bacterial waves are less attenuated. As $\chi_Q$ increases, the attraction between the messenger and the cooperative bacteria increases which in turn increases the speed of bacterial density wave subject to less attenuation. Finally, Fig. 4.4-a shows that cooperation improves the attenuation of the channel even if it is not as significant as in the case of delay.

In Fig. 4.4-c, the impact of cheating on attenuation is illustrated where $\mu_0 = 1.5 \times 10^{-5}\text{cm}^2/\text{s}$, $r_{coop} = 0.05$ cm, $\chi_Q = 4.5 \times 10^{-5}$ cm$^2$/s. Similar to the delay of the channel,

cheating can annihilate the positive effects of cooperation when the cheating frequency is high. For the cheating frequency of $\xi = 0.05$, i.e. there are only $5\%$ cheaters, the attenuation is not greatly affected. However, when the cheating frequency rises to $0.5$, half of the population quit participating in cooperation, and this results in the attenuation becoming more severe and getting closer to the attenuation level without any cooperation.

*Maximum Data Rate*

In Fig. 4.5, we illustrated the effect of cooperation where $r_{comp} = 0.2$ cm, $\chi_Q = 4.5 \times 10^{-5}$ cm$^2$/s. It is observed that the maximum data rate is decreasing with increasing distance since the bacterial density wave is widening while traveling as shown in Fig. 4.2. Due to this widening effect, the previous symbol's bacterial density wave overlaps more with the current symbol's bacterial density wave requiring to slow down the rate of transmission. Furthermore, Fig. 4.5 shows that the cooperative behavior improves the maximum data rate. This follows from the fact cooperation lowers the delay which in turn lowers the widening of the bacterial density wave. Thus, we can transmit more frequently without overlapping waves which results in increased data rate.

### 4.5.2 Impact of Competition

*Delay of The Channel*

In Fig. 4.3-b, the impact of competition on the delay of the bacterial nanonetwork channel is illustrated. The delay of the channel is evaluated for $r_{comp} = 0.05$ cm and $0.1$ cm and for $\chi_P = 1.5\times10^{-5}$ cm$^2$/s and $4.5\times10^{-5}$cm$^2$/s. It is observed that competition leads to higher delay for all the considered cases due to the negative effects on the bacterial chemotactic response as discussed in Section 4.4.2. Another observation is that the lower $r_{comp}$, i.e., the closer the competitive population to the messenger, will result in lower delay since the competitive effects driving the messenger bacteria away from the receiver are stronger when the second population gets closer. Moreover, when the chemotactic sensitivity of the

messenger bacteria to the competition molecules $\chi_P$ are higher, the chemotactic response to the competition gets stronger and decreases more the speed of the bacterial density wave. Hence, the bacterial wave travels slowly causing a higher delay. Note that, since the delay is inversely related to $r_{comp}$, a small increase in $r_{comp}$ causes larger deviation in delay than an increase in $\chi_P$ which is proportional to delay.

*Attenuation of The Channel*

Fig. 4.4-b presents the attenuation of the channel and the effects of competition on the attenuation. The attenuation is evaluated for $r_{comp} = 0.05 \text{ cm and } 0.1 \text{ cm}$ and for $\chi_P = 1.5 \times 10^{-5} \text{ cm}^2/\text{s and } 4.5 \times 10^{-5} \text{cm}^2/\text{s}$. With decreasing $r_{comp}$, the competitive interaction between the messenger and competing population rises which leads to a stronger attenuation. This arises since strong competitive repulsion slows down the bacterial density wave whose amplitude gets attenuated by the time dependent term in (4.24). Similarly, for higher chemotactic sensitivities $\chi_P$, the bacterial waves are less attenuated. As $\chi_P$ increases, the repulsion between the messenger and the cooperative bacteria increases which in turn decreases the speed of bacterial density wave subject to greater attenuation. Finally, Fig. 4.4-b shows that the attenuation has worsened with competition for all cases compared to the attenuation without any competition.

*Maximum Data Rate*

In Fig. 4.5, we illustrated the effect of cooperation where $r_{comp} = 0.2 \text{ cm}$, $\chi_Q = 4.5 \times 10^{-5} \text{ cm}^2/\text{s}$. Fig. 4.5 shows that the competitive behavior deteriorates the maximum data rate. This is due to the increasing effect of competition on delay which causes more widening of the bacterial density wave. Hence, the previous symbol's bacterial density wave overlaps more with the current symbol's bacterial density wave requiring to slow down the rate of transmission.

### 4.5.3 Impact of Joint Cooperation and Competition

To illustrate the effect of joint cooperation and competition, we considered that there are one cooperative and one competitive populations in the environment interacting with the messenger population. We considered four cases where we explore the effects of the distance and the chemotactic sensitivity of neighbor populations on the delay and attenuation.

*Delay of the Channel*

In Fig. 4.3-d, the joint effect of cooperation and competition on the delay is illustrated. Firstly, we consider the case where the chemotactic sensitivities of the cooperative and competitive populations are the same , i.e, $\chi_Q = \chi_P$, whereas the cooperative population is farther from the competitive population, i.e., $r_{coop} > r_{comp}$. In this case, since the competitive population is closer to the messenger population, competitive behavior is dominant which reflects as a higher delay than the no social interaction. Similarly, in the case where $\chi_Q = \chi_P$ and $r_{coop} < r_{comp}$, the cooperative behavior is dominant leading to a decreased delay.

Secondly, we consider the case where the distances of neighbor populations are the same, i.e., $r_{coop} > r_{comp}$, whereas the chemotactic sensitivity of the cooperative population is higher than the competitive one, i.e., $\chi_Q > \chi_P$. In this case, cooperative behavior is dominant since the messenger population is more sensitive to the cooperative behavior which shifts the delay in the cooperative direction to a value lower than the social interaction case. Similarly, in the case where $r_{coop} = r_{comp}$ and $\chi_Q < \chi_P$, the competitive behavior is dominant leading to an increased delay.

*Attenuation of the Channel*

In Fig. 4.4-d, the joint effect of cooperation and competition on the attenuation is illustrated. Firstly, we consider the case where the chemotactic sensitivities of the cooperative and competitive populations are the same , i.e, $\chi_Q = \chi_P$, whereas the cooperative popula-

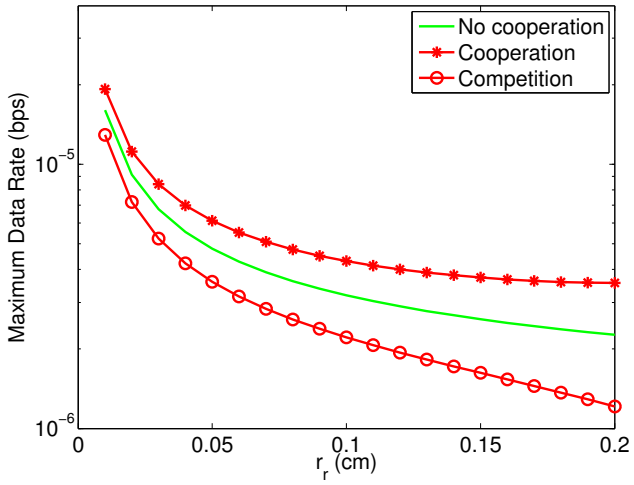


Figure 4.5: Maximum data rate of the channel

tion is farther from the competitive population, i.e., $r_{coop} > r_{comp}$. In this case, since the competitive population is closer to the messenger population, competitive behavior is dominant which reflects as a higher attenuation than the no social interaction case. Similarly, in the case where $\chi_Q = \chi_P$ and $r_{coop} < r_{comp}$, the cooperative behavior is dominant and the attenuation becomes lower.

Secondly, we consider the case where the distances of neighbor populations are the same, i.e., $r_{coop} = r_{comp}$, whereas the chemotactic sensitivity of the cooperative population is higher than the competitive one, i.e., $\chi_Q > \chi_P$. In this case, cooperative behavior is dominant since the messenger population is more sensitive to the cooperative behavior leading to a lower attenuation than the social interaction case. Similarly, in the case where $r_{coop} = r_{comp}$ and $\chi_Q < \chi_P$, the competitive behavior is dominant and the attenuation is higher than the no social interaction case.

## 4.6 Conclusion

The use of bacteria has been proposed for molecular communications due to their motility property as well as the fact that DNA plasmids with encoded information can be carried

by them. This MC technique is defined as bacterial nanonetworks. In this study, we first present the Keller-Segel model that describes the dynamics of the bacterial chemotaxis process. This is followed by expressing a traveling wave solution for the density of the propagating bacteria through chemotaxis, where the delay and attenuation of the bacterial nanonetwork channel are derived. Using this traveling wave modeling approach, the social behavior of bacteria, namely, cooperation, cheating and competition, is analyzed in terms of their effects on the delay and the attenuation of the channel. The numerical results show that the social behavior have a significant effect on the channel characteristics (the species we considered is *E. coli*). The cooperation between the bacteria improves the channel by lowering the delay and the attenuation. However, the benefits of cooperation are short-lived when the bacteria switch towards cheating behavior, and the performance worsens as the frequency of cheaters increases. Furthermore, the results show that the competition between the bacterial species deteriorates the channel by leading to higher delay and heavier attenuation. The objective of this study is to provide a model for the propagation of bacteria transferring information in the presence of other microorganism that may interact either positively or negatively depending on the environmental condition. By analyzing their interaction behavior, this will result in efficient design of bacterial nanonetworks that is realistically found in their natural environments.

# CHAPTER 5
# DISTRIBUTED MODULATION SCHEMES FOR BACTERIAL CHEMOTAXIS CHANNEL

## 5.1 Motivations and Related Work

In this chapter of the PhD thesis, we focus on biomedical applications of MC where biological components and systems are utilized to create artificial communication systems. This new paradigm for developing communication networks could pave the way for new forms of healthcare monitoring solutions, where artificial communication systems are developed from biological components and are integrated with the human body [76, 77, 78, 5]. This could lead to an in-body network system that provides fine granular sensing and early detection of diseases.

Numerous models for molecular communication have been proposed, including diffusion based systems where molecules that represent information are diffused into the environment [19], as well as FRET [16], and calcium signaling [79]. Besides these models, another approach is utilizing organisms as information carrier, and specifically bacteria. Bacteria have a number of properties that have been used to create molecular communication. In [12], the quorum sensing process was utilized to transfer information. In quorum sensing, the bacteria coordinate and signal each other by producing the molecules known as AHL (acyl homoserine lactone) according to their local population density. A bacteria population will produce AHL molecules that diffuse and travel through the microfluidic channels to a receiver which is another population of bacteria. Through the quorum sensing process, the receiver can sense the density of the population transmitting the signal.

In [80], programmed bacteria that emit attractants and repellants are used to localize and track targets. Through their cooperative communication process, the bacteria can search the

environment in a timely and efficient manner. This form of searching process can provide new solutions towards localization of diseased cells that are malignant. Another technique that has been proposed is utilizing the motility properties of bacteria and their ability to hold plasmids, which can potentially be used to encode and store information [55]. The motility is usually achieved through the flagella that extend from the bacteria body, enabling the bacteria to swim in a fluidic medium. Based on these properties, the bacteria nanonetwork is established by having the bacteria pick up plasmid with encoded information from a transmitter nanomachine, and swimming towards a receiver to unload the plasmid [81]. However, an issue with this form of information delivery is the process required to encode the information into the plasmids, and engineering the receiver to decode this information by first removing the plasmid from the bacteria, and searching through the DNA to find the genes that hold the encoded information. It requires a mechanism that can read the DNA which is not an easy task. A simpler approach is to use bioluminescence to decode the information by modulating the quantity of bacteria rather than the genes carried by the bacteria. The intensity of the bioluminescence indicates the modulation of the bacteria. Furthermore, information transfer in bacterial nanonetworks create long delays. To mitigate these delays we create parallel transmission mechanisms by introducing distributed receivers which are spatially separated. Using engineering plasmids, information carrying bioluminescence genes are distributed among bacteria groups to create **plasmid diversity**. We use multiple transmitter-receiver pairs, each bound to a different combination of the distributed genes, which are distinguished by the spatial separation, i.e., the receiver of each pair illuminate at a different location which leads us to create distinguishable parallel paths. Hence, the information transfer rate can be improved by sending information simultaneously from these parallel paths, i.e., distributed receivers.

The proposed modulation technique is achieved through different combinations of genes carried by the bacteria that can lead to bioluminescence. In this study, we focus on four different combinations of the genes on the plasmids, leading to $M$ distributed receivers.

According to the information that are to be transmitted the corresponding bacteria will be released from the transmitter. Bacteria will swim towards one of $M$ receivers to bind and conjugate with the non-motile bacteria that are stationary. Upon successful binding, the genes that are transferred and combined in the receiver bacteria will enable bioluminescence. We refer to this form of modulation as *Distributed modulation for bacterial nanonetworks* (For the rest of the article we will only refer to *Distributed modulation*).

In this study, we first simulated the bacteria propagation behavior in 3D to determine the probability distribution for the first passage time of bacteria which is modeled as an Inverse Gaussian Function. Then, we introduce *Binary Density Modulation*, *M-ary Density Modulation*, and *Distributed Modulation* schemes. We compare these schemes by evaluating the performance metrics such as the bit error probability as well as the achievable rate, where we vary the distances between the transmitter and receivers, as well as the average transmit power which corresponds to the quantity of bacteria released from the transmitter. The results from our analysis show that the Distributed Modulation scheme outperforms the other two schemes due to the minimization of ISI that can result from bacteria emitted during previous time slots. This in turn leads to higher achievable rates. The results also found that the achievable rate changes with the time slot length, since distinct bacteria for different symbols can be concurrently emitted from the transmitter, leading to smaller time slots required for each symbol transmission.

The contributions of this chapter can be listed as

- We determined of the first hitting time parameters of Brownian Motion by simulations conducted with BSim based on the physical parameters of system.
- We introduced the plasmid diversity and distributed receivers concepts to create diversity in bacterial nanonetworks.
- We proposed three modulation schemes and derived the corresponding probability of errors and achievable rates where distributed modulation outperforms the others and

stands out as a reliable candidate for modulation.

This chapter is organized as follows: Section 5.3 introduces the system model for bacterial nanonetworks by presenting the background information on the genes programmed into the plasmid leading to bioluminescence. In Section 5.2, an extensive literature review is given. In Section 5.3.2 the propagation model of the bacteria is presented. In Section 5.3.3 the bioluminescence occurring upon the reception of bacteria at the receiver is described. Section 5.4 presents the detailed model of the modulation schemes, while Section 5.5 presents the performance evaluation comparison between the three different schemes. Lastly, Section 5.6 concludes the chapter.

## 5.2 Related Work

Bacterial nanonetworks are studied in the literature from many different perspectives. In [25], the fundamentals of bacterial networks are discussed. The encoding and decoding of information on bacterial plasmid by conjugation are defined in communications engineering perspective. Furthermore, the motion of bacteria carrying plasmid messages inside various environments is defined as the propagation of the information. In [24], a simulation model is developed to study the channel capacity in bacterial nanonetworks. In both of these studies, bacteria is considered to move following run-and-tumble cycles as in our work, however, the motion is not analytically modeled. [25] only simulates the propagation channel but does not calculate any other communication metric whereas [24] does not consider the loss due to random motion of bacteria but incorporates it as a term in delay.

Another perspective to bacterial nanonetworks is presented in [82] where a simulation is performed to characterize the dynamics of bacterial nanonetworks. The BNSim is tool developed which takes into account chemotactic movement of bacteria, genetic circuits and intercellular interactions among bacteria for drug delivery applications. In [78], a mathematical model for capturing the dynamics of bacteria populations are derived for biological applications. In [77], a statistical physics model is proposed to study the dynamics of dense

networks of bacteria coupled with intercellular communication of bacteria. These studies focus mostly on swarming of the bacteria and how the bacteria population is distributed into the environment and whether they accumulate on the target.

Furthermore, in [83] a non-equilibrium statistical physics inspired model is proposed to study biological communication defined in many levels such as inside cell, intercellular, and interkingdom levels. [83] proposes new metrics for information theory where there is no definition of individual transmitter or receiver but each cell performs both functions. The mutual information is here defined between the concentration of an intracellular entity such as quorum sensing molecules and the physical behavior of bacteria such as bioluminescence.

Another perspective considered in [84], presents the information spreading with opportunistic communications in bacterial nanonetoworks using an epidemic approach similar to Delay Tolerant Networks and model analytically the number of bacteria receiving the plasmid carrying the information in a complex bacterial nanonetwork.

Despite all the previous efforts in the literature, there are still many problems in determining how to use the bacteria and their swarming capabilities in order to create efficient biological communication networks. Prior body of work concentrates on modelling and simulating the organization of bacterial populations and their motion with respect to environmental cues.

Our approach in this study combines different elements from state-of-the-art to move one step closer to realizing bacterial nanonetworks. Our work analyzes the performance of communication systems that can be build on top of these elements in terms of the achievable rate. Furthermore, we devise the novel concept of plasmid diversity and distributed receivers which improves the information transfer rate.

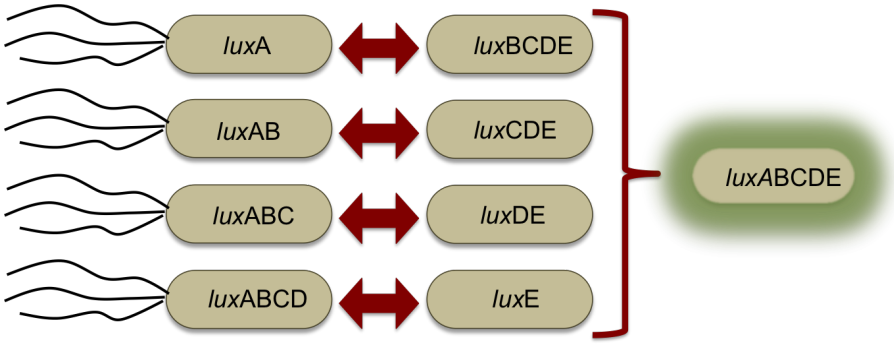


Figure 5.1: Illustration of genes *luxA*, *luxB*, *luxC*, *luxD*, and *luxE* distributed between the bacteria. The collection of all five genes will lead to bioluminescence.

## 5.3 System Model

Although previous works have proposed various modulation schemes for molecular communications, the majority of these works were focused on diffusion based systems [85], [86], [87]. The objective of our proposed approach is to develop a modulation scheme improving the data rate using bacterial properties. We utilize in total three different properties, namely, engineering plasmids, motility, as well as the conjugation process.

**Engineering plasmids**: Besides the chromosome, bacteria also have a circular DNA molecule that is known as plasmid. In Synthetic Biology, plasmids are usually engineered with different combination of genes that provides the bacteria new traits. One of these traits is engineering bioluminescence in the bacteria to emit visible light. We assume that the transmitter and receiver bacteria acquired a combination of *lux* genes by the engineering of plasmids before being deployed in the environment. Currently, it is very common and easy to modify the genetic material of bacteria using techniques like CRISPR [88]. Furthermore, the genes that we chose for this study, namely, *lux* genes which encodes bioluminescence proteins are very thoroughly studied in the literature and it is well-known how to create plasmids comprising of *lux* genes [89] since bioluminescence is frequently used as a reporting mechanism of the genomic level events [90].Bacterial cells produce light if they have all of the following five genes, namely, *luxA*, *luxB*, *luxC*, *luxD*, and *luxE*

[91]. In the event that any of these five genes are missing, no light will be produced. However, the bacteria may be able to pick any of these genes from plasmids of other organism in order to have the full collection that will lead to light emission. This is illustrated in Figure 5.1. Bioluminescence is very common in marine bacteria such as *Vibrio fishieri*, but the gene sequence responsible for luminescence can easily be transferred to other bacteria such as *E. coli* which is the bacteria considered in this study.

**Motility**: Bacteria are able to mobilize by utilizing flagella, which are hair like structures that extend from the body. In order to achieve motility, the flagella will form a single body that will act as a propeller to enable the bacteria to mobilize between different locations [92].

**Conjugation**: Bacteria are able to transfer and pass plasmids between each other. This process is known as conjugation. During conjugation, the bacteria will come together and form a physical connection through the **pilus** that allows copies of plasmids to be transferred [93]. Bacterial conjugation is a natural DNA transfer mechanism for bacteria [94, 95] which creates significantly dynamic genomes where lots of genes can be deleted or inserted easily. When two bacteria come close to each other they make a physical connection by joining their pili. Then, the plasmid of the donor bacteria gets nicked and a single strand DNA is transferred to the recipient cell. Both cells synthesize complementary DNA strands and both plasmids become circular again. Conjugation may happen between both the same species of bacteria or different species however the plasmid transfer rate is higher between similar strains. The plasmid transfer rate changes between $10^{-6}$ to $10^{-3}$ [96, 97].

These three different properties allow us to create molecular communication links for bacterial nanonetworks, which are illustrated in Figure 5.2. The information is coded through the genes *luxA*, *luxB*, *luxC*, *luxD*, and *luxE* that are inserted into the plasmid of the motile bacteria contained in the transmitter. The receiver consists of non-motile bacteria (i.e, the flagella have been removed) which is located at a distance $d$ apart. We considered that all pairs are parallel to each other as shown in Figure 5.2, so that no pair has advantage

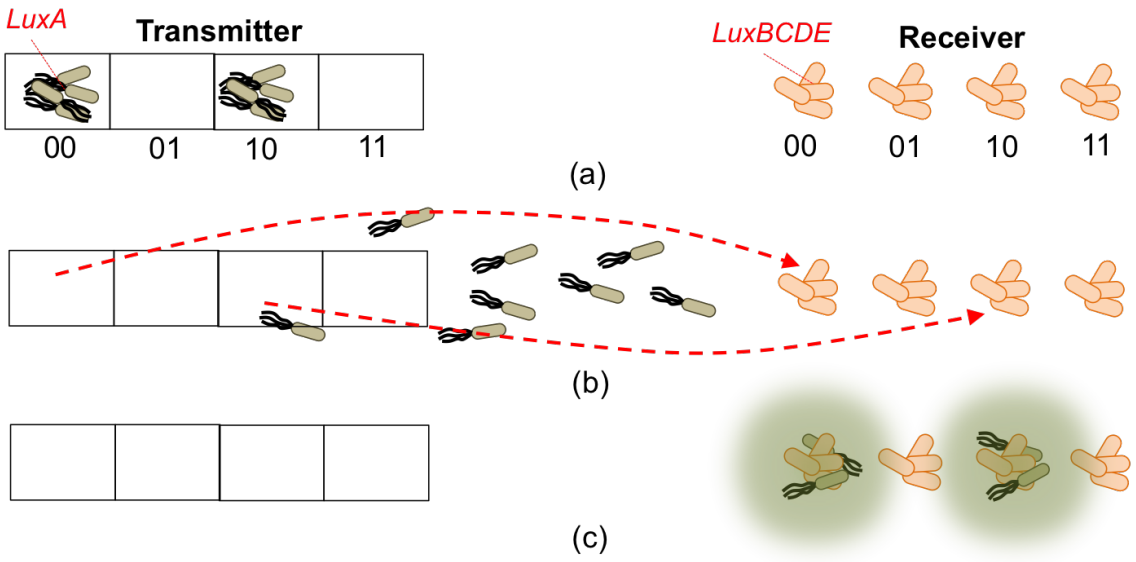


Figure 5.2: Illustration of modulation using bacterial nanonetworks with distributed receivers. The transmitter contains motile bacteria, while the receiver contains non-motile population. In this example, the digital bits "0010" is to be sent from the transmitter to the receiver. Each population of bacteria at the transmitter and receiver have combination of genes that will lead to bioluminescence (e.g. for digital bits "00", the transmitter bacteria contain *luxA*, while the receiver non-motile bacteria contain *luxBCDE*). (a) the motile bacteria are initially stored within the transmitter, (b) the bacteria are released from the transmitter, (c) the conjugation process at the receiver between the motile and non-motile bacteria.

over the others. However, in a more elaborate situation where the a priori probabilities of each symbol are known, the transmitter-receiver distance of the pair transferring the most probable symbol may be smaller to increase the rate.

We assume that the time is slotted and the transmitter releases $N_0$ genetically encoded bacteria at the beginning of each time slot which lasts $T_s$ sec. Furthermore, we assume that the transmitters and receivers are perfectly synchronized. The synchronization may be established using quorum sensing which activates certain intracellular mechanisms only when the bacteria population reaches a threshold [98], or using the extracellular noise common to all cells which induces collective dynamics [99], or a blind synchronization algorithm which implements the non-decision directed Maximum Likelihood (ML) criterion for the

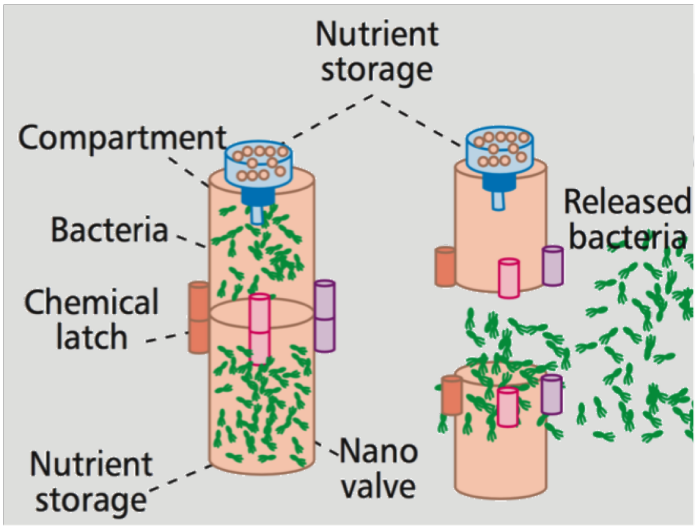


Figure 5.3: The transmitter model [**expl**]

estimation of channel delay [100].

### 5.3.1 Transmission Model

The transmitter contains compartments storing the bacteria with different gene combinations representing two digital bits, as illustrated in Figure 5.2. The transmitter can be modeled as a container with chemical latches opening and closing to release bacteria as shown in Figure 5.3. The opening and closing process of the latch can be stimulated chemically. In order to have a reusable transmitter, a nutrient harvesting process can be mounted into the nutrient storage [56]. In Figure 5.2, the bits ”00” consist of the transmitter motile bacteria plasmids having *luxA*, while the non-motile bacteria are the receiver having *luxBCDE* genes in their plasmid. Therefore, the combination of genes for each pair of bits between the transmitter and receiver is unique. At the beginning of each time slot, the transmitter releases these bacteria into the medium where they propagate randomly.

Since the bacteria follow a Brownian motion, bacteria will be dispersed in the environment and only a portion of the released bacteria will be able to reach the receiver. In the following section we will introduce a propagation model for the motile transmitter bacteria.

### 5.3.2 Propagation Model

Bacteria can follow either a random or directed motion. When there is no specific source of attraction, bacteria move in the environment randomly following a Brownian motion model. When there is a source of attraction such as nutrition, light or magnetic field, bacteria move towards it following a chemotactic movement model [101]. In this study, we assume that there is no specific source of attraction in the environment.

The Brownian motion of bacteria is governed by a sequence of run-and-tumble process. This means that they run straight at constant speed $v$ for a random time duration $t_r$, then tumbles without changing position for $t_t$, and choose a new direction with a random angle $\theta$, and this is followed by the run phase. Repeating this sequence, the bacteria move randomly in the environment. To characterize this movement, we ran 3D simulations in a confined environment to obtain the properties of the first passage time of bacteria released from the transmitter reaching the receiver. In particular, we performed 3D discrete time simulation of bacteria using run-and-tumble model for $\Delta t$ time intervals.

The simulation is conducted using *BSim*[102] simulator, an agent-based computational tool to model the dynamics of bacterial population moving in a 3D environment. For the simulation, a 3D container of $1\ mm^3$ size is considered, where the surfaces of the container are solid. As the size of the container is quite big considering the size of the bacteria and the velocity of the bacterial movement, the collisions and reflections between the bacteria and container walls can be ignored for our total simulation time. The receivers and transmitters are set at opposite sides from the center of the container at equal distances. Four transmitters and four corresponding receivers are placed for various distances. Both the transmitters and receivers are circular in shape with a very small radius. The bacteria are considered to successfully reach the target once it collides with that receiver. In order to determine the impact of successfully reaching the target, the radius of the receivers are varied for various runs. We assume that the population of bacteria moving inside the container will remain the same during the transmission period due to sufficient supply of nutrients [12]. A sample of

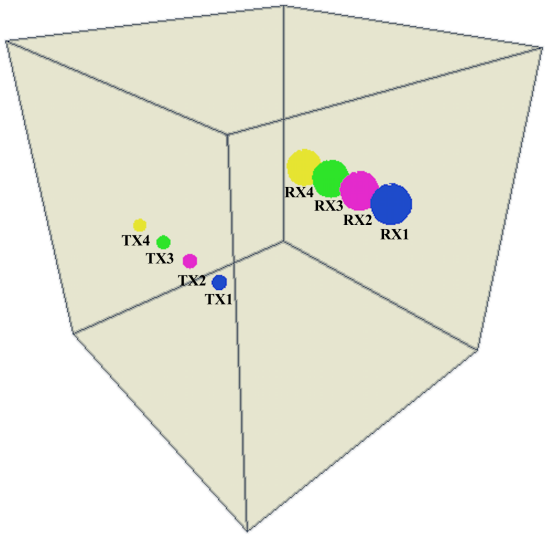


Figure 5.4: Initial state of simulation environment.

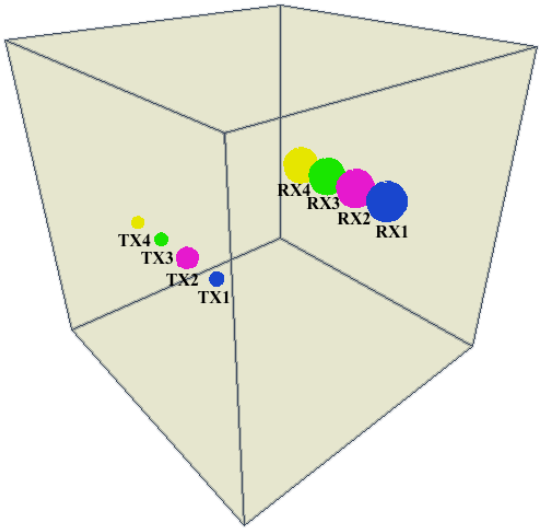


Figure 5.5: Bacteria are released from the sender (green coloured).

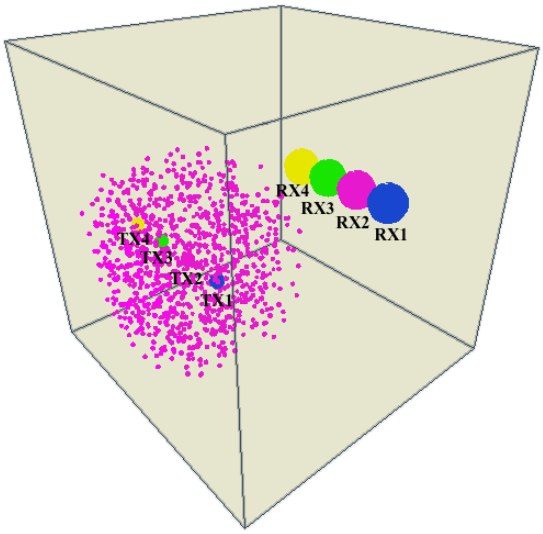


Figure 5.6: Bacteria are moving away from the sender.

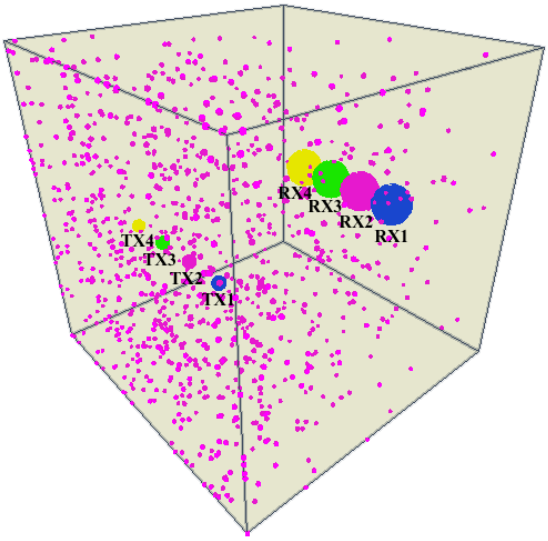


Figure 5.7: Some of the bacteria reached to different receivers.

Table 5.1: Simulation Parameters

| **Parameter Name** | **Value** |
|---|---|
| Temperature | 305 K |
| Viscosity | 2.7e-3 Pa s |
| Radius of the bacteria | 1 $\mu m$ |
| Flagella force | 1 pN |
| Mean time to end a run | 0.86 sec |
| Mean time of end a tumble | 0.14 sec |
| The maximum tumbling angle | 180 degree |
| Boltzman constant | 1.38e-23 |
| Number of Bacteria | 10000 |
| Max. Bacteria lifetime | 6 hours |
| Distances | 500, 1000, 1500 $\mu m$ |
| Receiver radius | 100, 200, 300 $\mu m$ |
| Simulation duration | 6 hours |
| Timestamp | 0.01 seconds |

the transmitter and receivers locations, their initial state, the bacteria release and movement, as well as their propagation towards the receivers are illustrated in Figure 5.4, 5.5, 5.6 and 5.7 respectively. For our simulation, we have considered three different distances between the transmitters and corresponding receivers and 3 different receiver volumes. There are two states of bacterial movement, which are running when the flagella are rotating counter clockwise and tumbling when the flagella are rotating clockwise. The tumbling angles are random values and follow a gamma distribution. The maximum tumbling angle is set as 180 degree. Other parameters for the simulation is listed into Table 5.1.

Since it is known that the first passage time of the random walk is represented by an inverse probability distribution function [103], we compared our simulation results with an inverse Gaussian pdf. The distribution obtained from the simulation for the first passage time of a bacterium at the receiver is very similar to an inverse Gaussian distribution, as shown in Figure 5.8, which is expressed as

$$f(t) = \left[\frac{\lambda}{2\pi t^3}\right]^{1/2} \exp\left(-\frac{\lambda(t-\nu)^2}{2\mu^2 t}\right), \tag{5.1}$$

Table 5.2: Fitted Inverse Gaussian Parameters

| **Distance** ($\mu m$) | **RX Volume** ($\mu m^3$) | $\nu$ | $\lambda$ |
|---|---|---|---|
| 500 | 100 | 2993.37 | 1044.080 |
| 500 | 200 | 2971.459 | 1092.047 |
| 500 | 300 | 3033.642 | 1113.672 |
| 1000 | 100 | 5880.463 | 4594.112 |
| 1000 | 200 | 5726.056 | 4651.549 |
| 1000 | 300 | 5742.775 | 2532.088 |
| 1500 | 100 | 8083.802 | 11887.945 |
| 1500 | 200 | 8017.303 | 11568.980 |
| 1500 | 300 | 8126.618 | 11760.664 |

where the coefficients $\lambda$ and $\nu$ depend on the run-and-tumble parameters of the bacteria, the distance between transmitter and receiver, and the receiver volume.

By curve-fitting we compute $\lambda$ and $\nu$ from our simulation setup for a range of transmitter-receiver distance and receiver volume (Table 5.2). This characterization of the bacterial motion enables us to model the propagation of bacteria between different locations.

The probability of a bacterium arriving to the receiver in a time slot $T_s$ is [104]

$$q = \int_0^{T_s} f(t)dt. \tag{5.2}$$

If $N_0$ bacteria are released from the transmitter at the beginning of the time slot, we can compute the number of bacteria arriving to the receiver, $N_a$, with the following binomial distribution

$$N_a(N_0) \sim Binomial(N_0, q). \tag{5.3}$$

When the number of bacteria released from the transmitter, $N_0$ is large, this binomial distribution can be approximated by a Gaussian distribution $\mathcal{N}(\mu, \sigma^2)$ where the mean and variance are [85]

$$\mu = N_0 q, \quad \sigma^2 = N_0 q(1-q). \tag{5.4}$$

According to Figure 7, it is observed that the probability distribution function for the

first passage time has a long tail. Therefore, there will be bacteria arriving to the receiver after the intended time slot causing inter-symbol interference between each symbol sent in consecutive time slots. Hence, the total number of bacteria arriving in the current time slot, i.e., for the current symbol, is reformulated by adding the bacteria released in this time slot and the remaining bacteria released in the previous time slots causing the inter-symbol interference. If the time slot length is very large, the ISI effects will be lower but data rate will be slowed down too since there is more time between consecutive symbols. Hence, we choose the time slot length as short as possible after which the pdf of arrival of bacteria becomes flat. In other words, we choose the time slot length as the point where the pdf drops below 0.00005. In this study, for distances $d = 500, 1000, 1500\ \mu m$ with a receiver volume of $100\ \mu m^3$, the time slot lengths are chosen as $T_s = 1774, 4690, 7383\ seconds$, respectively.

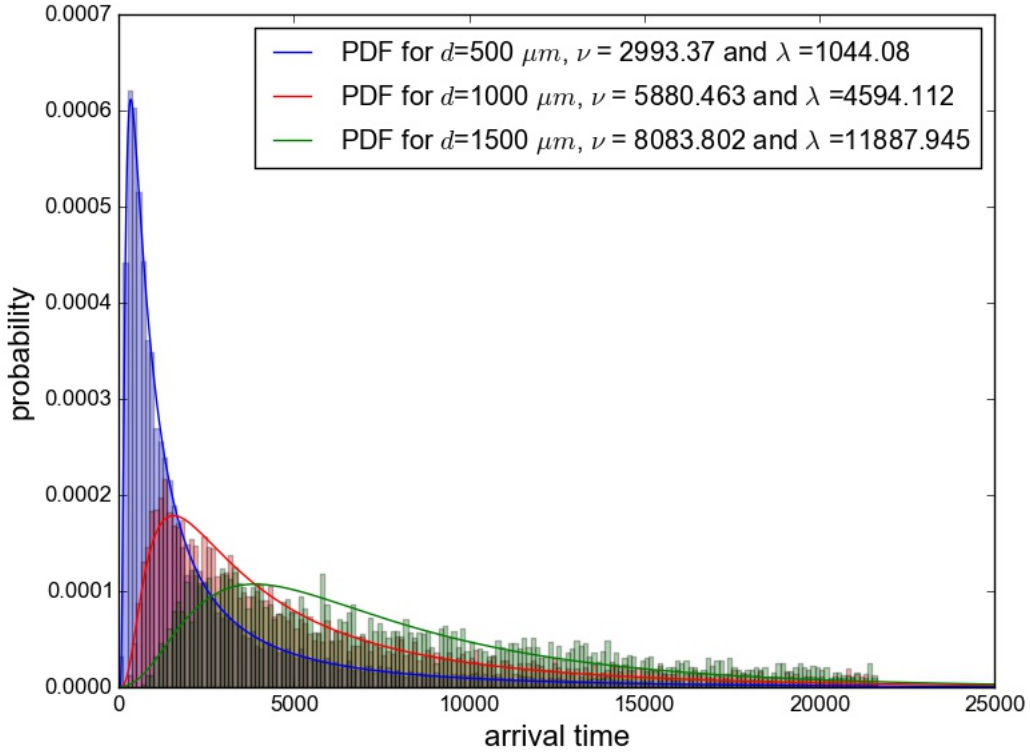


Figure 5.8: Probability Distribution Functions (PDF) of the arrival time of the bacteria for various distances (receiver volume = 100 $\mu m^3$).

When we calculate the probabilities that bacteria released in previous slots arrive in the current time slot, it is observed that the largest contribution comes from the immediate previous time slot. For example, for $d = 500\mu m$ and receiver volume of $100\mu m^3$, the probability that a bacteria arrives in the current time slot $q$ is $0.6$, whereas the probability from the immediate previous slot $q_p = 0.17$, and the probability for the third and forth slots are $0.07$ and $0.03$, respectively. Hence, we can assume that only the previous time slot contributes to the inter-symbol interference. This leads us to define the total number of bacteria arriving to the receiver as follows

$$N_T(s_c, s_p) = N_a(n_{s_c}) + N_p(n_{s_p}), \tag{5.5}$$

where $n_{s_c}$ is the number of bacteria released in the current time slot and $n_{s_p}$ is the number of bacteria released in the previous time slot, and the number of bacteria released in the previous slot but arriving in the current time slot is denoted as $N_p(n_{s_p})$. The $s_c$ represents the symbol sent in the current time slot and $s_p$ represents the symbol sent in the previous time slot.

$N_p(n_{s_p})$ can similarly be approximated by a Gaussian distribution $\mathcal{N}(\mu_p, \sigma_p^2)$ where the mean and the variance are

$$\mu_p = n_{s_p} q_p \qquad \sigma_p^2 = n_{s_p} q_p (1 - q_p), \tag{5.6}$$

where $q_p$ is probability of bacteria which was released in the previous time slot arriving in the current time slot. This probability $q_p$ is expressed as

$$q_p = \int_{T_s}^{2T_s} f(t)dt. \tag{5.7}$$

Since $N_a$ and $N_p$ are independent Gaussian random variables, the probability distribution of $N_T(s_c, s_p)$ becomes also Gaussian distributed $\mathcal{N}(\mu_T, \sigma_T^2)$ with mean and variance

$$\mu_T = \mu + \mu_p \qquad \sigma_T^2 = \sigma^2 + \sigma_p^2. \tag{5.8}$$

The $N_T$ bacteria who arrived to the receiver will conjugate and transfer their message to the receiver bacteria according to the reception model discussed in the next section.

### 5.3.3 Reception Model

When the motile bacteria from the transmitter reach the receiver, they conjugate with the non-motile bacteria in the receiver to transfer the plasmids, in order to create the full set of genes required for bioluminescence. The number of conjugated receiver bacteria $N_r$ increases with every incoming motile bacteria from the transmitter. Hence, the intensity of light due to bioluminescence increases with the number of incoming bacteria at the receiver. In this section, we denote the measured light intensity as $L(s_c, s_p)$ and we express it in terms of the total number of bacteria released from the transmitter arriving to the receiver $N_T(s_c, s_p)$.

Since the conjugation process takes a couple of minutes [93] which is very short compared to the propagation time in the order of hours [55], we can neglect the time required for conjugation.

In a bacteria population, conjugation does not take place between all the bacteria. Only a certain ratio of motile bacteria from the transmitter will conjugate with the bacteria at the receiver. We call the ratio of conjugated bacteria to the organisms released from the transmitter as transfer frequency and it is denoted by $\alpha_c$. Hence, the number of receiver bacteria which are conjugated with the transmitter bacteria is found as $N_r = \alpha_c N_T$. The $\alpha_c$ is a parameter that relates to the bacterial species as well as environmental genetic factors [105].

When the density of conjugated bacteria reaches a critical density, the receiver starts shining light significantly. This phenomenon is called quorum sensing where bacterial cells produce a small autoinducer molecule which diffuses in and out of the cell whose

concentration increases with the increasing bacterial cell density. The bioluminescence genes are controlled by this autoinducer molecule. When the autoinducer concentration increases above a threshold level, the bioluminescence genes become active and the light becomes observable.

The relation between the bacterial cell density and the autoinducer concentration is found by [69]

$$\frac{dA}{dt} = v_A N_r - d_A A, \tag{5.9}$$

where A is the autoinducer concentration, $v_A$ is autoinducer production rate and $d_A$ is the autoinducer degradation rate.

The autoinducer forms a complex with bacterial cell receptors with a probability of $\rho(t)$. The dynamics of this probability is described by [106]

$$\frac{d\rho}{dt} = -\kappa\rho + A\gamma(1-\rho), \tag{5.10}$$

where $\kappa$ is the dissociation rate and $\gamma$ is the complex formation rate, and $\rho$ represents the probability that autoinducer forms a complex with cell receptors.

When cell receptors are bound with the autoinducer, it activates the *lux* genes associated with bioluminescence. Although the detailed biochemistry of bioluminescence is unknown, the gene expression can be approximated by a two-step process for the production of the bioluminescent proteins and the light as

$$\begin{aligned} \frac{dS}{dt} &= (b_0\rho + a_0) - b_1 S \\ \frac{dL}{dt} &= a_1 S - b_2 L, \end{aligned} \tag{5.11}$$

where $L$ is the amount of light, $S$ is a post-transcriptional messenger, and $b_0, a_0, a_1, b_1, b_2$ are constants [106]. $a_0$ represents the basal production of bioluminescence proteins in the absence of autoinducer [91], $b_0$ represents the production rate of the post-transctriptional messenger in the presence of autoinducer, $a_1$ is the rate of light production, $b_1$ denotes the

decay rate of the post-transcriptional messenger and $b_2$ denotes the decay rate of light.

At the end of the time slot, the system will come to a steady-state where the autoinducer concentration is

$$A_s = \frac{v_A N_r}{d_A}. \tag{5.12}$$

Accordingly, the probability of forming a complex at steady-state is

$$\rho_s = \frac{A_s \gamma}{A_s \gamma + \kappa}. \tag{5.13}$$

Then, the light intensity at the steady-state is expressed as

$$L_s = \frac{a_1(b_0 \rho_s + a_0)}{b_1 b_2}. \tag{5.14}$$

In our study, the receiver is a population of bacteria whose members are noisy inherently. However, the effect of the discrepancies and uncertainties between each bacterium is less significant when the response of the population is studied instead of the response of each individual bacterium. Hence, we assume that the noise in the reception process is negligible compared to the noise resulting from the propagation process which is the main source of noise in this study.

In Section 5.3.2, we have found that the number of bacteria arriving to the receiver $N_T$ has a Gaussian distribution with mean $\mu_T$ and variance $\sigma_T^2$. Thus, the number of conjugated bacteria $N_r$ can be easily described also by a Gaussian distribution with mean $\alpha_c \mu_T$ and variance ${\alpha_c}^2 \sigma_T^2$.

Since the steady-state autoinducer concentration $A$ is a linear function of the number of conjugated bacteria $N_r$, the probability of the autoinducer concentration also follows a Gaussian distribution with mean $\mu_A = (v_A/d_A)\alpha_c \mu_T$ and mean $\sigma_A^2 = (v_A/d_A){\alpha_c}^2 \sigma_T^2$.

According to (5.13), the probability distribution of $\rho$ is changing nonlinearly with au-

toinducer concentration $A_s$. Hence, the pdf of $\rho$ can be described as follows

$$f_{\rho_s} = \frac{f_{A_s}\left(\frac{\rho_s \kappa}{\gamma(1-\rho_s)}\right)}{\gamma(1-\rho_s)^2/\kappa}, \tag{5.15}$$

where $f_{A_s}$ is the Gaussian probability distribution of $A_s$.

Similarly, the probability distribution for the light can be found by

$$f_{L_s} = \frac{f_{\rho_s}\left(L_s b_1 b_2/(a_1 b_0)\right)}{a_1 b_0/(b_1 b_2)}. \tag{5.16}$$

## 5.4 Modulation Schemes

In Section 5.3, we described the bacterial propagation model as well as the reception model that will indicate a successful transfer of plasmids at the receiver. We investigated the propagation of bacteria from transmitter to the receiver and the reception by bacteria located in the receiver. Based on our simulation, as well as previous works, we have found that the propagation of bacteria suffers very long delays, which in turn will affect the end-to-end data rate of the communication system. In order to increase the rate of the information transfer, we suggest two modulation schemes exploiting the engineering plasmid property that allows us to program different combination of genes.

### 5.4.1 Modulation with a Single Receiver

In this modulation scheme, a single transmitter and receiver pair is considered.

*Binary Density Modulation*

When the information to be transmitted for the time slot is the symbol $0$, no bacterium is sent from the transmitter. Since there is no transmitter bacterium arriving to the receiver, no bioluminescence is observed. However, when the information is the symbol $1$, $N_0$ bacteria is released from the transmitter at the beginning of the time slot and when they deliver

the message to the receiver bacteria by conjugation, the receiver bacteria produce visible light. To detect the information sent, the light intensity is compared to a threshold above which symbol $1$ is decoded and below which symbol $0$ is decoded. This modulation scheme resembles to an *ON-OFF* Keying modulation for conventional communication system.

We assume that the symbols for binary density modulation $s_i$ can be either $0$ or $1$. Also, we assume that all symbols are equiprobable and independent of each other. For binary density modulation, the total probability of error can be calculated by

$$P_e = \sum_{s_c=0}^{1} P(s_c)P(\hat{s}_c \neq s_c|s_c) \tag{5.17}$$

where $P(s_c)$ is the a priori probability of transmitting symbol $s_c$ and $P(\hat{s}_c \neq s_c|s_c)$ denotes the probability of incorrect decoding given the current symbol, where $\hat{s}_c$ is the current received symbol.

Since there are ISI effects, it is necessary to take into account the interference of the previous symbol on the current symbol. Thus, the incorrect decoding probabilities are expressed in terms of previous symbol as follows

$$P(\hat{s}_c \neq s_c|s_c) = \sum_{s_p=0}^{1} P(s_p)P(\hat{s}_c \neq s_c|s_c, s_p), \tag{5.18}$$

since the transmitted symbols are independent and the incorrect decoding probability $P(\hat{s}_c \neq s_c|s_c, s_p)$ depends on the current and previous symbols.

If we set the threshold for light intensity to $\tau_L$, the incorrect decoding probabilities become

$$P(\hat{s}_c = 1|s_c = 0, s_p) = P(L_s(s_c, s_p) > \tau_L|s_c = 0, s_p) \tag{5.19}$$

$$P(\hat{s}_c = 0|s_c = 1, s_p) = P(L_s(s_c, s_p) < \tau_L|s_c = 1, s_p) \tag{5.20}$$

The light intensity $L_s(s_c, s_p)$ is found by replacing the number of released bacteria for

the current and previous symbols $n_{s_c}$ and $n_{s_p}$ for $N_T(s_c, s_p)$ in (5.5) with

$$n_{s_i} = \begin{cases} N_0, & \text{if } s_i = 1 \\ 0, & \text{if } s_i = 0 \end{cases} \tag{5.21}$$

The threshold depends on the camera system used to measure the light and might change with the experimental setup, i.e., the sensitivity of the camera, ambient light, growth conditions of the bacteria and the bacteria species.

Since all the symbols are equally likely the error probability can be calculated by

$$P_e = \frac{1}{4}\left(\sum_{s_p=0}^{1} F_{L_s(1,s_p)}(\tau_L) + \sum_{s_p=0}^{1}\left(1 - F_{L_s(0,s_p)}(\tau_L)\right)\right). \tag{5.22}$$

where $F_{L_s(s_c,s_p)}$ is the cumulative density function of the pdf of $L_s(s_c, s_p)$ derived in (5.16).

*M-ary Density Modulation*

In *M-ary* density modulation, instead of using two symbols, we can introduce $M$ symbols, i.e., $M$ levels of bacterial density representing $log_2(M)$ bits. By thresholding the bioluminescence intensity at the receiver with $M - 1$ thresholds, one of these $M$ levels can be decoded. This modulation scheme resembles to an *Amplitude Shift Keying* (*ASK*) modulation from conventional communication system.

We consider the case $M = 4$ representing 2 bits of information where transmitted symbols are $\{0, 1, 2, 3\}$ corresponding to $\{0, N_0/3, 2N_0/3, N_0\}$ released bacteria at the transmitter, respectively. For the rest of the text, M-ary density modulation refers to the modulation with $M = 4$. We further assume that all symbols are equally likely and independent from each other.

For M-ary density modulation, the total probability of error can be calculated by

$$P_e = \sum_{s_c=0}^{3} P(s_c) P(\hat{s}_c \neq s_c | s_c) \tag{5.23}$$

where $P(s_c)$ is the a priori probability of transmitting symbol $s_c$ and $P(\hat{s}_c \neq s_c|s_c)$ denotes

the incorrect decoding probability given $s_c$, where $\hat{s}_c$ is the current received symbol.

To take into account the effect of ISI, we further elaborate (5.23) by conditioning it with the previous symbol $s_p$. We express the incorrect decoding probabilities given $s_c$ when $s_p \in \{0, 1, 2, 3\}$ as

$$P(\hat{s}_c \neq s_c | s_c) = \sum_{s_p=0}^{3} P(s_p) P(\hat{s}_c \neq s_c | s_c, s_p), \tag{5.24}$$

since the current and previous symbols are independent of each other.

To detect the 4 transmitted levels, 3 thresholds are needed. If we set the thresholds for light intensity to $\tau_{L_0}, \tau_{L_1}, \tau_{L_2}$, where $\tau_{L_i}$ differentiates between $\hat{s}_c = i$ and $\hat{s}_c = i + 1$, the incorrect decoding probabilities become

$$P(\hat{s}_c \neq s_c | s_c = 0, s_p) = P(L_s(s_c, s_p) > \tau_{L_0} | s_c = 0, s_p) \tag{5.25}$$

$$P(\hat{s}_c \neq s_c | s_c = 1, s_p) = P(L_s(s_c, s_p) < \tau_{L_0} \text{ or } L_s(s_c, s_p) > \tau_{L_1} | s_c = 1, s_p) \tag{5.26}$$

$$P(\hat{s}_c \neq s_c | s_c = 2, s_p) = P(L_s(s_c, s_p) < \tau_{L_1} \text{ or } L_s(s_c, s_p) > \tau_{L_2} | s_c = 2, s_p) \tag{5.27}$$

$$P(\hat{s}_c \neq s_c | s_c = 3, s_p) = P(L_s(s_c, s_p) < \tau_{L_2} | s_c = 3, s_p) \tag{5.28}$$

The light intensity $L_s(s_c, s_p)$ is found by replacing the number of bacteria released for

current and previous symbols $n_{s_c}$ and $n_{s_p}$ in $N_T(s_c, s_p)$ in (5.5) with

$$n_{s_i} = \begin{cases} N_0, & \text{if } s_i = 3 \\ 2N_0/3, & \text{if } s_i = 2 \\ N_0/3, & \text{if } s_i = 1 \\ 0, & \text{if } s_i = 0 \end{cases} \tag{5.29}$$

The incorrect decoding probabilities given in (5.25), (5.26), (5.27), (5.28) can be found by using the pdf of $L_s$ given in (5.16).

If all the symbols are equally likely, the probability of error can be expressed as

$$\begin{aligned} P_e = & \frac{1}{16} \Bigg( \sum_{s_p=0}^{3} (1 - F_{L_s(0,s_p)}(\tau_{L_0})) \\ & + \sum_{s_p=0}^{3} (F_{L_s(1,s_p)}(\tau_{L_1}) + 1 - F_{L_s(1,s_p)}(\tau_{L_0})) \\ & + \sum_{s_p=0}^{3} (F_{L_s(2,s_p)}(\tau_{L_2}) + 1 - F_{L_s(2,s_p)}(\tau_{L_1})) \\ & + \sum_{s_p=0}^{3} F_{L_s(3,s_p)}(\tau_{L_2}) \Bigg) \end{aligned}, \tag{5.30}$$

where $F_{L_s(s_c,s_p)}$ is the cumulative density function of the pdf of $L_s(s_c, s_p)$ derived in (5.16).

### 5.4.2 Modulation with Multiple Receivers

In this section, we introduce a novel modulation scheme called distributed modulation using bacterial nanonetworks where multiple transmitter and receiver pairs are used. Since the detection of the light is realized by a camera, the light intensity at different location in an image can be measured. Hence if we place $M$ receivers in the environment spatially separated from each other, we can create a new modulation scheme where the transmitter between each pair no longer represents one bit but $log_2(M)$ bits as shown in Figure 5.2. In this study, we consider that $M = 4$, i.e., but the analysis can easily be extended to include

more receivers. When an information $00$ is to be sent, the associated transmitter releases bacteria which propagate in the environment reaching the complementary receiver.

Each transmitter-receiver pair is associated with one of the following symbols $\{0, 1, 2, 3\}$ and only one transmitter-receiver pair is active at each time slot. Since we assume that the a priori probabilities of symbols are not known, we place the pairs such that transmitter-receiver distance is the same for all pairs. If it is known that a symbol has a higher probability, then the transmitter and the receiver of the corresponding pair can be positioned closer to increase the rate. Since we have 4 different transmitters and receivers, there are 4 light intensities to measure corresponding to each receiver which we denote as $L_{s,i}$ for $i^{th}$ receiver. Each receiver is assumed to have the same threshold $\tau_L$. If the light intensity of a receiver is above $\tau_L$, the corresponding symbol will be received. We assume that all symbol are equally likely and independent of each other.

The total probability of error for this modulation scheme can be calculated by

$$P_e = \sum_{s_c=0}^{3} P(s_c) P(\hat{s}_c \neq s_c | s_c) \tag{5.31}$$

where $P_{s_c}(s_c)$ is the a priori probability of transmitting symbol $s_c$ and $P(\hat{s}_c \neq s_c | s_c)$ denotes the incorrect decoding probability given $s_c$, where $\hat{s}_c$ is the current received symbol. Since all 4 transmitter-receiver pairs are parallel $P(\hat{s}_c \neq s_c | s_c)$ is the same for all symbols, i.e, for all tx-rx pairs. Hence, (5.31) becomes

$$P_e = P(\hat{s}_c \neq s_c | s_c). \tag{5.32}$$

To incorporate the effects of ISI, we condition the incorrect decoding probability with

the previous symbol $s_p$ and express it as

$$\begin{aligned} P(\hat{s}_c \neq s_c|s_c) = \\ = \sum_{s_p \neq s_c} P(s_p) P(\hat{s}_c \neq s_c|s_c, s_p, s_p \neq s_c) \\ + P(s_p = s_c|s_c) P(\hat{s}_c \neq s_c|s_c, s_p, s_p = s_c), \end{aligned} \tag{5.33}$$

where the first term corresponds to the case where the previous symbol is not equal to the current symbol, i.e., the previous symbol was sent from a different transmitter. One source of error in this case is that remaining bacteria from the previous symbol activating the receivers for the other symbols than the current one. The other source of error is that there is not enough bacteria released from the transmitter of the current symbol to activate the corresponding receiver. The second term of (5.33) represents the case where the previous symbol is equal to the current symbol. In this case, the number of bacteria from the previous symbol is added to the number of bacteria for the current symbol. The only source of error is that there is not enough bacteria to activate the intended receiver. There is no possibility that the other receivers will be activated since there is no remaining bacteria from the previous slot for them.

If we set the thresholds for the light intensity to $\tau_L$ for each pair, the incorrect decoding probabilities are expressed as

$$\begin{aligned} P(\hat{s}_c \neq s_c|s_c, s_p, s_p \neq s_c) = \\ = P(L_{s,s_p}^{(s_p \neq s_c)} > \tau_L|s_c, s_p, s_p \neq s_c) \\ + P(L_{s,s_c}^{(s_p \neq s_c)} < \tau_L \ \& \ L_{s,s_p}^{(s_p \neq s_c)} < \tau_L|s_c, s_p, s_p \neq s_c), \end{aligned} \tag{5.34}$$

$$\begin{aligned} P(\hat{s}_c \neq s_c|s_c, s_p, s_p = s_c) = \\ = P(L_{s,s_c}{}^{(s_p = s_c)} < \tau_L|s_c, s_p, s_c = s_p). \end{aligned} \tag{5.35}$$

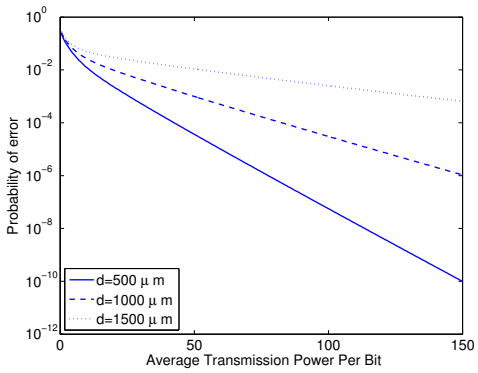


(a)

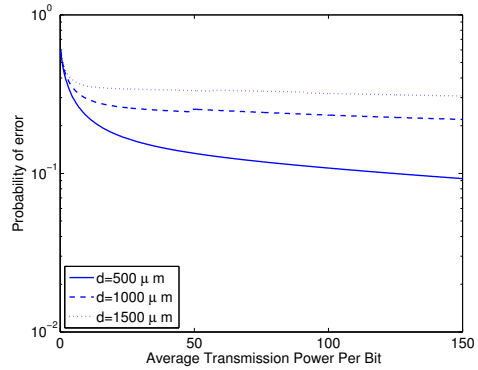


(b)

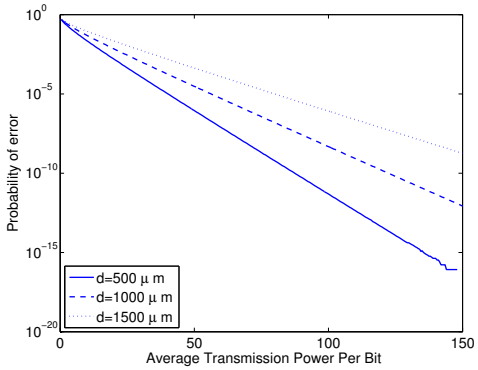


(c)

Figure 5.9: Probability of error for different modulation schemes for varying distances (a) Binary Density Modulation. (b) M-ary Density Modulation. (c) Modulation with Distributed Receivers.

$L_{s,s_c}^{(s_c,s_p)}$ is found by replacing $n_{s_c}$ and $n_{s_p}$ in $N_T(s_c, s_p)$ in (5.5) with $n_{s_c} = N_0$ and with

$$n_{s_p} = \begin{cases} N_0, & \text{if } s_c = s_p \\ 0, & \text{if } s_c \neq s_p \end{cases} \tag{5.36}$$

$L_{s,s_p}^{(s_c,s_p)}$ is found by replacing $n_{s_c}$ and $n_{s_p}$ in $N_T(s_c, s_p)$ in (5.5) with $n_{s_c} = 0$ and with

$$n_{s_p} = \begin{cases} 0, & \text{if } s_c = s_p \\ N_0, & \text{if } s_c \neq s_p \end{cases} \tag{5.37}$$

The incorrect decoding probabilities (5.34, 5.35) can be found by using the probability distribution of $L_s$ given in (5.16).

If all the symbols are equally likely, the probability of error can be expressed as

$$\begin{aligned} P_e = \frac{3}{4}\left(1 - F_{L_{s,s_p}^{(s_c\neq s_p)}}(\tau_L) + F_{L_{s,s_c}^{(s_c\neq s_p)}}(\tau_L) F_{L_{s,s_p}^{(s_c\neq s_p)}}(\tau_L)\right) \\ + \frac{1}{4} F_{L_{s,s_c}^{(s_c=s_p)}}(\tau_L); \end{aligned} \tag{5.38}$$

where $F_{L_{s,i}(s_c,s_p)}$ is the cumulative density function of the pdf of $L_s(s_c, s_p)$ derived in (5.16).

### 5.4.3 Achievable Rate

We define the achievable rate $R$ that maximizes the mutual information between the transmitted symbol and the received symbol as follows

$$\begin{aligned} R = & \\ & = \max_{\tau_L} \; I(X;Y) \\ & = \max_{\tau_L} \sum_X \sum_Y P(X,Y) log_2 \left(\frac{P(X,Y)}{P(X)P(Y)}\right). \end{aligned} \tag{5.39}$$

## 5.5 Performance Evaluation

In this section, to compare the performance of the three different modulation schemes we evaluate the probability of bit error and achievable rates against the average transmission power per bit for each type of the modulation that we proposed in Section 5.4. In this study, the transmission power is defined as the number of bacteria released from the transmitter.

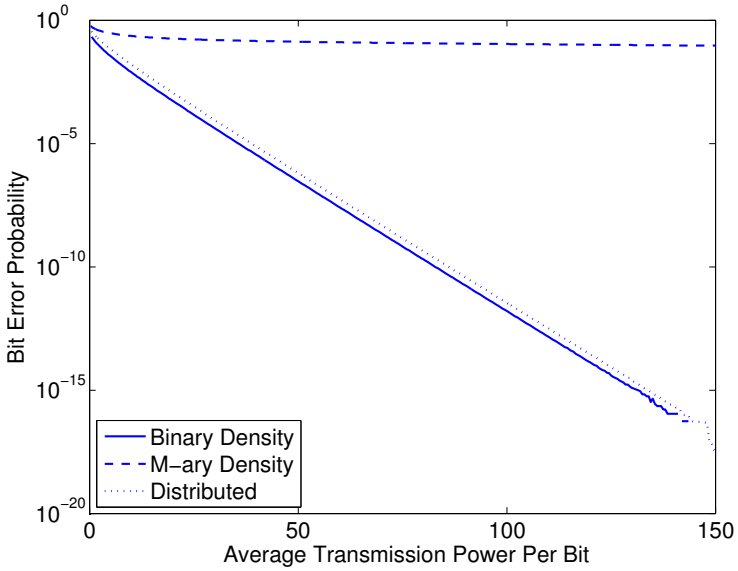


Figure 5.10: Bit Error Probability comparison between Binary Density, M-ary Density, and Distributed Modulation schemes.

For fair comparison between modulation schemes, the average transmission power per bit, i.e, average number of bacteria released per bit is used. Firstly, we use the simulations from Section 5.3.2 to observe the arrival times of bacteria for varying transmitter-receiver distances. The inverse Gaussian model that we fitted to the simulation for the arrival time shows that the arrival probability does not change significantly after a certain time due to its long flat tail. Hence, we chose $d = 500, 1000, 1500\ \mu m$ with a receiver volume of $100\ \mu m^2$, the time slot lengths are chosen as $T_s = 2557, 6159, 9095\ seconds$, respectively as discussed in Section 5.3.2.

Using these $T_s$ values, the probability of error and achievable rate of the three different modulation schemes are evaluated for optimum thresholds values which are found by minimizing the probability of errors for varying transmission powers. In Figure 5.9, the probability of errors for each modulation scheme are shown for varying transmitter-receiver distances. For all modulation schemes, probability of error is decreasing significantly with the increasing average transmission power per bit, i.e., the number of bacteria released from the transmitter which is expected. When the number of bacteria released from the trans-

mitter increases, the number of bacteria arriving the receiver in- creases in turn increasing the correct detection probability. This decrease in probability of error is less significant for *M-ary* density modulation since increasing transmission power increases the separation between symbol levels while also contributing to the ISI where the residual bacteria from the previous symbol cause errors. Furthermore, as seen from Figure 5.9, the distance has a considerable effect on probability of error for all three modulation schemes. Since the bacteria propagate randomly, it is harder to reach the receiver when they have to travel longer distances which results in an increase in probability or error.

To compare the probability of errors of the proposed modulation schemes, the probability of errors are converted to bit error probability for fair comparison. In Figure 5.10, bit error probabilities for $d = 500\mu m$ are plotted versus the average transmission power per bit. Distributed modulation and the binary density modulation perform very similarly, the probability of error decreases with the increasing transmission power per bit. However, for M-ary density modulation, increasing the transmission power does not ameliorate the bit error probability.

In this study, we considered *M-ary* modulation with $M = 4$, transmitting $log_2(M) = 2$ bits per symbol. The achievable rates comparison between binary and *M-ary* modulation with $M = 4$ is illustrated in Figure 5.11. For *M-ary* modulation, the achievable rate increases very quickly with increasing transmission power whereas for binary modulation, the achievable rate requires a lot of power for a small increase in rate.

Similarly, the achievable rates of *M-ary* density modulation and distributed modulation schemes are compared in Figure 5.12. Asymptotically, both schemes reach the rate of 2 bits per/slot as expected. However, to attain the same rate, distributed modulation requires larger quantity of less transmission power than the *M-ary* density modulation. Considering the distributed modulation's lower error probability and higher rate, it can be considered as an efficient modulation scheme.

Another factor influencing the achievable rate is the length of time slot. To examine

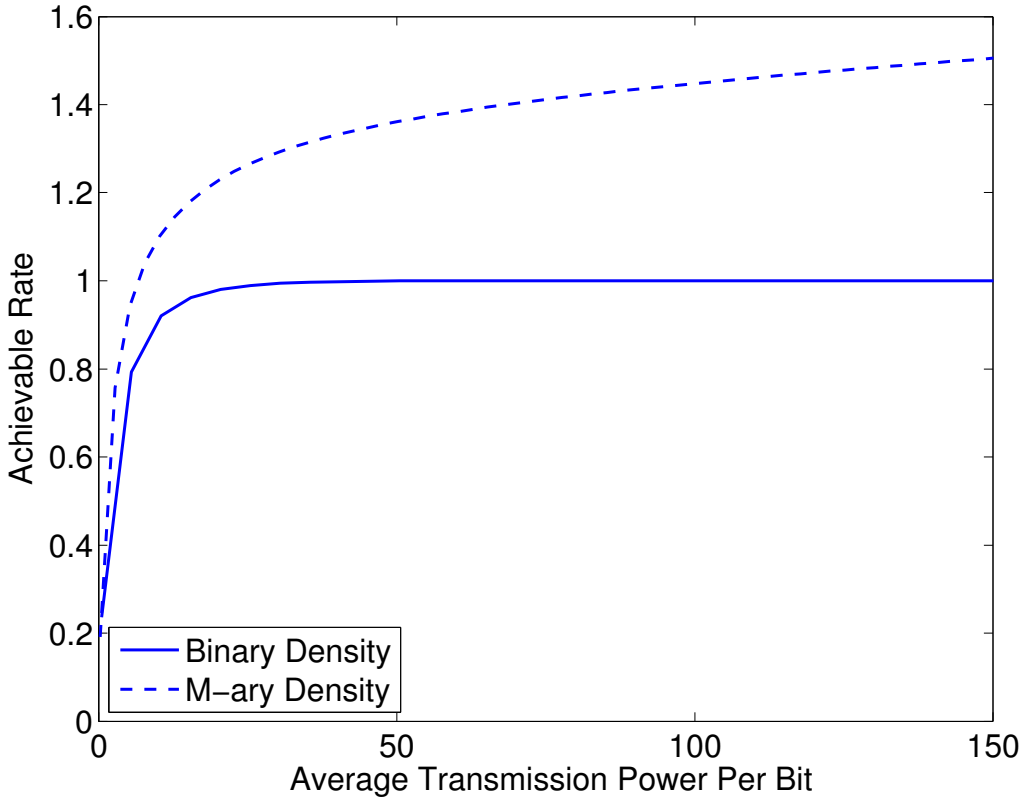


Figure 5.11: Achievable rate for binary density and m-ary density modulation.

its effect, the achievable rate versus time slot length is presented in Figure 5.13 for various transmission powers. When the duration of the time slot increases, there are more bacteria reaching the receiver and delivering its message. Hence, the rate per time slot increases. However, when the time slot becomes too large, this rate is divided by the large time slot length which in turn decreases the rate per second.

## 5.6 Conclusion

Bacterial nanonetworks is one proposed model for molecular communication that utilizes bacteria as information carriers between the transmitter and receiver. While this bio-compatible approach can allow information to be transmitted up to millimeter distances, there are numerous complexities in developing encoding techniques of the plasmids at the

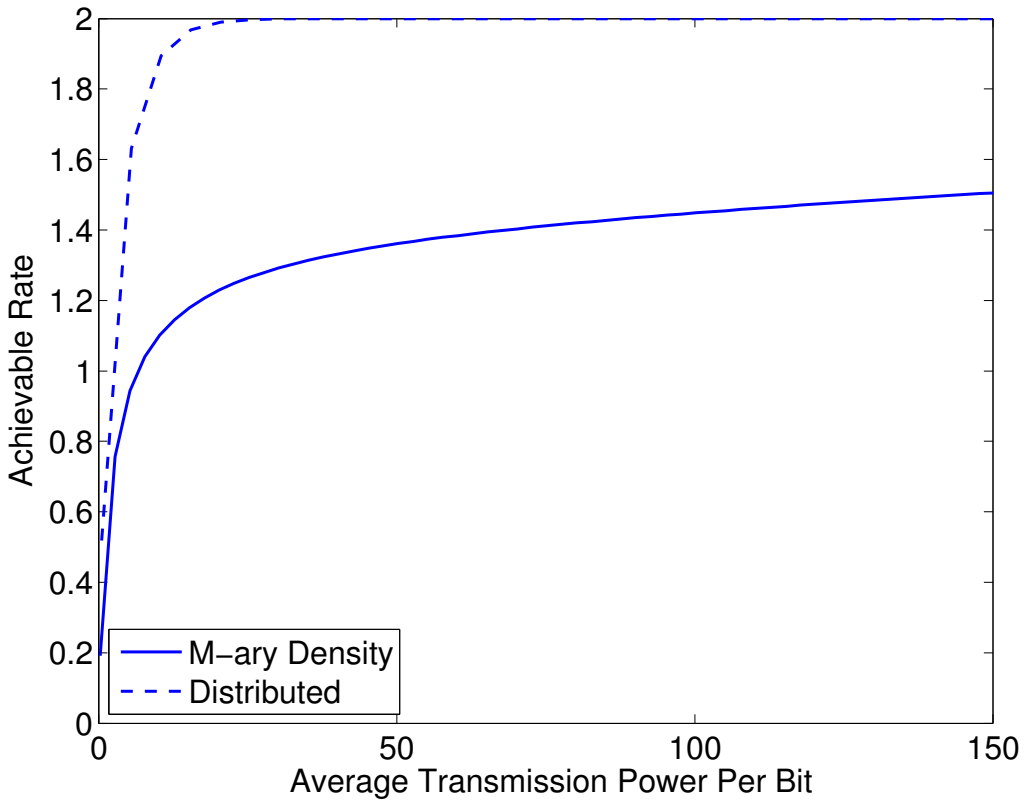


Figure 5.12: Achievable rate for m-ary density and distributed modulation.

transmitter, as well as decoding at the receiver. A simpler approach could be achieved through ON-OFF keying where the population of the bacteria represents the digital bits that are to be transmitted. However, the long propagation period of the bacteria leads to low data rate. In order to improve the performance, this study proposed incorporating another property which is the encoding of different combination of genes into the plasmid, where the different combinations can represent a series of bits. The transmitter motile bacteria will swim towards the non-motile bacteria at the receiver to conjugate and transfer the plasmids with the encoded genes. This will lead to the non-motile bacteria at the receiver to receive a full set of genes that will lead to bioluminescence. Through these different combination of genes, parallel transmission of bits can be achieved, and this in turn will lead to lower bit error probability as well as higher achievable data rate. The performance

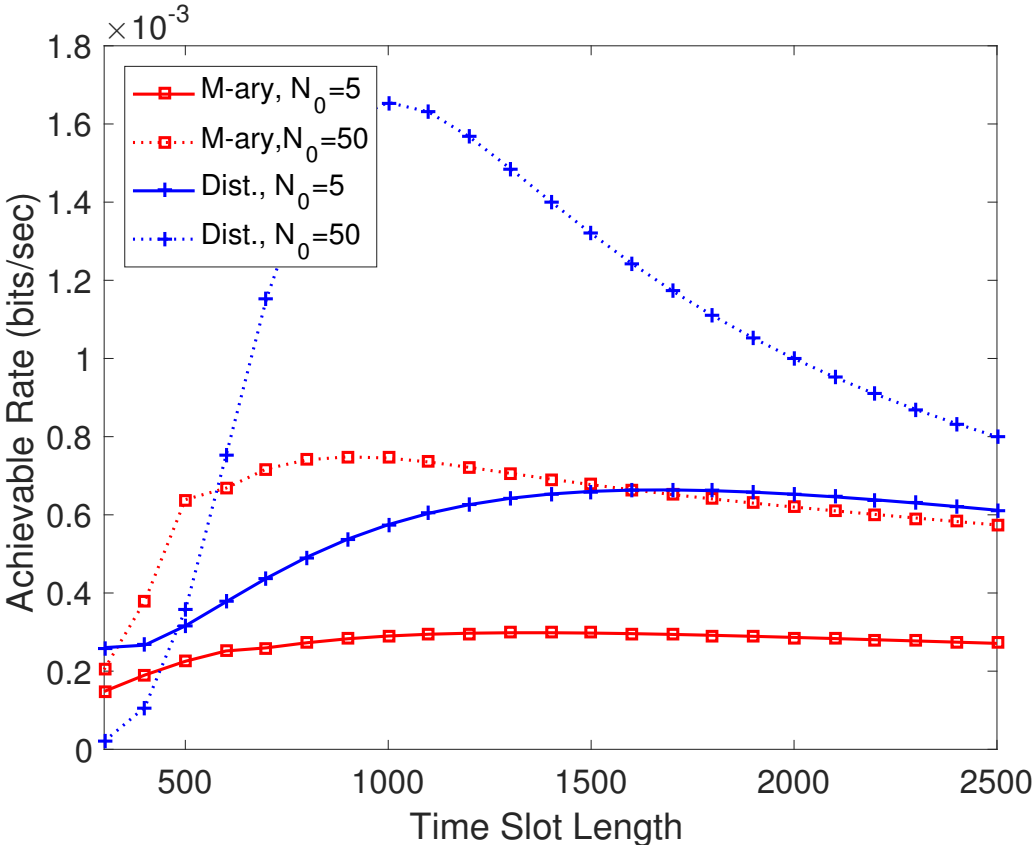


Figure 5.13: Achievable rate for m-ary density and distributed modulation.

evaluation compared the distributed modulation scheme presented in this study with the Binary Density Modulation as well as the M-ary Density Modulation scheme, and found that the performance improvement can be established for varying distances, quantity of bacteria emitted, as well as time slots. This proposed approach has shown how incorporating other known cellular functions, such as engineering different combination of genes into the plasmids, can be incorporated into bacterial nanonetworks to further improve their performance. This would, therefore, lay the foundation for incorporating other functionalities and properties in the future to further improve the performance and open up new opportunities for novel healthcare applications.

# CHAPTER 6

# MICROBIOME-GUT-BRAIN AXIS AS AN INFRASTRUCTURE FOR INTERNET OF BIO-NANOTHINGS

## 6.1 Motivations and Related Work

The IoBNT is envisioned to be a heterogeneous network of electronic and biological devices, deployed inside and outside of the body as shown in Fig. 6.1, communicating through different means, ranging from electromagnetic waves and coupling, electrical and mechanical stimulation, to Molecular Communication (MC) [1]. Electronic devices comprise implantable and wearable electronic devices such as brain implants, pacemakers, and smart watches, whereas biological devices comprise manipulated natural cell and tissues or man-made synthetic ones such as engineered immune system cells, engineered gut microbes, and artificial cornea.

Developing the IoBNT communication network infrastructure requires the following main prerequisites: (i) integrating accurate and predictable models of communication and networking parameters, (ii) minimizing the interference with natural body functions in order to prevent any psychological or physical discomfort, (iii) interconnecting heterogeneous devices (electrical and molecular), (iv) accessibility from outside the body in a minimally invasive fashion.

These requirements greatly reduce the practicality of classical telecommunications solutions, especially for realizing intra-body IoBNT links [2]. The direct contact of the IoBNT devices with the human body, where cells and multicellular organs naturally communicate and interconnect into networks, suggests the possibility to exploit these biological communications for the interconnection of these devices. Therefore, in this chapter we detail a conceptual framework for the realization of a network infrastructure where **artifi-**

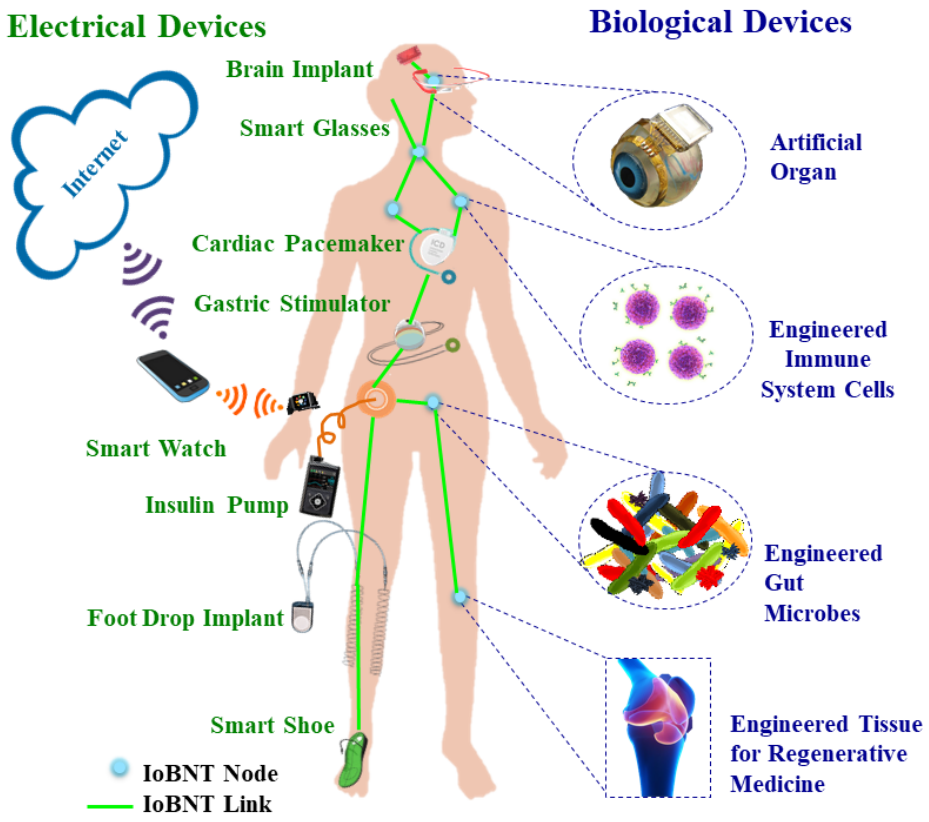


Figure 6.1: The Internet of Bio-NanoThings paradigm.

**cial communications between wearable/implantable devices are realized by exploiting natural biological communications systems in the human body**.

The focus of the conceptual framework introduced in this chapter will be the **Microbiome-Gut-Brain Axis (MGBA)**, where electrical signals propagating through the nervous system are converted to molecular signals that influence the gut microbial communities, and *vice versa*. The information propagates by means of natural communication links and interfaces, which are present in the nervous system, the endocrine system, and the immune system [107]. The holistic nature of the MBGA encompasses electrical and molecular communication domains and interfaces between them. The accessibility of MBGA from the external environment through the alimentary canal, and the presence of microbial cells, which are genetically programmable as biological devices, make this system particularly interesting to explore in light of the IoBNT paradigm. A direct connection with the MGBA

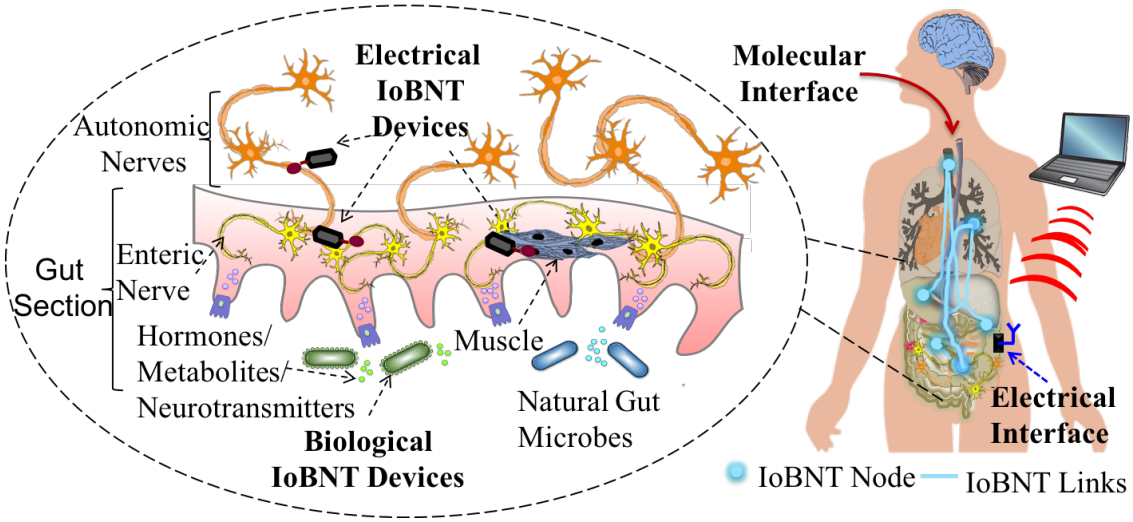


Figure 6.2: Microbiome-Gut-Brain-Axis IoBNT communication network infrastructure.

will also provide a large amount of data about the health of the central and autonomous nervous system, as well as the gut.

The objective of this chapter of the PhD thesis is the present an application of bacteria-based MC for IoBNT where natural MC channels in the body involving native bacteria of the gut and the enteric nervous system are suggested to form an infrastructure for the communication of artificial information to interconnect implantable devices.

We specifically focus on the **utilization of the MGBA as an IoBNT communication network infrastructure** to transmit and receive information generated by and/or directed to electronic and biological devices, as shown in Fig. 6.2, where this infrastructure is also envisioned to communicate with the external environment through dedicated molecular (alimentary canal) and electrical (wireless data transfer through skin) interfaces.

To this end, we present a methodology that comprises both analytical and experimental efforts. The analytical effort builds on top of neuroscience and bioinformatics to abstract and model with reliable mathematical expressions the propagation of device-sourced information through biological tissues utilized as communication channels, which include the modeling of i) electrical communications between devices connected through nerves in the gut muscle, enteric, and autonomic systems; ii) molecular communications involving bio-

logical devices and natural gut microbes through interactions with hormones, metabolites and neurotransmitters, and iii) the heterogeneous electrical and molecular communications interface between the gut and the central nervous system. The experimental effort is based on the design of a unique integrated network probe device composed of a hub connected to an ensemble of electrical and molecular stimulation and sensing interfaces. This probe device is intended to be first utilized in an *in vitro* environment, which is composed of an innovative gut-on-a-chip system able to co-culture cells that compose the MGBA. Then, an implantable version of the probe, which explores wireless power and data transfer technology to establish connectivity with the external environment, is to be utilized into laboratory rats to collect *in vivo* data on the MGBA communications. On top of these models and experiments, as part of our methodology we introduce design elements, opportunities, and challenges to realize the aforementioned IoBNT network infrastructure.

This chapter is organized as follows. In Sec. 6.2, we detail how analytical models of communication channels for device-to-device communications can be derived from models of biochemical processes underlying the MGBA. In Sec. 6.3, we describe a methodology to design devices to derive empirical data to complement the analytical channel models in *in vivo* and *in vitro* settings. In Sec. 6.4, based on the MGBA-based channel models, we describe the main element of a network infrastructure of IoBNT applications, as well as the main features of a simulation environment to aid the design of such networks. Finally, in Sec. 6.5, we draw our conclusions.

## 6.2 Analytical Methodology

The MGBA refers to the bidirectional communication network between the brain and the gastrointestinal tract, which in general includes the Central Nervous System (CNS), the Autonomic Nervous System (ANS), the Enteric Nervous System (ENS), the gastrointestinal tract, and its microbiome [107]. According to recent studies [108, 109, 110], through the MGBA, the gut microbiota influences brain functions, behavior, stress and pain modu-

lation systems, and brain neurotransmitter systems, whereas the brain controls gut motility, gut wall permeability and microbial composition. On the one hand, the electrical stimulation sent from the CNS goes through the autonomic nerves reaching the enteric nerves, enteric muscles, and further the cells in the intestinal walls, surrounded by the gut mucosa. The incoming electrical signals are transduced to molecular signals by these cells and then released to the gut lumen (internal space of the gut) in the form of secretion of acids and mucus, and immune system products. These molecular signals affect the communication among gut microbes and alters their community composition [111]. On the other hand, the changes in the gut microbial community interactions, composition, or secretion of compounds such as hormones, metabolites and neurotransmitters, at the gut mucosa are detected by the cells in the intestinal walls as molecular signals, which are transduced to electrical signals by these cells and propagate back to the CNS through the ENS and ANS [110].

Along with the fundamental expertise accumulated on molecular communication and nanonetworks [112], in recent years the ability to successfully apply fundamental communication engineering abstractions, concepts, and modeling strategies to characterize biological systems has been demonstrated. Examples can be found in the study of drug propagation in the cardiovascular system [113], information flow through engineered bacteria [114] and gut microbes [115], and communications via peripheral nerves [116].

In this study, by stemming from some of the aforementioned examples, we describe the ambitious challenge of modeling the complete, complex, and heterogeneous MGBA communications. In this direction, it is essential to define physical channel models of *electrical communications* through nerves and muscles; *molecular communications* involving gut microbes and their interactions with hormones, metabolites and neurotransmitters; and the *transduction between electrical and molecular communications* through the MGBA. Within each of the aforementioned modeling efforts, the MGBA-based channels need to be characterized in terms of

(i) admissible input-output value and frequency ranges within biocompatible boundaries,

(ii) delay between a stimulation onset and the sensing of its consequences after propagation through the channels,

(iii) noise and variability of the input-output response,

(iv) cross-talk with natural communications and with other simultaneous stimulations.

### 6.2.1 Physical Channel Models of Communications Through Enteric and Autonomic Nerves, and Muscle Activity

The modeling of electrical communication channels through the MGBA stems from neuroscience literature [117], where the processes underlying electrical signal propagation through neurons are described. Different options for electrical stimulation and electrical activity sensing should be considered for transmitting information signals between devices through the ENS. These signals should be minimally interfering with the natural gut functions, but at the same time exploiting any possible stimulation pattern to maximize the information capacity between a stimulation and a sensing location.

Previous efforts on modeling the information transmission through neurons by communication theory focus on the propagation of signals carrying natural information but lack the methodology describing how artificial information can be transmitted without interfering with the natural information flow. In particular, in [118], the authors develop a physical channel model of the neuro-spike propagation between two interconnected neurons investigating the probability of error and delay. In [119], a specific part of the neuron, the synapse, is investigated to characterize the propagation of the spiking rate function between neurons. In [120], multiple synaptic paths directed to a single postsynaptic terminal is modeled and the information rate per spike is derived. This work has been extended to compute the ergodic capacity of the synaptic Multiple-Input Multiple-Output (MIMO) communication

channel [121]. Another approach models neuron-to-neuron communication by a frequency response dividing it into intra-neuronal and inter-neuronal blocks [122].

To tackle the problem of transmitting information signals between devices interfaced with neurons, we briefly review the system proposed in [116, 123]. In particular, this system utilizes the so-called **subthreshold electrical stimulation**, which potentially allows the propagation of artificial information from one end of the neuron to the other end minimally interfering with the natural neuro-spike communications occurring at the same neuron.

As shown in Fig. 6.3, we consider the **Sender**, which modulates the injection of electrical current $I_i(t)$ into the soma according to the signal to be transmitted. The **Channel** corresponds to the membrane potential perturbation resulting from the current injection, and its propagation along the axon. The **Receiver** recovers the transmitted signal by reading the membrane potential $V_o(t)$ at a distance $x$ from the soma along the axon. This system can be described with a linear channel model by leveraging the quasi-active model of the neuron's membrane from neurophysiology literature [124]. This linear model of electrical signalling through a single neuron is valid only when the membrane potential maintains a value less than $V_{th}$, named subthreshold condition, which typically ranges from -60 mV to -55 mV, where there is no stimulation of a neuro-spike, or Action Potential (AP) [117]. This threshold defines the admissible input-output values of this communication system. An analytical model of the transimpedance ($V_o/I_i$) of a single neuron is derived as function of the input frequency components. By studying this model for the propagation of electrical signals through a neuron, the frequency range, the attenuation, and the delay can be extracted as parameters that will be the constraints for the design of modulation and coding techniques and medium access control protocols, described in Sec. 6.4.1.

To obtain channel models of electrical communications in the MGBA over its neurons, the aforementioned studies should be complemented by existing mathematical and computational models from enteric neurobiology [125]. These computational models represent

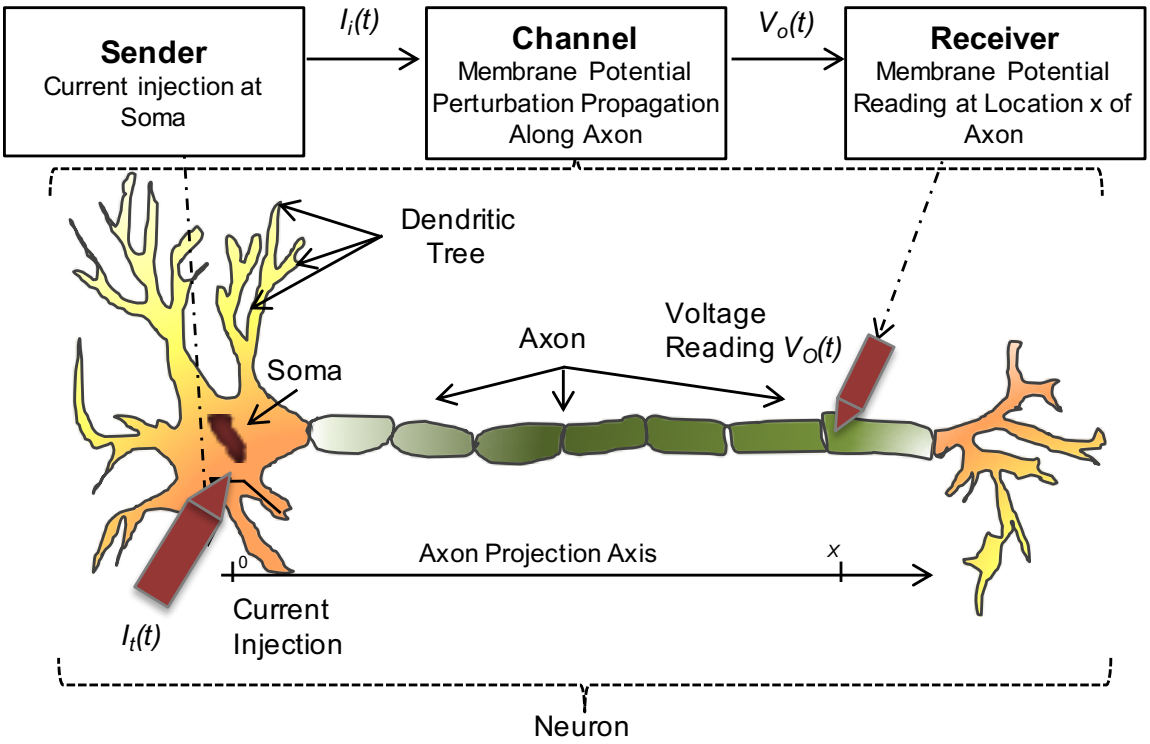


Figure 6.3: Scheme of a single-neuron-based communication system [116].

the natural communication processes in enteric nerves, their interconnections with the autonomic nerves, and the impact of these communications on muscle dynamics. Models describing the chemistry, the morphology, and the connectivity of the ENS neurons can be found in the literature [125]. In addition, the result of electrical signals in the ENS such as muscle contractions and mucosal secretion are observable and measurable [126]. These two properties make the ENS stand out in terms of possibility to obtain quite accurate models compared to other parts of the nervous system [127]. For this aim, biophysics-based mathematical models of individual neurons, *e.g.*, Intrinsic Sensory Neurons (ISN), should be considered. ISNs are the building blocks of ENS since they connect every neuron type in the ENS and make recurrent connections with themselves [128].

To capture the peculiarities of the enteric neurons, the aforementioned channel models should be revisited by considering cross-talk interactions with natural AP-based communications through leaky-integrate-and-fire models [129] coupled with the After-Hyperpolarizing

(AH) potential characteristic of enteric neurons, which represents the decrease of the membrane potential below the resting potential following the peak of the AP [127]. Furthermore, the synaptic models should be refined for different types of enteric neurons adopting either slow [130] or fast [131] Excitatory PostSynaptic Potential (EPSP) at the receiving neuron. The observable output of the ENS, *i.e.*, the mechanical contraction of smooth muscles stimulated by electrical signals, can be modeled based on the conductance model [132] of muscle fibers.

On top of these models describing single neurons and connection of neurons, the topology of neuron interconnections is built either randomly into anatomically relevant mesh structures [132] or following the topology extracted by experiments. In addition, models of the interconnection with the autonomic nerves, and the correlated myoelectrical activity of the smooth muscle should be incorporated, as described in [125]. Noise should be also considered by integrating stochastic models, such as [133, 134]. Another noise source is the person-to-person variability in the ENS mesh structure, which should be taken into account to increase the reliability of the communication channels in the IoBNT infrastructure.

### 6.2.2 Physical Channel Models of Communications Through the Gut Microbial Community

As part of the conceptual framework detailed in this study, communication channels in the gut are based on the paradigm of MC [1], where the transmission, propagation, and reception of information is realized through molecules and chemical reactions. In particular, in our framework the communications through the gut are based on the release and sensing of molecules and/or the manipulation of the microbial community composition in the mucosa and lumen. The release of molecules can be realized through ingestion, injection, or by engineered microbes, and sensing can be realized through excretion samples, biological sensors, or engineered microbes as well. As in Sec. 6.2.1, this information transmission should be minimally interfering with the natural gut functions, and at the same time maximize the information capacity of these channels.

To evaluate the feasibility of such channels, the theoretical information transmission performance in terms of mutual information has been estimated in [114] for an *E. coli* bacterium, and in [115] for other two gut bacteria species. This estimation is based on the bacteria metabolism, defined as the complex network of chemical reactions that underlie the conversion of chemical compounds to energy, cellular building blocks, and waste. The transmitted information is encoded into the release rate, concentration, molecule type or release times of chemical compounds in the proximity of the bacterial cells, where the chemical compounds participate in metabolic chemical reactions within the bacterial cells as shown in Fig. 6.4. These chemical reactions are chained into pathways, where input chemical compounds are broken down generating energy, and at the same time biomass, *i.e.*, cellular components, are built up consuming energy. The transmitted information is modulated at the microbes into changes in the cell's behavior such as the growth (biomass) rate, and rates of uptake/secretion of chemical compounds to/from the environment in response to the released chemical compounds. These changes then reflect into the gut microbial community behavior and composition. The transmitted information can then be received by another device by means of the aforementioned sensing techniques, or transduced by the MBGA into nervous system activity, as described in Sec. 6.2.3.

To model the aforementioned communication system at a single microbe cell, in [115] the cell metabolism is abstracted as a series of two channels, *i.e.*, the Enzyme Expression Regulation Channel and the Metabolic Reaction Channel, as shown in Fig. 6.4. Advances in DNA sequencing and metagenomics studies provide a wealth of data on the gut microbes, their metabolism, and their interactions, including their organization into interdependent consortia [135], such as the gut microbial community. The methodology proposed to obtain these channel models stems from bioinformatics techniques for metabolic network modeling and simulation applied to these data, *i.e.* **GEnome-scale Modeling (GEM)** and **Flux Balance Analysis (FBA)** [136]. The results obtained in [115] in terms of mutual information of these channels demonstrate the potential of utilizing species within the

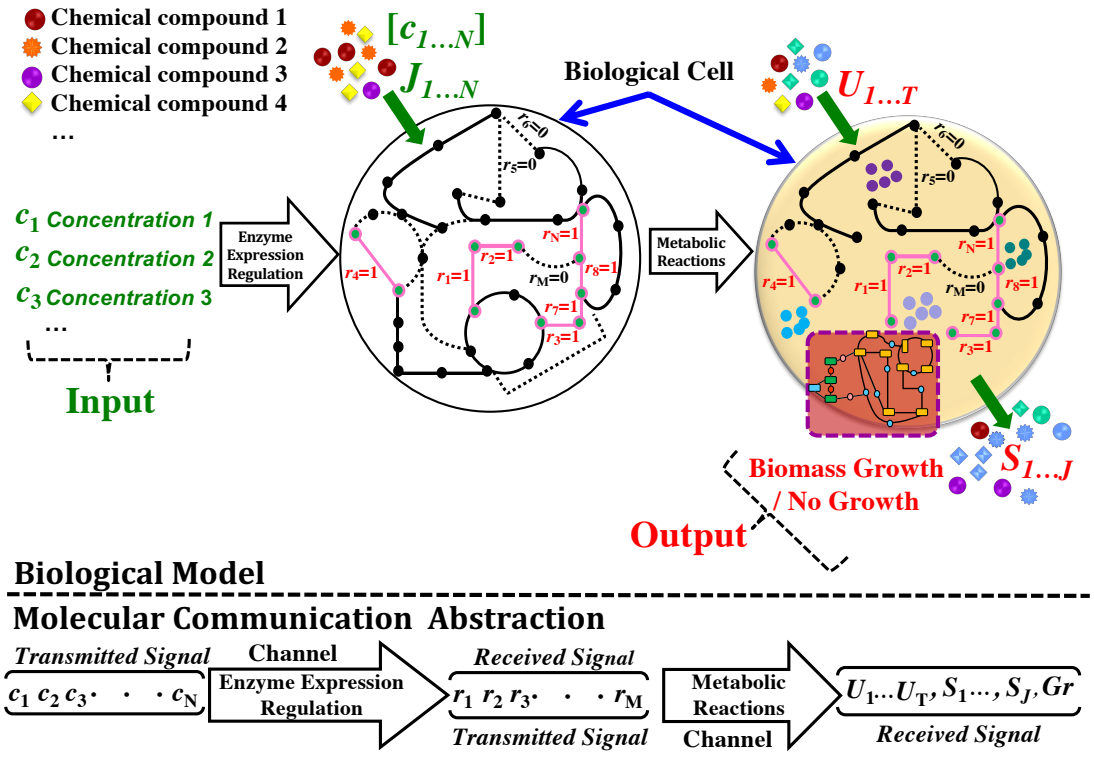


Figure 6.4: Scheme of a molecular communication channel based on microbial metabolism [115].

gut microbial community to propagate information. In particular, it is observed that the encoding of information into different compounds results into different values of mutual information, which opens the road for optimizing these communication channels with a proper design of information encoding schemes based on molecule release.

To generalize the aforementioned channel models to cover multiple microbe cells and possibly the entire microbial community, a potential approach is to combine multi-community metabolic simulation techniques [137, 138], and ecological models of microbial community dynamics and stability [139] with the theory of diffusion-based and advection-based molecular communication, *e.g.*, as utilized in [113] to model the propagation of information in the cardiovascular system. For the former, mixed-bag FBA and multi-species FBA consider a joint metabolic model of multiple species in steady state, possibly interacting [137], while dynamic FBA (dFBA) [140] focuses on the temporal dynamics of a metabolic model

for a single input chemical compound at a time. In contrast, an approach based on ecological mathematical models [139] can include the effects of variable perturbations to the community evolution, such as when microbes are added to the community, or flushed away. A diffusion-based molecular communication channel model, able to represent the diffusion of the molecules between microbes within the mucosa and along the lumen can be derived from the mathematical expression of the molecular diffusion through mucus, *e.g.*, in [141]. By combining these diverse models, similar communication channel metrics as mentioned in Sec. 6.2.1 can be derived. In addition, the cross-talk with natural processes should also be evaluated in terms of how much a particular stimulation pattern could result in an unhealthy perturbation of the microbial community dynamics.

### 6.2.3 Communications from/to Nervous System to/from Gut Microbiome

The MBGA is characterized by an intercommunication of the aforementioned electrical and molecular channels detailed in Sec. 6.2.1 and 6.2.2, respectively. We intend to harness this feature to develop a communication gateway between devices interfaced to different systems, *i.e.*, from gut (mucosa, lumen) to the nervous system (ENS, muscles) and *vice versa*. To model this intercommunication, we propose to consider the following main mechanisms:

(i) the modulation of gut microbial community composition alters the chemistry in the gut with consequent modulation of the ENS activity;

(ii) the modulation of the microbial metabolism results in a modulation of secrete metabolites, such as Short-Chain Fatty Acids (SCFA), that have neuroactive properties, or in neurotransmitter themselves, which again modulate the ENS activity;

(iii) the release of signaling molecules (that are small molecules different from the metabolites) by neurons alters the microbial community interactions

(iv) the muscular activity, *e.g.*, a contraction, can mechanically displace the gut microbiota and even change its composition.

As a consequence, the ENS activity model and the microbial metabolic models should be combined with models of the release of signaling molecules and electrical/molecular signal transduction mechanisms, respectively. Furthermore, a biomechanical model such as in [142] and its connection to the ENS model, in particular the myoelectrical activity of the smooth muscle and the aforementioned ecological models, is required to account for the muscular activity. All these modeling efforts should be tuned and validated by in-vitro and in-vivo experiments, projected in Sec. 6.3. In addition, the propagation of molecules across the intestinal wall and tissues can be modeled according to diffusion and convection equations [143]. Unlike previous literature on diffusion-based MC models [114, 19], analogous to free-space channel model in wireless communication, the transport in interstitial space, where molecules should navigate around the cells, diffuse inside and outside of cells is analogous to channel models with reflection and refraction in crowded environments.

## 6.3 Experimental Methodology

The analytical methodology proposed in Sec. 6.2 is based on physiological models of the MGBA and its components. These models are in part sourced by existing literature, where available, and in part complemented and tested with the results of the experimental methodology described in this section. In this direction, a **complete gut-on-a-chip (GOAC)** model [144] able to grow samples of the gut tissues, their innervation, and the gut microbial community, with stimulation and sensing interfaces for *in vitro* experiments will be developed for testing electrical and molecular (6.2.2) channels individually, and their interconnection as described in respectively Sec. 6.2.1, 6.2.2, and 6.2.3, respectively. Subsequently, *in vivo* experiments will be conducted on rats using the **Integrated Network Probe Device (INPD)** described in Sec. 6.3.1, capable of spanning all possible stimulation and sensing

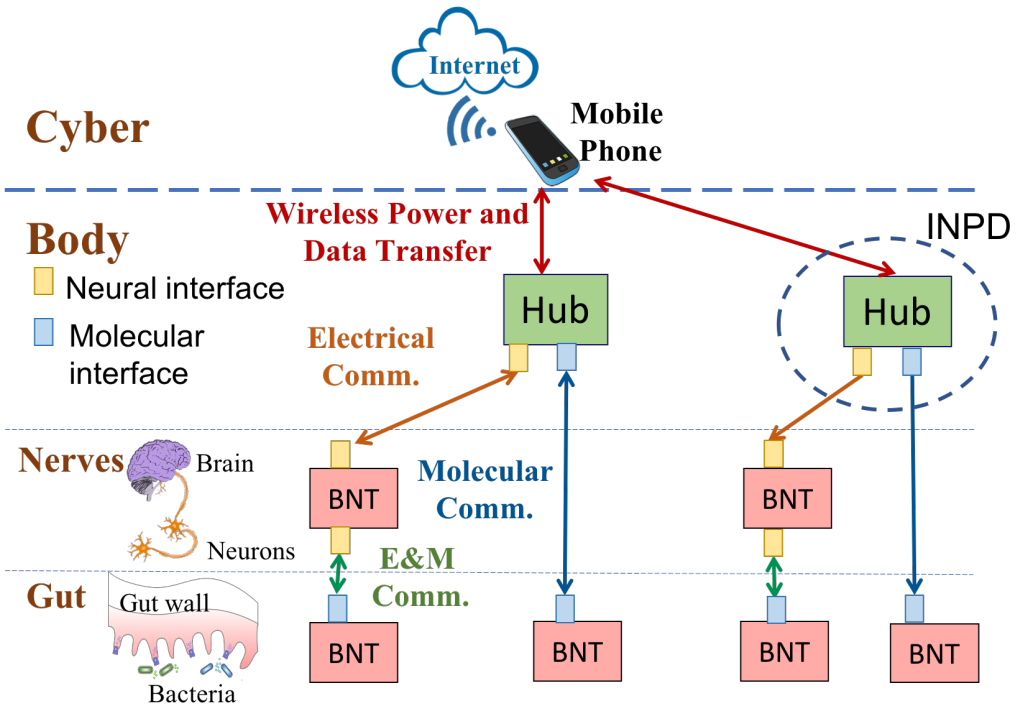


Figure 6.5: Scheme of the design of the integrated network probe device proposed for the experimental methodology described in this study.

modalities of interest for the development and the validation of the MGBA communication channels, towards the realization of the intrabody IoBNT communication network infrastructure described in Sec. 6.4.

### 6.3.1 Devices for Experimental Validation of MGBA Channel Models

To support the experimental methodology, interfaces to sense/actuate signals on different MGBA parameters, as well as hub devices that integrate these signals, are envisioned to be utilized both for *in vitro* and as an INPD for *in vivo* experiments, as described in Sec. 6.3.2 and Sec. 6.3.3, respectively. This device will record and control signals to/from all the components constituting the MGBA communications such as electrical signals through ANS, ENS, the gut muscular tissue, and molecular signals such as the concentration of molecules (hormones, metabolites, neurotransmitters), as well as the microbial community composition. To this end, we envision a design with multiple **electrical and molecular interfaces** to electrical and molecular stimulators and sensors, *i.e.*, **Bio-NanoThings (BNT)**,

and one or more **Hubs** that connect these interfaces to the outside of the body through a wireless power and data transfer link compatible with the Enercage-HC2 system presented in Sec. 6.3.3, as illustrated in Fig. 6.5. These interfaces will implement the transmitters and receivers introduced in Sec. 6.2. After the testing stage, these interfaces and their connected circuits can be separated from the aforementioned hubs and be the bases to design standalone wearable and implantable IoBNT devices capable of communicating via intrabody MGBA channels.

### 6.3.2 *In vitro* Experimental Platform based on Organ-on-a-chip Device

The *in vitro* GOAC environment is expected to mimic actual gut functions in a more controllable, low noise environment as a first step towards *in vivo* experiments, allowing us to refine the channel models developed using the methodology described in Sec. 6.2, and subsequently the accuracy of the simulator described in Sec. 6.4.3. Organ-on-a-chip (OOAC) microfluidic devices aim to create minimal functional units of tissue or organs by reconstituting key structural and physical features. Researchers have fabricated chips to model several tissues and organs, including liver [145], hearth [146], kidney [147], lung [148], intestine [149], and muscle [150], among others. For example, a human GOAC microfluidic device has been developed to study interactions between on-chip cultured human intestinal epithelial cells and the gut microbiome in a setting that mimics the human intestinal microenvironment [151]. In such systems, selected *in vivo* human gut components can be incorporated to create an *in vitro* gut-on-a-chip system. The microfluidic nature of OOAC systems can be exploited to establish a well-defined and controllable microenvironment for the envisioned GOAC capable of monitoring and controlling pH, temperature, delivery of nutrients/oxygen/drugs, and removal of waste. Physiological peristaltic motions, *i.e.*, the natural muscular contractions, can also be mimicked at the chip level through integration of vacuum side chambers to study the mechanical activity.

Due to its controllability, GOAC provides a perfect experimental testbed to study the

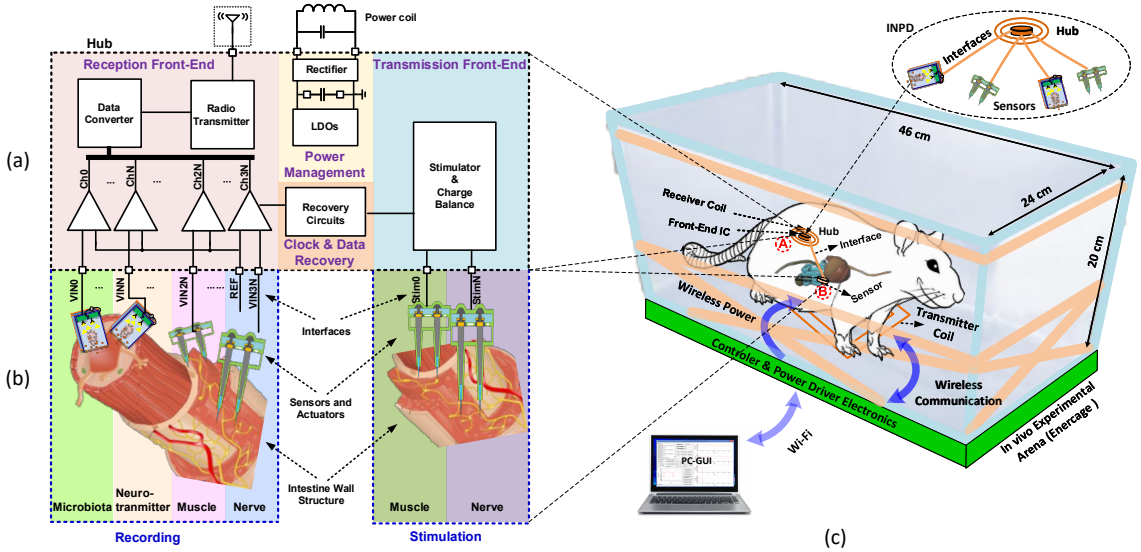


Figure 6.6: Schematic of a) the hub and b) the biological interfaces of the integrated network probe device, and c) *in-vivo* experimental arena.

MGBA communication channels where the individual communication links can be isolated and tested. Also, this platform limits noise and variability among the individuals compared to an *in vivo* setting, which helps in the definition of general models. Moreover, this *in vitro* platform will be also utilized to test the devices and interfaces designed considering the criteria described in Sec. 6.3.1 to assure accurate operations and biocompatibility before conducting *in vivo* experiments. In this controlled environment by tuning system parameters to extremes, limits of operation without damaging tissues and altering the microbial balance will be examined.

While GOAC systems can achieve control over specific individual aspects of the tissue environment, existing examples are still relatively simple compared to the actual gut ecosystem. To create a GOAC more reflective of the physiological function under test is a challenge that needs to be addressed. Other challenges include culturing human intestinal cells, living microbiota and enteric nerves in the same chip while maintaining cell viability.

### 6.3.3 *In vivo* Experimental Platform

Following the *in vitro* experiments, refined channel models for communications over the MGBA and tested devices capable of interfacing with the MGBA will be integrated to be tested further in an *in vivo* experimental platform. In order to capture other unexpected properties of the actual body environment and dynamically measure communication parameters, *in vivo* experiments should be on animal models. In preclinical studies, researchers prefer to use small animal models such as rodents because of lower cost, rapid growth, ease of maintenance, and similarity of their biological and behavioral characteristics to those of humans. Here, we describe our methodology based on rat models, which are very suitable to observe the overall effects on a living subject in its natural environment.

A wireless experimental arena, called **EnerCage-HC2**, will host the rats to provide more natural conditions for long time continuous experiments than conventional methods which limit their mobility by tethered wires [152, 153, 154]. Any device implanted in the rat will be connected to the cage using magnetic induction links for wireless power and data transfer. The EnerCage-HC2 system, presented in [155], is built around a standard homecage using a new 4-coil inductive link which powers wirelessly and communicates with a stimulating headstage [156]. Wireless power, in the EnerCage system, is delivered in the near-field domain at 13.56 MHz, a Federal Communications Commission (FCC) approved operating frequency for Industrial, Scientific, and Medical (ISM) applications.

For *in vivo* experiments, a novel device implanted in the rat's body as shown in Fig. 6.6 is needed to stimulate and record electrical and molecular signals exchanged over the MGBA to test the aforementioned MGBA channels. The details of design for this implantable device which will be directly in contact with MGBA components such as nerves and gut microbes via its interfaces, as described in Sec. 6.3.1. This device will also be connected to the EnerCage-HC2 to relay commands from outside the body to the device and the information collected from the body to the outside during the tests. Using this device, the limits of operation to interfere with the natural body functions and to alter cells or tissues

will be tested in order to define electrical and molecular signals' limits for biocompatibility. While passing electrical signals through neurons or molecular signals through tissues, the time, frequency and location that is not used by the natural functions will be identified similar to cognitive radio networks where secondary users use spectrum left vacant by the primary users. Furthermore, long term experiments should be conducted to observe and minimize the effects of electrical signals stimulating neurons on the degradation of neural fibers or the effects of molecular signals stimulating bacteria on the composition and livelihood of the gut microbiome.

### 6.3.4 Integrated Network Probe Device Hub

A compact novel hub should be serving as the main part of the INPD that operates wirelessly in conjunction with the existing smart *in vivo* experimental arena, Enercage-HC2, described in Sec. 6.3.3. The integrated hub should include electronic circuits to drive electrical and molecular interfaces, and process them to be transmitted to outside the body. The electrical interfaces are electrodes that record and stimulate smooth muscle activity from gut serosa muscle membranes, *i.e.,* membrane found on the outer wall of the organs of the abdominal cavity, record local neural activity from enteric, vagus nerve, *i.e., nerve running through brain to abdomen controlling hearts, lungs, and digestive track*, and autonomic nervous systems, and the molecular interfaces are the biosensors to detect microbial activity and concentrations of molecules, such as neurotransmitters, hormones, and metabolites in the gut mucosa. A rendered view of the wireless hub system, including its interfaces with the target biological environment of the MGBA, is depicted in Fig. 6.6-a and b. Moreover, the location of the hub in the rat body under the skin, and its utilization in the EnerCage experimental arena, are illustrated in Fig. 6.6-c.

Even though an ultrasound-powered, mote-sized Implantable Medical Device (IMD) has been recently proposed to record neural activity from the peripheral nervous system [157], to the best of our knowledge, the researchers do not demonstrate the functionality

of that system on a freely behaving animal. *Moreover, electronics for joint stimulation and recording of enteric nerves, muscles, and microbial activity have not yet been considered or demonstrated.* Hence, a novel design is required for the implantable hub adopting a System-on-a-Chip approach (SoC) for ultimate miniaturization. The SoC should utilize ultra-low power and ultra-low noise Application-Specific Integrated Circuit (ASIC) design techniques to deal with multiple stringent constraints imposed on the interface modules and wireless powering and communication in a wireless smart arena. These constraints include the following:

- non-uniform and non-linear responses from the biosensors and electrodes,
- strong rejection of artifacts coming from the stimulator on the recording side,
- reliable power transfer in every location of the smart experiment arena with record-setting RF-to-DC power conversion efficiency,
- sub-threshold operation of the analog front-end for ultra-low power operation,
- minimum silicon footprint for cost reduction and ease of implantation with minimal damage,
- input-referred noise well below that of the transducer.

In addition, bio-compatibility should be kept in mind when designing and fabricating the hub. For example, in an effort to minimize the heat generated in the wireless power delivery and management blocks to prevent possible tissue damage, and satisfy the regulatory requirements, such as electromagnetic power specific absorption rate (SAR), the wireless power transmission link should operate at relatively low frequencies with minimal absorption in the tissue, minimum power consumption, and minimum area to be implantable. This is a challenge but not a major concern, since the operating frequency in molecular sensing systems is within Hz range [158], while in neural recording system is within tens of kHz range [159], hence wireless transmission link can be used sparsely to generate less heat.

Finally, *considering the difficulties in placement and attachment in a moving environment, such as the gut,* the hub will be assembled on a compact and flexible substrate, which can be surgically implanted under the skin or in the abdominal area (point A in Fig. 6.6-c), close to where molecular and electrical sensors/actuators should be implanted (point B in Fig. 6.6-c).

Recording channels should employ ultra-low-noise amplifiers, followed by ultra-low-power data converters to prepare data packets for transmission via EnerCage to a computer outside of the cage. The same computer should be programmed to initiate modulation of the nerves and muscle systems based on closed-loop algorithms that analyze the incoming data or animal behavior. The SoC should also include data/clock recovery and efficient stimulation circuits to convey outside-sourced information to the nervous and muscular systems. A power management unit will convert wireless RF power to multiple DC supplies required by other circuit blocks in the hub. The main blocks of the implantable hub presented in Fig.s 6.6-a and -b are the transmission front-end, the reception front-end, data recovery, and the power management unit, detailed in the following.

*Transmission Front-End*

While molecular signals can be stimulated externally by the ingestion of a pill or injection of a substance which does not require specific circuitry at the implantable hub, here we focus on the hub requirements for the electrical stimulation of the nerve cells through the neural interfaces detailed in Sec. 6.3.5. Conventional nerve stimulation studies mostly focus on Deep Brain Stimulation (DBS), which has been widely accepted as an effective therapy method for the partial cure of Parkinsons disease, tremor, and dystonia [160, 161]. In the electrical stimulation methods, Voltage-Controlled Stimulation (VCS), Current-Controlled Stimulation (CCS), and Switched-Capacitor Stimulation (SCS) are the most common topologies. VCS enables power-efficient stimulation; however, variations in the electrode position and accordingly in the electrode impedance [162] over time com-

plicates limiting and balancing the stimulation charge [163, 164]. Whereas CCS provides precise charge control and safe operation, it has low power efficiency due to the dropout voltage across its current sources [165, 166]. SCS, designed in [167], takes advantage of both the high efficiency of VCS and the safety of CCS using capacitor banks to transfer quantized amount of charge to the tissue. We have presented the first integrated wireless SCS SoC with inductive capacitor charging and charge-based stimulation capabilities, which can improve both stimulator efficiency and stimulus efficacy in DBS in [168]. The amount and the shape of the stimulus current for different stimulation scenarios for muscle and nerve manipulation can be adjusted via a current steering Digital to Analog Converter (DAC), which can be controlled by the user through the wireless link of the EnerCage.

*Reception Front-End*

A multimodal-sensing module that captures signals from the enteric nerve system, the gut microbial activity, and muscular movements to realize signal reception from both electrical and molecular channels should be developed. For nerve and muscle activity sensing, it is required to detect ultra-low voltage levels on the order of micro volts [152, 169], which should be considered in conjunction with the ultra-low energy consumption requirements of an IMD imposed by wireless powering [170]. For detecting molecules and microbial activity via biosensors, the reception circuit will require current detection components with wide range sensing capability and high linearity performance [171]. For this, it is key to identify the low-end sensitivity, *i.e.*, the minimum detectable signal for the system. The design of low-current detection instrumentation pertaining amperometric bio-sensors is widely explored in [172].

Another important challenge to realize the reception front-end is the adaptation of the electronic system to biological systems in terms of accommodating very different time scales. In fact, the dynamics of a biomolecular event, such as a change in the gut microbial composition, may happen in a longer time frame than electrical events at the nervous

systems, *i.e.*, minutes or even hours compared to milliseconds. Therefore, the electronic system should be designed to accommodate a very long integration time with respect to more classical electrical systems [173].

To digitize the sensed analog signal, following the reception front-end, a new hybrid ADC architecture should be developed, which combines ultra-low power, high resolution, and small footprint specifications. Following the ADC, digitized electrical and biochemical signals should be compressed, packetized, and wirelessly transmitted from inside the host body to the Internet via EnerCage and a computer.

*Power Management Unit*

Since the integrated hub is considered to be small and arbitrarily placed, electromagnetically-coupled Wireless Power Transmission (WPT) links pose a challenge, as demonstrated in [174, 175]. The Power Management Unit (PMU) may overcome this challenge by including an active voltage-multiplying rectifier, a duty-cycled wireless charging system, and a power-control loop. This unique PMU should operate in a way that each IMD, regardless of its orientation inside the host body, utilizes the lowest amount of power trickling into the entire array of implants, while ensuring correct bio-signal acquisition, pre-processing, ADC, and back telemetry operations.

### 6.3.5 Neural and Molecular Gut Interfaces for the Integrated Network Probe Device

In this section, we investigate possible solutions for neural and molecular interfaces connected to the implantable hub (wirelessly or wired depending on the location of the interest area) in order to stimulate and sense electrical and molecular signals at different locations of the MGBA. The stimulated and sensed data should be processed to obtain the parameters of the underlying physical channels discussed in Sec. 6.2.

*Electrical and Mechanical Activity Sensors and Stimulators*

Recording and stimulation of the central nervous system (*i.e.*, brain and spinal cord) is heavily studied and various types of microelectrodes capable of capturing and influencing the electrical activity of CNS such as the Utah Microelectrode Array [176] and the Michigan Probe [177] are been introduced. At the same time, the recording and stimulation of the ENS capable of interfacing with enteric neurons and gut muscles have not been fully explored to date. The motility of the gut, and the complex intestinal wall structure pose challenges for stable placement and efficient operation of electrodes to be implanted for this purpose. To design and develop electrodes specifically tailored for enteric neuron interfacing, the membrane potentials and conductance of enteric neurons, which are different than previously studied systems, should be taken into account [178]. Besides, the aspect ratios should be adjusted to suit the target areas varying with respect to the gut layer of interest. The particular geometry of the electrodes and their coating should be also tailored to minimize tissue damage and provide bio-compatibility.

*Molecular (Hormones, Neurotransmitters, Metabolites) Sensors and Stimulators*

As mentioned above,the gut microbiota and the ENS interface through neural and hormonal signals between immune cells, enteric neurons, smooth muscle cells, interstitial cells, and the gut microbiome. Furthermore, gut microbes can influence the ENS by producing hormones which act as local neurotransmitters (*e.g.*, GABA (gamma-aminobutyric acid), serotonin, melatonin, histamine, acetylcholine), by Short-Chain Fatty Acids (SCFAs) (*e.g.*, butyric acid, propionic acid and acetic acid), and by generating catecholamines in the lumen of the gut [107, 179]. Therefore, the effect of gut microbes on the MGBA can be studied by the manipulation of gut microbial community composition through the modulation of neurotransmitters, food, antibiotics, and probiotics.

The first step for designing molecular sensors and stimulators is to utilize the *in vitro* GOAC described in Sec. 6.3.2 as a development platform, where the microfluidic environ-

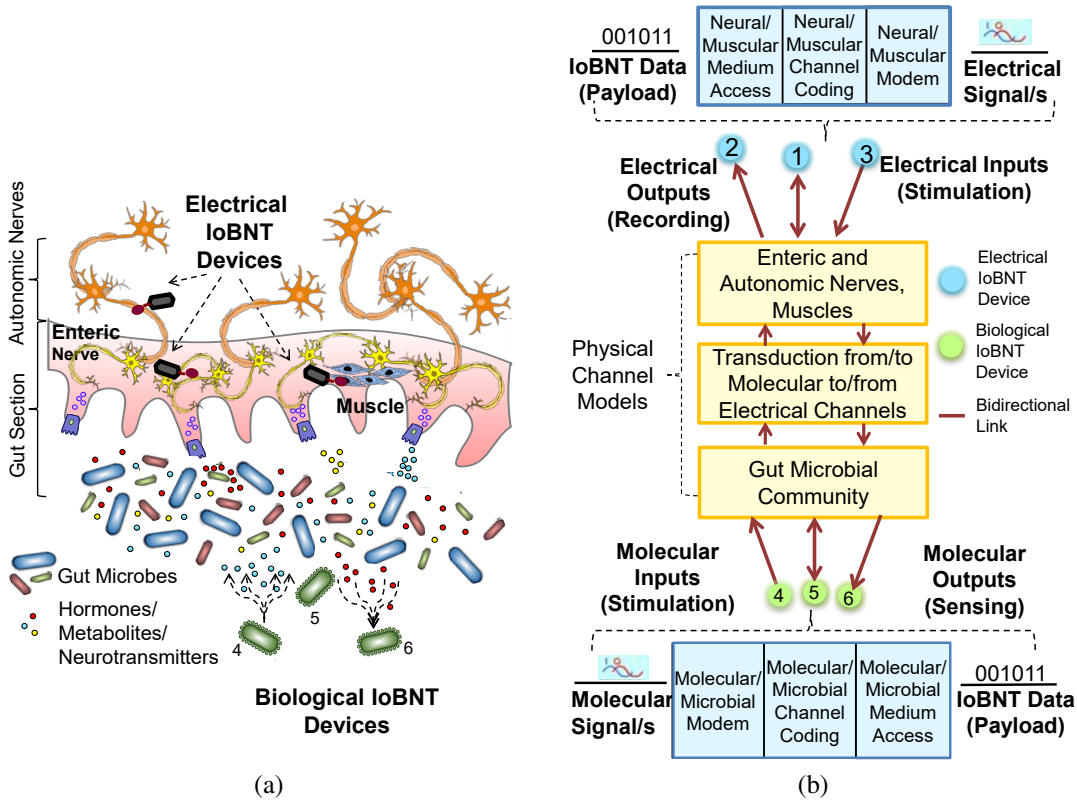


Figure 6.7: (a) The communication processes involved in MGBA stimulation and sensing. (b) The corresponding proposed physical channel models and IoBNT network infrastructure components.

ment allows to simulate the effect of the release of molecular signals to manipulate the microbial community composition in real time. While the optically transparent nature of the GOAC device will allow optical measurements and imaging, platinum surface electrodes integrated on the system can be used for electrochemical detection of molecules [180, 181] such as hormones, neurotransmitters, and metabolites in real time. Over multiple rounds of stimulation, the amount and kinetics of the interaction of molecules of interest with the microbial community can be analyzed in real time. To realize sensors able to test electrical to molecular channels, neurons will be stimulated using the electrodes within a range of frequencies and amplitudes, and the corresponding molecular sensors will be tuned to observe the corresponsing changes in the lumen by electrochemical sensors in terms of

concentration of hormones, neurotransmitters, and other relevant molecules.

In addition to the aforementioned interfaces, necessary to generate and transmit signals through the MGBA, supplementary capability of measuring additional pertinent information from the gut environment should also be included in the implanted electronics, with sensors to evaluate the correlation between the MGBA communications channels and other physiological parameters, such as stress-strain, pH, temperature, heartbeat rate, and blood pressure.

## 6.4 Internet of Bio-NanoThings Communication Network Infrastructure

To interconnect IoBNT devices through the MGBA channels investigated analytically and experimentally with the methodologies described in Sec. 6.2 and Sec. 6.3, respectively, a network infrastructure needs to be defined regulating access to resources for all biological and electrical devices as shown in Fig. 6.7-a. Resources in this context can be considered as the limited number and variability of molecules in the environment, the energy consumed by the devices for transmission and reception, and the transmission time and location clear of natural communications in the body. The components of this infrastructure constitute channel coding, medium access, and modulation/demodulation (modem) modules, tailored to the transmission of information via electrical or molecular stimulation, the propagation of information along MGBA, and the reception of information via electrical or molecular sensors, as shown in Fig. 6.7-b.

By jointly investigating neural/muscular and molecular/microbial medium access, channel coding and modulation in a cross-layer fashion, we aim to increase the data rate as high as possible to approach the theoretical channel capacity over MGBA channels determined by the models described in Sec. 6.2. The design of the infrastructure including these modules should generate electrical or molecular signal waveforms within the admissible input-output value and frequency ranges while minimizing delay and noise, and minimizing disruption to the natural communications in the MGBA necessary to maintain

its homeostasis (healthy state). Furthermore, the wired structures of neuronal communication and the wireless structure of bacterial communication should be exploited to develop a reliable addressing through the MGBA. By taking into account the peculiarities of the MGBA, in the following we will discuss the cross-layer design of electrical and molecular infrastructure components.

### 6.4.1 Electrical Infrastructure Components

The electrical infrastructure components are responsible for stimulating and sensing the electrical activity for electrical communications through channels based on enteric and autonomic nerves, where the underlying biological processes of electrical signal propagation will be leveraged to design novel modulation, channel coding, and medium access solutions for IoBNT. Considering the subthreshold communication described as in Sec. 6.2.1 over a single neuron as illustrated in Fig. 6.3, the sender should limit the current injected to the soma such that it does not create a membrane potential exceeding the threshold which in turn creates a "spike" to carry the information to the next neuron over the synapse [123].

If an amplitude modulation scheme is considered for this communication link, the modulator component of the sender should select current levels representing symbols within the subthreshold potential range [182] with the modulation depth limited by the subthreshold noise [134]. To avoid crossing the threshold, *i.e.*, interfering with natural communications, the medium access component should avoid the simultaneous transmission from multiple sources, whose input currents when summed up might create a membrane potential larger than the threshold. Besides, the channel coding component should increase the frequency of symbols corresponding to lower membrane potentials so that even when multiple signals are summed up, there is less chance of crossing the threshold. All these three modules should be jointly designed to accommodate more users with higher data rates while still keeping cross-talk to natural communications below the limit.

Furthermore, the synaptic transmission, which is the release of molecules called neuro-

transmitters by a pre-synaptic to a post-synaptic neuron capturing these neurotransmitters, brings a new dimension to the waveform design. Since in ENS, neurons operate with more than one type of neurotransmitter [183], the type of neurotransmitter can be used either to add one more dimension to the amplitude-frequency domain of modulation, or to assign different neurotransmitters to different users allowing simultaneous transmission over the same channel.

### 6.4.2 Molecular Infrastructure Components

The molecular infrastructure components are responsible for stimulating and sensing molecular activity to realize molecular communications through the gut mucosa and lumen, as described in Sec. 6.2.2, where the intestinal wall, gut microbial communities, and food intake contribute to the molecular composition of the gastrointestinal tract. The microbes' behavior in terms of uptake and consumption of chemical compounds, and their growth rate will be leveraged to design novel modulation, channel coding, and medium access solutions for IoBNT. Joint design of these three components is necessary due to the requirement of minimal disruption to natural communication occurring in the gut.

Keeping disruption to natural communications over MGBA at minimum for molecular signals translates into avoiding dysbiosis, *i.e.*, the disruption of microbial balance in the gut, which might cause severe diseases such as Crohn's disease or colorectal cancer [184]. Considering the microbial community structure described in Sec. 6.2.2, and illustrated in Fig. 6.4, the excess or lack of a chemical compound can interfere with the metabolic reactions, and in turn disrupt the growth balance of the community. To avoid a break in this balance, information should not be encoded on the properties of a molecular signal composed of probiotics promoting the reproduction of only one microbial species in the medium. If a concentration based modulation scheme is adopted where molecular signals are represented by chemical compound concentrations, the modulator should adjust the concentration levels such that any change in these will still transmit the information but not

disrupt the community structure [138]. The medium access module should also contribute to keeping this balance by regulating the simultaneous access to the chemical compounds while trying to give enough resources to all the transmitters for a timely and successful information delivery. Medium access control techniques tailored for molecular communication such as amplitude division multiple access and molecular code division multiple access schemes can be adapted to the MGBA environment to satisfy the aforementioned requirements.

### 6.4.3 Biomolecular Intrabody Network Simulator

A new simulator for heterogeneous intrabody communication networks should be developed as part of the framework to aid the design of MGBA-based IoBNT networks. This simulator will incorporate the physical channel models described in Sec. 6.2 and aid in the estimation of the performance of these channels as well as the aforementioned network infrastructure components in terms of attenuation, delay, noise, capacity, cross-talk and interference.

Even though several open-source network simulators exist today, such as ns-3 [185], these cannot be directly used for biomolecular intrabody communication because: (i) these simulators are built on top of well-defined propagation models for electromagnetic or acoustic communication, where instead we would require computational models describing the underlying biological processes; (ii) these simulators are developed with the classic network protocol stack in mind, where instead the limited capability of IoBNT devices will requite to design the infrastructure in a cross-layer fashion as discussed in Sec. 6.4.

The main challenges of a biomolecular intrabody network simulator are discussed below:

- *Computational models:* Considering the complex and massively interacting gut-microbiome structure, creating a complete model for simulating the gut, capable of accounting for all the microbial species and all the different tissues throughout the

nine meters of the gastrointestinal tract, poses a great challenge. Existing models, focusing either on a specific tissue or specific interaction in the gut, should be integrated to built a spatio-temporal multiscale representation of the gut ranging from nanoseconds to years and from molecules to systems. A challenge to achieve this goal stands in incorporating the complete physical structure of the gut and its potential changes to the models. Another challenge arises from the need of immense computational power and vast amounts of storage to run these computational models, which can be addressed by high performance computing.

- *Flexibility to design modulation, channel coding, and medium access schemes:* Considering the biochemical nature of signaling, a distinction between different communication stack layers is not as straightforward as in classical networking [1]. The simulator should provide flexibility to design modulation, channel coding, and medium access, as well as allowing cross-layer design for both electrical and molecular channels.

- *Performance evaluation:* To provide insightful results, the simulator is required to compute not only communication parameters such as delay and achievable rate, but also other parameters representing biocompatibility constraints and the constraints on the proposed devices such as measuring cross-talk with natural communications and metabolic burden on genetically engineered bacteria. The simulator should also be able to obtain results in multiple spatio-temporal scales as mentioned above.

## 6.5 Conclusion

This chapter of the PhD thesis presents fundamental challenges in the development of a self-sustainable and bio-compatible network infrastructure to interconnect the next-generation electrical and biological wearable and implantable devices, *i.e.*, Internet of Bio-NanoThings. Microbiome-Gut-Brain Axis is investigated as a possible infrastructure to build this net-

work of Bio-NanoThings inside the human body. The challenges and the requirements to realize the proposed infrastructure are addressed and the analytical and experimental methodologies are given as a roadmap for future studies. This novel communication concept using MGBA as an intrabody communication infrastructure will provide transformative bio-inspired communication systems and network architectures, with future impact on applications for health-care (*e.g.*, systems for advanced and perpetual tele-health monitoring and control).

# CHAPTER 7
# INTERNET OF BIO-NANOTHINGS FOR EARLY DETECTION OF INFECTIONS

## 7.1 Motivationd and Related Work

The state-of-the-art diagnostics, monitoring, and therapy in clinical settings are limited by the imprecise nature of current methods and use of devices that are either external, or when implanted, suffer from large size. A breakthrough is eminent since we are at a critical crossroad in bio-medical research in which our ability to miniaturize sensors and electronics is unprecedented, and our understanding of biological systems enables manipulation and control of behavior of cells. These technologies will be leveraged to create Internet of Bio-NanoThings (IoBNT), first introduced in [2], as a paradigm-shifting concept for communication and network engineering, which tackles challenges of developing efficient techniques for the transfer of information, communication, and networking within the biochemical domain, while enabling a connection to the electrical domain of the Internet through a bio-cyber interface.

IoBNT is envisioned to be a heterogeneous network of nanoscale bio-electronic components and engineered biological cells, so called *Bio-NanoThings (BNT)*, communicating via electromagnetic waves, and by molecular communication, as illustrated in Fig.7.1. The objective of this concept is to directly interact with the cells enabling more accurate sensing and eventually control of complicated biological dynamics of the human body in real time. The approach taken in IoBNT requires the engineered cells to sense, process, and communicate among each other and with external devices that provide remote and minimally invasive ways of interrogation in the IoBNT concept. The realization of IoBNT starts with the design of implantable submilimeter BNTs which are capable of sensing bio-

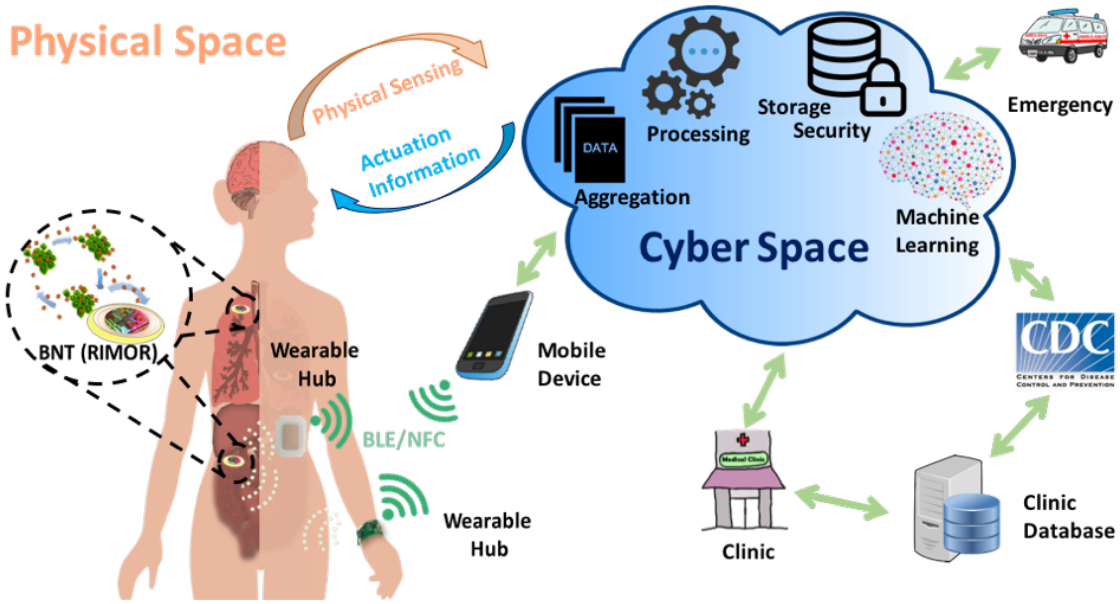


Figure 7.1: IoBNT Concept.

chemical information in the human body and transmitting the sensed information remotely to a wearable hub outside of the body.

In this chapter, we discuss how IoBNT concept may be applied to early detection and mitigation of infectious diseases. Existing technologies for the detection of infections are usually based on the culture of microbial organisms causing the infection found in the samples collected from the patients or using polymerase chain reaction (PCR) requiring bulky devices heating and cooling the samples and reagents for enzymatic reactions to identify the molecular structure of microorganisms. IoBNT framework separates itself from these existing technologies by enabling *in vivo* continuous monitoring of infections through implanted nanoscale sensors detecting communication among infectious organisms within the body. Then, these sensors report to a wearable mobile hub which forwards the collected data to healthcare professionals. Hence, the patient does not need to visit a laboratory to get tested and also infections can be detected early, even before symptoms appear, prompting the patient to seek medical advice. This way, the risk of premature death of vulnerable patients can be reduced.

Early detection of infections is very critical especially for cancer patients who are at

immuno-suppressive state after chemotherapy and vulnerable to serious infections which is a major reason for mortality. As another example, in the case of cystic fibrosis, a genetic disorder with no cure, mostly affecting lungs, infections occur wave by wave and cause the death of the patient. Thus, early detection of lung infections will improve both the quality of life of cystic fibrosis patients and increase their life expectancy. Moreover, detecting infections at an early stage in at risk patient populations will allow the timely administration of antibiotics and other drugs shortening the stay in hospital for treatment and decrease mortality [186], and both resulting in significant reduction in healthcare costs. In addition to this, with the rise of antibiotic resistance among infectious bacteria, treating infections is becoming more and more challenging for health professionals. Applying the wrong antibiotic delays the therapy and can reduce the survival rate as much as five-fold [187]. Furthermore, this IoBNT application can be used to track the efficiency of antibiotics.

This framework not only benefits individuals' health but also contributes to public health. In the case of an epidemic or pandemic, the continuous monitoring of infections provided by IoBNT systems is very valuable. Especially since they are already integrated with mobile devices and remote data analytics tools; IoBNT can be easily configured for tracking, tracing, and quarantining people.

The proposed system will continuously monitor the tissues at risk of serious infection to detect it earlier than conventional methods which requires culturing the bacteria in a laboratory to increase its quantity to detectable levels, which typically takes 48-72 hours [188]. While alternative molecular methods such as enzyme-linked immunoabsorbent assay (ELISA) and polymerase chain reaction (PCR) provide higher sensitivity and specificity within a shorter assay time, they require complex instrumentation and skilled operators limiting their use to clinical laboratories. As such, these methods are not suitable for continuous *in vivo* monitoring for early detection of infections.

The approach considered in this study is based on the proposed system eavesdropping on the quorum sensing (QS) communication among infectious bacteria in the tissue by

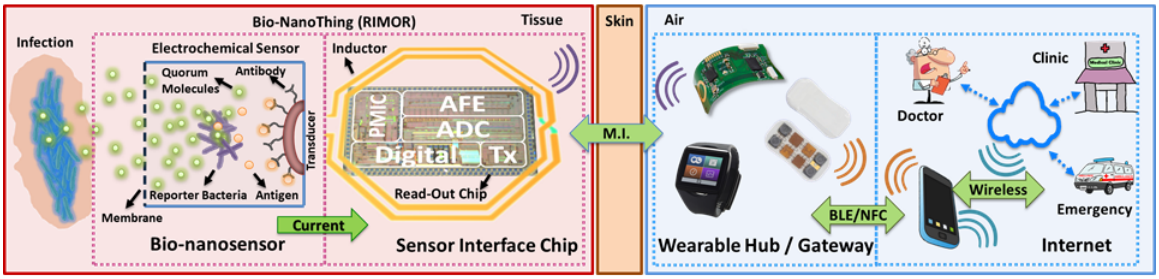


Figure 7.2: Overview of PANACEA System.

distributed BNTs which host electronic devices and highly miniaturized bio-sensors. QS is a method of communication where bacteria coordinate their behavior by exchange of molecules. By listening in to QS via BNTs, the spatio-temporal distribution of abnormally growing bacteria in tissue can be obtained to detect an infection even before the patient shows symptoms. QS signals are transformed into electrical signals measured and converted into raw data relayed through the coil/antenna to the wearable hub, which may come in the form of a patch, bandage, or smartwatch. The wearable hub forwards the raw data via access networks such as wi-fi or cellular systems to the Internet where it is processed and delivered to interested parties such as healthcare institutes and emergency services, and send an actuator information if required. Fig. 7.2 summarizes the overview of a design of IoBNT for infection detection application.

Besides the early detection of infections, we can use IoBNT framework to help us with the mitigation of infections by incorporating active and passive drug delivery systems. For passive drug delivery, external devices can be configured to release the pre-programmed drug recipe or send a message to patients to take the personalized medicine. For active drug delivery, a mechanism can be incorporated in the implantable devices to release drugs.

Although numerous studies have been conducted in IoBNT paradigm focusing on the communication and networking aspects, there is a lack of validation platforms. Implementing devices that can receive and process biochemical domain signals, i.e., the building blocks of IoBNT is not a trivial task. A broad expertise from various fields, such as genetic engineering of bacteria, bio-nano molecular sensing, and implantable and wearable bio-

interface designs is needed. Hardship of bringing a multi-disciplinary expertise makes it a daunting task for researchers. As a firs step of creating validation platforms for IoBNT, we introduce a novel design for a device serving as a BNT, capable of working in biological environment.

The research on IoBNTs will make contributions in many broad directions discussed in the following sections of this chapter which we divide into two, namely, development of Bio-NanoThings depicted in light of the advancements in synthetic biology and nanotechnology discussed in Section 7.2, and development of communication channels and networks among Bio-NanoThings and the Internet discussed in Section 7.3. Finally, we conclude the chapter by future research directions and challenges.

## 7.2 Development of Bio-NanoThings

The first aspect of the framework described in this chapter is the development of Bio-NanoThings which are main devices of IoBNTs. In this section, a realistic design solution for a hybrid Bio-NanoThing is described for the first time in literature and required features of BNTs for infection detection application are discussed. A BNT device, consists of mainly three parts: a bio-nanosensor, a sensor-interface chip, and a coil/antenna. BNTs can be utilized for detecting the quorum sensing signals of infectious bacteria and for wirelessly transferring the sensed data of infection to a wearable hub outside of the body as depicted in Fig. 7.2. The miniature BNT can be deployed both as implantable and wearable device in the body.

In this section, we focus on the design and fabrication of a novel sub-millimeter sized bio-nanosensor, its interface chip, and a coil/antenna as the components of BNT as illustrated in Fig. 7.2. First, we introduce various sensing modules and explain the methods of implementing the bio-nanosensor. Then, we move on to the design of ultra-low power interface circuits with wide range of sensing capabilities and high-efficiency wireless power transfer circuits along associated coil/antenna.

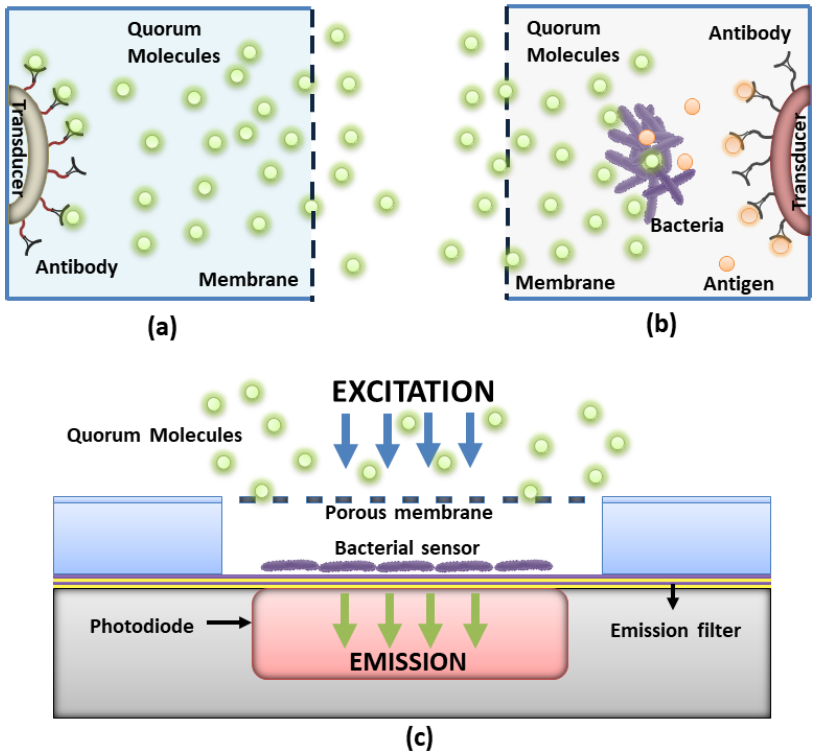


Figure 7.3: Bio-sensor with a) direct electro-chemical, b) bacterial sensor, c) optical measurement.

### 7.2.1 Bio-nanosensor

An infection is the invasion of various healthy human tissues by pathogenic bacteria that are multiplying and disrupting tissues' operation, causing diseases. To detect it with IoBNT, we design BNTs exploiting quorum sensing communication of bacteria infecting human body detected by bio-nanosensors. Quorum sensing is the major cell-to-cell communication mechanism where bacteria produce and release chemical signal molecules whose external concentration increases as a function of increasing cell-population density[189]. Therefore, by sensing the concentration of its quorum sensing molecules, it is possible to estimate the density of the infectious bacteria population.

There are many alternative ways to design the biosensor of BNT. An alternative method can be the direct detection of QS molecules of the bacteria of interest via antibodies [190] attached to a transducer, depicted in Fig. 7.3.a. Other methods include utilizing an-

other species of bacteria as a detector in the sensor. The engineered bacteria of the bio-nanosensor sense MC signals generated by the infectious bacteria and catalyze a chemical process to produce an electro-active product [191], as depicted in Fig. 7.3.b or produce light detected by the transducer which converts light into electrical current, depicted in Fig. 7.3.c.

Researchers widely utilize bacterial sensors with engineered synthetic pathways for molecular sensing [192]. The main advantage of bacterial sensors is that they are equipped with membrane receptors evolved to interact with the target of interest with high sensitivity and specificity. In the bacterial sensor, a genetically engineered *E. coli* K12 strain, which is harmless to human, can be employed to bind to QS molecules and produce an optical signal as bio-luminescence/fluorescence or molecular signals easy to be detected by electrochemical sensors. An *E. coli* strain either expresses the lux genes (light output) or catalyzes a chemical process to produce an electroactive product (chemical output). For physical transduction, electrochemical, mass-based, magnetic, or optical approaches can be evaluated and compared for the highest achievable specificity and sensitivity.

In this study, we elaborate on bacterial sensors for QS with light output and optical transducers, both already having established design processes. The design of bio-nanosensor has two steps. First step is designing a microfluidic reservoir that harbors the bacterial sensor colony. The reservoir should be sealed with a porous membrane with pores small enough to entrap the bacteria while allowing diffusion of QS molecules. Second step is designing an optical transducer that consists of light emitting diodes for excitation and a photo-diode array placed in close proximity of the colony to detect low levels of fluorescence emission from the bacterial sensor colony. Over the photo-diode array, a distributed Bragg reflector that specifically blocks the excitation wavelength to maximize the sensitivity, can be constructed. Finally, the bacterial sensors needs to be introduced into the chamber and immobilized on the functionalized surface.

From micro-electro-mechanical systems' perspective, to develop the proposed bio-

nanosensor architecture, there are many challenges to be tackled: (i) *Bacterial sensor growth:* Ideally, we would like to have a constant number of live bacterial sensors that only as act chemical transducers. Live bacteria however replicate. Hence, keeping the bacterial sensor population steady within the reservoir is a major challenge. (ii) *Bacterial noise:* Live bacteria interact with the environment and adapt. Therefore, the effect of stochastic behavior of bacteria on the sensor performance should be analyzed. There are approaches to address these challenges, namely, physical and chemical means for population control. Physical approaches include use of confinement of bacteria mechanically [193], thermally [194] or optically [195]. Mechanical confinement makes use of membranes to force a monolayer of bacteria. Thermal control is based on joule heating through integrated heaters on the perimeter of the colony. Likewise, structured UV illumination is used to inactivate bacteria in the perimeter regions. For chemical control, bacteriostatic antibiotics such as tetracycline as well as selectively patterned antibacterial coatings such as silver nanoparticles [60] are other alternatives to balance the death and reproduction rate within the bacterial colony. (iii) *High sensitivity:* The overall sensitivity of the system will depend on the efficiency of individual transduction steps and their integration. To optimize device sensitivity, the bacteria strains that produce more fluorescent molecules per sensed quorum sensing molecule through evolution should be identified. Photodiodes, and the filter can be designed to help minimize cross-talk. An array of photodiodes under the colony as well as use of lenses to focus light from large area bacteria population onto the photodiodes might also help to solve this challenge. (iv) *Specificity:* It should be confirmed that the detection is specific to the molecule of interest. Bacteria species have diverse quorum sensing molecules ranging from N-acyl homoserine lacton (AHL) molecules for Gram-negative bacteria to modified oligopeptides (autoinducer peptides, AIP) for Gram–positive bacteria. Bacterial sensors are genetically engineered to only respond specifically to the quorum sensing molecule of interest unique to the infectious bacteria that is being detected. Hence, many bacterial sensors developed for biological studies of quorum sensing

can be incorporated in the bio-nanosensor alleviating the specificity challenge.

### 7.2.2 Sensor-Interface Chip

To increase the reliability of the infection detection system in the decision making mechanism, we consider to have more than one modality. Therefore, a multimodal-sensing paradigm, incorporating both optical (florescence/bioluminescence) and electro-chemical sensing mechanisms, that maximizes both sensitivity and specificity of BNTs should be adopted. Even though florescence/bioluminescence has been studied extensively and used in various biomedical applications [196, 173, 197, 198, 199], detection of low light is still a key challenge. Similar to low light detection, in electrochemical sensing, it is required to detect ultra-low current levels on the order of picoamperes to nanoamperes [200], which should be considered in conjunction with ultra low power requirement in an implementable medical device (IMD). In an effort to minimize the heat generated in the wireless power delivery and management blocks, and prevent possible tissue damage in compliance with regulatory requirements, such as specific electromagnetic power absorption limits [201, 202] a low $\mu$W-level sensor-interface chip is necessary. Considering these requirements, the sensor-interface chip has mainly four parts:

*Analog front-end (AFE)*

AFE circuit, which interacts with bio-nanosensors, requires a current and/or impedance detection circuit with wide range sensing capability and high linearity performance preferably at various frequencies [171]. Another important issue for the AFE circuit is the adaptation of the electronic system to biological systems. The timing between two appearances of a biological event may take a very long time, *i.e.*, minutes or even hours range. Furthermore, this may happen very slowly. Therefore, the electronic system should be capable of long integration time [173]. At the same time, aggressive duty cycling that significantly reduces the average power consumption of the circuit down to low $\mu$W level should be deployed.

Beside low power sensing and long integration capability, to minimize the effect of in-body noise to the sensed data, the AFE circuit should be very low noise.

*Analog-to-digital converter (ADC)*

specific absorption rate (SAR) ADCs are among the lowest power consuming architectures with amazingly low 0.88 pJ per conversion levels reported in [203]. However, to achieve both low power and high resolution, they occupy a large area on chip. Delta-sigma ADCs can achieve high resolution at relatively low power levels and very small foot-prints [204]. However, they need high clock frequency and generate large data volume those need to be decimated in the digital domain. Existing ADC circuits need a trade off between large-area occupation and low-power consumption. In [158], on the other hand, researchers sensed fluorescence produced by bacteria through a simplified discrete-time comparator-based ADC, which quantifies with threshold crossing. A solution for BNT might be a new hybrid ADC architecture by combining the ultra-low power highly popular SAR architecture for most significant bits (MSB), with high resolution and and small foot-print delta-sigma modulation for the least significant bits (LSB) [205].

*Power management IC*

In this proposed system, the wireless reading range of BNTs is projected to be more than 15 cm, so that the physicians are able to eventually implant BNTs at a desired location within the body. Therefore, the anticipated amount of delivered power even after optimization of the multi-coil wireless power transmission (WPT) link [206, 207] would be around several tens of $\mu$W. This is a major challenge but not a major concern, because the operating frequency in bacterial sensing systems is in Hz range. Thus, in an adaptive heavily duty-cycled architecture, it is possible to build an extremely efficient charging mechanism to harvest the low incoming electromagnetic energy from the wireless power link, store it in high charge density, yet very small off-chip capacitors - boosting the voltage level [208,

209] - and use it over a short period of time when the bio-nanosensors are activated, the AFE conditions/pre-processes the acquired signals, the ADC samples and digitizes them, and the back telemetry link send the resulting data to the wireless/wearable hub outside the host body.

*Wireless data transmitter*

Following ADC, digitized optical and biochemical signals are compressed, packetized, and wirelessly transmitted from inside the host body to the external wearable Internet hub. Since the available power to the BNTs will be limited to $\mu$W level, load shift keying (LSK) or passive back telemetry can be incorporated. Beside the back telemetry switch, the data communication block includes forward data modulation, encoding, and encryption (if necessary) to improve data integrity and security. Since the optimal power carrier frequency might be in the range of hundreds of MHz range, the L and C values are much smaller; therefore, the back telemetry link can offer a much higher bandwidth than what has been demonstrated in the traditional 13.56 MHz RFID links. In this system, a high bandwidth is not desired because of transmitting high volume of data. Instead, it is desired to apply aggressive duty cycling and the need to send small amount of collected data in a very short period of time. Using impulse-radio based transmission, which eliminates carrier signal to save power, is an alternative mean of data transmission which can be incorporated in this IoBNT application.

### 7.2.3 Coil/Antenna

WPT plays an increasingly important role in energizing IMDs that are either too small or inefficient for primary batteries to power [210]. Although researchers have considered powering smaller IMDs via ultrasound, laser, and ultra-high frequency (UHF) fields [211], WPT to IMDs is still considered the safest and most reliable technique to establish power/data link between one or more transmitter (Tx) and one or more receiver (Rx) coils

that are electromagnetically coupled in the near field [212, 213, 214]. Since these IMDs are small and arbitrarily placed, the design of an electromagnetically coupled WPT link poses a great challenge. The link should deliver enough power to the load (PDL) while ensuring that the temperature and human body exposure to electromagnetic (EM) field remain within safe limits. EM exposure is defined by the specific absorption rate (SAR) that should not exceed 1.6 W/kg for safe operation within 3 kHz  300 GHz band [202]. The essential components of WPT are coil and antenna. Hence the design of coil/antenna needs special concentration. The operating frequency, $f$, and the EM field intensity strongly impact the Tx-Rx coil/antenna geometry design, power source characteristics, power transfer efficiency (PTE), and PDL. In an effort to increase the received power on a small mm-sized in-body coil, the optimization of the coil design and the choice of $f$ are key aspects of the overall design.

Power efficient and reliable energy harvesting and wireless communication links based on magnetic induction requires a precisely designed miniaturized coil to connect BNTs to the wearable hub, which is a key challenge.

### 7.3 Communication Networks Among Bio-NanoThings

Since the severity of infection is directly related to the amount of infectious bacteria, it is the target to be detected using BNTs, described in Section 7.2. To this end, we consider quorum sensing (QS) of bacteria as an indicator of infection. QS is a cell-to-cell communication mechanism where bacteria produce and release chemical signaling molecules whose concentration reflects bacterial cell density [215] as explained in Section 7.2. By measuring the spatio-temporal concentration of QS molecules unique to target bacteria by a network of submilimeter sized BNTs deployed in tissues in large numbers, we can estimate the amount of infectious bacteria and learn about the progress of the infection.

QS communication of bacteria can be abstracted using molecular communication theory which studies the information exchange through emission, propagation, and reception

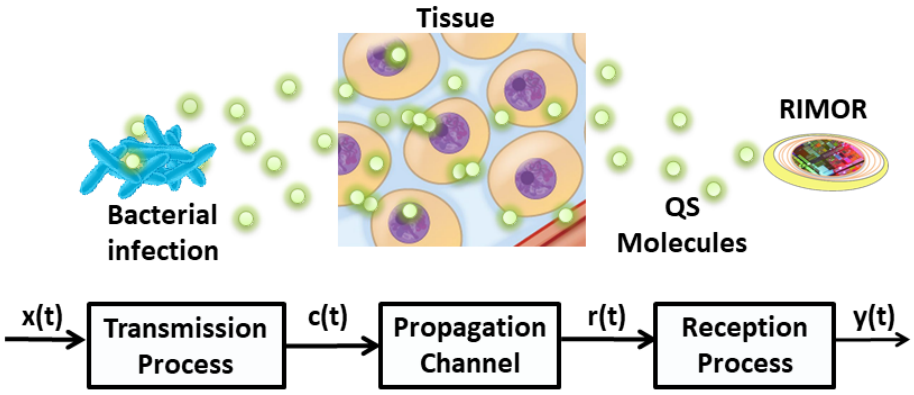


Figure 7.4: End-to-end model for MC Channel for infection.

of molecules [1]. MC theory focuses on the biological communication mechanisms based on transport of molecules for the information flow among biological cells, tissues, and organisms spontaneously evolved in nature. According to the transport media, different channel models can ve devised such as diffusion-based, flow-based, and molecular motors [112, 216, 217, 218]. Our prior works on bacteria-based molecular communication specifically on how to use bacteria as biotransceiver device for MC [219] and as active message carriers [220, 221]. MC paradigm helps with modeling the principles of multi-scale molecular and biological phenomena realistically without the over-complication of system biology models, and the limitations of experimental approaches. MC abstraction of QS helps us to model and analyze the propagation of QS molecules from the infection site to BNTs providing us a tool to estimate the original location and amount of bacteria at the infection site.

### 7.3.1 MC Channel for Infection

The amount of infectious bacteria can be considered as the message transmitted by the concentration of QS molecules diffusing through tissue reaching BNTs. This channel can be represented with an end-to-end model similar to [112] as shown in Fig. 7.4.

The first process in this MC channel is the transmission process, i.e., production and release of QS molecules by infectious bacteria. This QS mechanism can be modeled by

one of the many QS models [222] considering a population of bacteria as a single entity and abstracting all the intermediate biochemical reactions to reduce the system to a set of coupled nonlinear differential equations. In the transmission process, the differences among individual bacterium in a population and the random spatial distribution of bacteria can be introduced as noise sources.

The next step is the propagation process, i.e., the transport of QS molecules through the tissue where they diffuse through the cells and in fluid between the cells. As a starting point, only local infections where infectious bacteria is yet to reach bloodstream are considered. The movement of small molecules such as QS molecules in the interstitial space (small spaces between biological structures) occurs by diffusion and convection modeled by the general mass transport balance depending on the flow velocity of the interstitial fluid, the diffusion coefficient, and the reaction rates that account for consumption, degradation and binding to the cells. The values of the transport coefficients are determined by the structure of the interstitial space and the physicochemical properties of QS molecules.

Unlike the previous studies on diffusion-based MC model [112], which is analogous to free-space channel model in wireless communication, the transport in interstitial space is more complex where QS molecules should navigate around the cells, diffuse inside and outside of cells that is analogous to channel models with multipath, shadowing, reflection and refraction in a crowded environment. The noise for the propagation process arises from the random nature of diffusion and the dynamic properties of interstitial fluid such as flow rate and pressure.

The last step is the reception process where QS molecules arrive to the vicinity of BNTs and may be detected by the bio-nanosensors. As decribed in Section 7.2 bacterial bio-nanosensors which sense the concentration of QS molecules by the receptors of bacteria coupled to generation of bioluminescence and/or fluorescence detected by photodiodes constitute the MC receivers. The speed of this signal transduction is limited by the time required to produce bioluminescence, fluorescence or electroactive proteins (reporter). The

delay arising from this phenomena can be compensated by a very sensitive photodiode that can even detect one reporter protein.

To estimate the number of bacteria from the concentration measured by BNTs, we need to fully understand all these three processes, and analyze the delay, the attenuation and the noise of each process. The delay and attenuation models dictate the sensor and receiver design to maximize the infection detection. The capacity of this MC channel derived using the models describing these processes and the respective noises represent the accuracy of the estimation of infection.

In a more realistic infection scenario, multiple tissues in an organ might be infected simultaneously creating multiple transmitters at different locations. However, BNTs can sense a limited area around themselves. Hence, multiple BNTs can be deployed to monitor multiple transmitters in a larger area. This resembles a MIMO MC system with multiple transmitters and multiple receivers as shown in Fig. 7.5. QS molecules follow different paths while arriving to different BNTs located far from each other. Hence, the received QS concentrations experience different delay and attenuation profiles. By combining the data sensed by all BNTs, it is possible to more accurately detect the level of infection and generate a map of probable infection locations. By exploiting these multiple channels, novel localization techniques can be developed for MC that will indicate the infection sites in this scenario. This MIMO model is also useful to determine the locations and the amount of BNTs that is needed to implant in the body for an efficient detection and whole coverage of organs at risk.

### 7.3.2 MC Channel for Drug Delivery

To create a closed loop system, the proposed IoBNT application can include an actuator mechanism implemented in a passive or an active drug delivery form. For passive drug delivery, humans in the decision loop can be incorporated by including healthcare providers' opinions into the delivery logic. According to that, an external device that releases the pre-

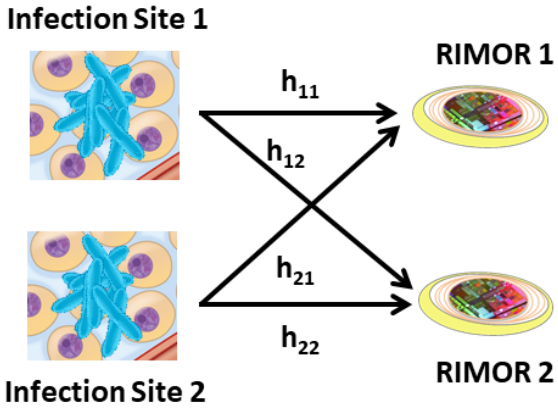


Figure 7.5: End-to-end model for MC Channel for infection.

programmed drug recipe or sends a message to patients to take the personalized medicine might be configured. For active drug delivery, a drug can be released directly from BNTs or the wearable hub. As an extension of QS eavesdropping concept, another alternative actuator mechanism is quorum quenching, i.e., prevention of quorum sensing by disrupting the signaling. By interrupting their quorum sensing communication and preventing quorum sensing controlled virulence mechanisms, infectious bacteria may be prevented from infecting healthy tissues [223].

Besides modeling bacterial infection, MC paradigm has also been used for modeling drug delivery systems (DDS) as an abstraction of the propagation of drug particles in the body [224, 225] which can be used for the mitigation of infection by administering antibiotics. By bringing abstractions traditionally used to characterize the functions of networking and computing systems, MC can formulate DDS problems in a way to be tackled with the mathematical tools used in communications, such as stochastic analysis, information theory and control theory. The biodistribution of drugs through the blood vessels is modeled with particle advection and diffusion combined with other physicochemical processes such as absorption, reaction, and adhesion. However, this model studies only the drug injected in blood vessels. Other passive drug delivery methods such as orally administered antibiotics requires the abstraction of absorption of drugs through gastro-intestinal system and mixing in the blood from MC perspective. For active drug delivery systems

such as implanted and dressing/patch drug delivery, the controlled drug release should be incorporated into MC paradigm.

## 7.4 Communication of BNT Networks with Internet

BNT networks are composed of mixed types of devices such as electronic and cell-based, as well as various types of communication such as MC and near field communication as shown in Fig. 7.2. In order to enable IoBNT operation, the realization of the interfaces between different domains is essential. This will provide the seamless interconnection of cyberspace and the biological environment towards the ultimate goal of "cell-connected-to-Internet".

The most challenging interface in IoBNT is the transduction of MC signals into electrical signals, which can be realized by RIMORs, where the sensor bacteria receive MC signals in the form of QS molecules and generate bioluminescence and/or fluorescence that is captured by photodiodes creating a current. Since this interface is dependent on the sensor bacteria, it is acquiring the inherent noisy behavior of biological systems. Furthermore, since sensor bacteria need time to produce bioluminescence and/or fluorescence proteins, this interface adds delay on top of the already large propagation delays in MC.

Another challenge is that MC networks require their own protocols due to peculiarities of MC channels and the limited computation capability of MC devices. The networking protocols for MC are extensively studied such as the TEC-SMART MAC protocol, amplitude source addressing. The next challenge for heterogeneous IoBNT networks is to find a solution to integrate these protocols with conventional network protocols on cyber side of IoBNTs. It is critical to develop novel protocols for IoBNT networks satisfying the requirements of both the molecular world and electrical world of networks.

After being converted into electrical signals, the data coming from MC channels is forwarded to outside of the body by BNTs to a wearable hub using near-field communication techniques. Magnetic-induction, ultrasound or radio frequency can be used to ensure both

the data and power delivery to the implanted BNTs. This wireless and wearable controller hub is responsible to transmit data received from BNTs to the Internet. Standard protocols such as BLE or NFC can be used for data transmission. A compact flexible printed circuit board (Flex-PCB), which can be easily attached to the body in the abdominal area, e.g. in the form of a patch, close to where BNTs are implanted, or a device similar to a smart watch can form the wearable hub.

## 7.5 Simulation Results

In this section, we quantitatively illustrate the feasibility of the IoBNT framework described in the previous sections targeting specifically infections caused by *Pseudomonas aeruginosa (P. aeruginosa)* bacterial species, a leading cause of hospital-acquired infections.

*P. aeruginosa* is resistant to a large spectrum of antibiotics and can infect various organs such as lungs, urinary tract, kidney, and skin [226] which can even lead to death [227]. *P. aeruginosa* infections affect the most the patients who are struggling with other diseases such as cancer, cystic fibrosis and burns, thus with weak immune system. Infection in cancer patients is associated with 8.5% of all cancer deaths at a cost of $3.4 billion per year [228]. Most of cystic fibrosis patients are infected by *P. aeruginosa* which by the time they reach the age 7 and after that they suffer chronical lung infections increasing the rate of mortality [229].

In clinical laboratories, plate culturing is used to determine the presence of *P. aeruginosa* in the samples collected from the patients. Plate culturing is the gold standard for bacteria detection which is the method of multiplying bacteria inoculated in Petri dishes with predetermined culture mediums for identification of the species. Typically, it takes *P. aeruginosa* 16-24 hours to grow from streaking onto plates in rich medium [230]. The aim of our simulations is to show that in case of an infection, the IoBNT framework discussed in this study can detect the presence of the bacteria earlier than 16-24 hours time period to be considered as an early detection.

For the simulation scenario, we consider a wound infection where bacteria first attach to damaged skin and colonize the wound which is pretty common in burns [231]. During the growth of bacteria in the wound, quorum sensing is fundamental to the initiation, propagation, and maintenance of acute *P. aeruginosa* infection. Quorum sensing molecules for *P. aeruginosa* are the autoinducers 3-oxo-C12-homoserine lactone (3-oxo-C12-HSL) and N-butyryl homoserine lactone (C4-HSL) [232]. These QS molecules are produced proportional to the bacterial density, i.e., the strength of the infection.

We simulate the diffusion of quorum sensing molecules (QS molecules) in soft tissues near damaged skin as the MC channel described in Section 7.3 to determine the amount of QS molecules reaching the BNTs. Then, we calculate the time it takes for the BNTs to detect alarming amount of QS molecules indicating the start of an infection to demonstrate that the proposed IoBNT framework in this chapter has potential for early detection of infections.

### 7.5.1 Bacterial Growth and Quorum Sensing

During infection, *P. aeruginosa* adheres to the epithelium of the skin and starts to reproduce and release toxins penetrating into the body through the cells of the skin or through the gaps in between the damaged cells of the wound [231]. With the activation of quorum sensing which encourages the accumulation of *P. aeruginosa*, the destruction of the epithelium begins which will no longer act as a barrier against the entry of bacteria in the tissues and later into the bloodstream.

The growth of infectious bacteria in a wound follow the logistic equation [233] expressed as

$$\frac{dN}{dt} = rN\left(1 - \frac{N}{K}\right), \tag{7.1}$$

where $N(t)$ represents the bacterial population density, $r$ is the bacterial growth rate, and $K$ is the carrying capacity [234].

Assuming quorum sensing is already activated in the initial colony of bacteria, the QS

molecule production can be expressed as

$$\frac{dA}{dt} = D_w \nabla^2 A + kN - \beta A, \tag{7.2}$$

where $A(t)$ represents the QS molecule concentration, $D_w$ corresponds to the diffusion of QS molecules in the wound, $k$ is the production rate of QS molecules, and $\beta$ is the degradation rate of QS molecules [233]. Since we are considering a small wound on surface, we will assume that bacteria is homogeneously distributed in the wound and QS molecules do not diffuse within the wound, hence we assume the first term in (7.2) is $0$.

### 7.5.2 Molecule Transport in Tissues

Cells receive nutrients and oxygen from blood and emit waste, metabolites, and carbon dioxide into the extracellular space, i.e., the volume outside cells in tissues filled with interstitial fluid into which cells and blood vessels are embedded. In some tissues, the extracellular space also contain extracellular matrix composed of materials such as collagen and fibers providing a structure for cells to adhere. This complex structure impedes the transport of molecules through the tissues.

In molecular communication theory, the most used transport equation is free diffusion of molecules in a semi-infinite space [3]. The channel models, inter-symbol interference expressions, noise models, and detection algorithms are mostly based on unrestricted movement of molecules. However, in biological environments, especially for *in vivo* applications, molecules are always found in a confined environment surrounded by biological cells hindering their diffusion by acting as obstacles. Therefore, in this study, we consider the more realistic diffusion in porous medium which can account for the diffusion of molecules in tissues through the interstitial fluid in between the cells constituting that tissue [143].

As seen in Fig. 7.6, cells in the extracellular space can be very dense leaving very small

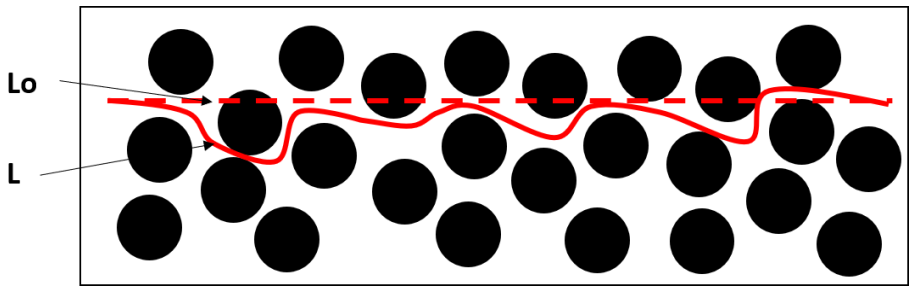


Figure 7.6: Diffusion in porous medium.

space for the interstitial fluid flow which is often modeled with Darcy's Law describing fluid flow through a porous medium. In that case, the transport of molecules in extracellular space is due to both diffusion and convection of molecules.

The propagation of quorum sensing molecule concentration in tissues is described by mass transport equation in porous media as

$$\frac{\partial C}{\partial t} = \frac{D}{\lambda^2} \cdot \nabla^2 C + \frac{Q}{\alpha} - \frac{f(C)}{\alpha} - v \cdot \nabla C, \tag{7.3}$$

where $C$ corresponds to the concentration of the quorum sensing molecule, $D$ is the diffusion coefficient, $\lambda$ is the tortuosity, and $\alpha$ is the volume fraction. The term $f(C)$ represents the clearance, loss, and uptake [235].

The structure of the tissue is represented in the transport equation (7.3) through two non-dimensional parameters, namely, the volume fraction $\alpha$, and the tortuosity $\lambda$. Volume fraction is defined as

$$\alpha = \frac{\text{volume of ECS}}{\text{volume of tissue}}, \tag{7.4}$$

which describes the geometry of the ECS as a diffusion medium. Tortuosity is a complex measure of how cellular obstructions are hindering the diffusion incorporating several geometric effects and the interstitial fluid viscosity. Often, tortuosity is determined empirically using

$$\lambda = (D/D^*)^{1/2}, \tag{7.5}$$

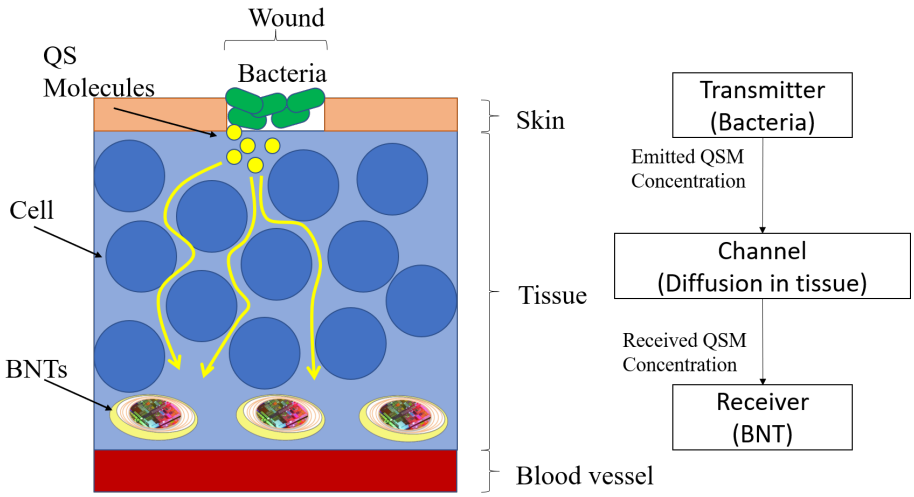


Figure 7.7: MC channel for infection detection.

comparing the diffusion coefficients in free solution to that in obstructed medium determined with experiments [236].

Using the above-mentioned porous diffusion theory, we are considering the molecular communication channel for infection described in Sec. 7.3, where the transmitter is the infectious bacteria emitting QS molecules and BNTs are receivers in a wound environment as shown in Fig. 7.7. We consider a cross-section of soft tissue with a wound on the skin hosting bacteria. As the bacterial population increases, the concentration of QS molecules also increases and these molecules diffuse through the tissue arriving the BNTs where they are captured by ligand-binding. Upon capturing QS molecules, BNTs measure the concentration of QS molecules and report to the wearable hub if a critical threshold is reached.

### 7.5.3 COMSOL Simulations

To simulate this MC channel, we use COMSOL which is finite element based multiphysics simulator capable of both simulating the growth of the bacteria and the propagation of QS molecules in the given simulation geometry. The physics interface of Transport of Diluted Species is used for the diffusion of QS Molecules in 2D. The simulation domain

implemented in COMSOL is shown in Fig. 7.8 for a 1 mm x 1mm soft tissue.

The initial bacteria population in the wound is modeled to be contained in the skin and the BNT of 0.1 mm x 0.1 mm is placed at (500 $\mu m$,200 $\mu m$) in the middle of the domain towards the blood vessel. To be able to evaluate the porous diffusion equation given in (7.3) in this domain, the boundary conditions should be set. The first boundary condition is at the interface of skin with tissue at y= 1 mm. Since QS molecules are only diffusing through the tissue and not towards outside of the body, we set a no flux boundary condition expressed as

$$\frac{\partial C}{\partial t} = 0, \qquad \text{at y= 1 mm.} \tag{7.6}$$

The second boundary condition is for the tissue/blood vessel interface at y= 0 mm. Here, we assume that all the QS molecules reaching this interface are washed away by bloodstream. Hence, we set a zero concentration boundary condition expressed as

$$C = 0, \qquad \text{at y= 0 mm.} \tag{7.7}$$

Also, we have assumed that initially there is no QS molecules in the tissue which corresponds to a zero concentration initial value in the domain expressed as

$$C(x, y) = 0, \qquad \text{at t=0 sec.} \tag{7.8}$$

The simulation parameters are the diffusion coefficient of the QS molecule for ***P. aeruginosa***, $D = 4.3 \times 10^{-11}\ m^2/s$, the bacterial growth rate, carrying capacity, $K = 3 \times 10^9\ cells/ml^{-1}$ , $r = 0.6\ h^{-1}$, QS production rate, $k = 74000\ h^{-1}$, QS degradation rate, $\beta = 600\ h^{-1}$ [233].

Furthermore, we assumed that $f(C) = 0$ since the loss of QS molecules in the tissue is negligible when there is a high production during the infection. Also, the velocity of the interstitial fluid, $v$, is assumed to be $0$ since interstitial fluid flow rates are very small and

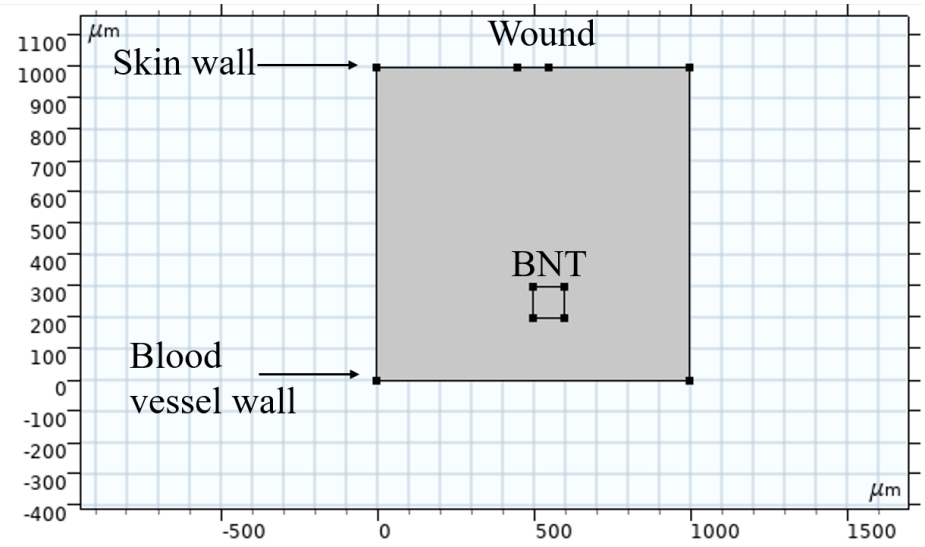


Figure 7.8: COMSOL simulation domain.

the transport is mainly dominated by the diffusion and not the convection [143].

In Fig. 7.11, the QS molecule concentration distribution in the field after 8000 sec is shown. This illustrates how QS molecules are propagating towards BNTs. To understand the impact of the porous diffusion and the tissue structure, we have plotted the concentration at the BNT with respect to time for varying volume fraction and tortuosity parameters.

In Fig. 7.9, the concentration of QS molecules with respect to time is plotted for a constant tortuosity, $\lambda = 1.45$, and for two values of volume fraction $\alpha = 0.25, 0.5$. It is observed that the higher the volume fraction, the lower the QS concentration at the receiver. Since the total tissue volume considered is fixed, the higher volume fraction corresponds to a larger volume of extracellular space as defined in (7.4) creating more possibilities for QS molecule to diffuse which in turn results in lower number of molecules reaching the receiver.

In Fig. 7.10, the concentration of QS molecules with respect to time is plotted for a constant volume fraction, $\alpha = 0.25$, and for two values of tortuosity, $\lambda = 1.45, 1.75$. It is observed that the higher the tortuosity, the lower the QS concentration at the receiver. The tortuosity depends both on geometry and viscosity of the diffusion medium. A higher value for tortuosity corresponds to a lower effective diffusion coefficient. Hence, in Fig. 7.10, it

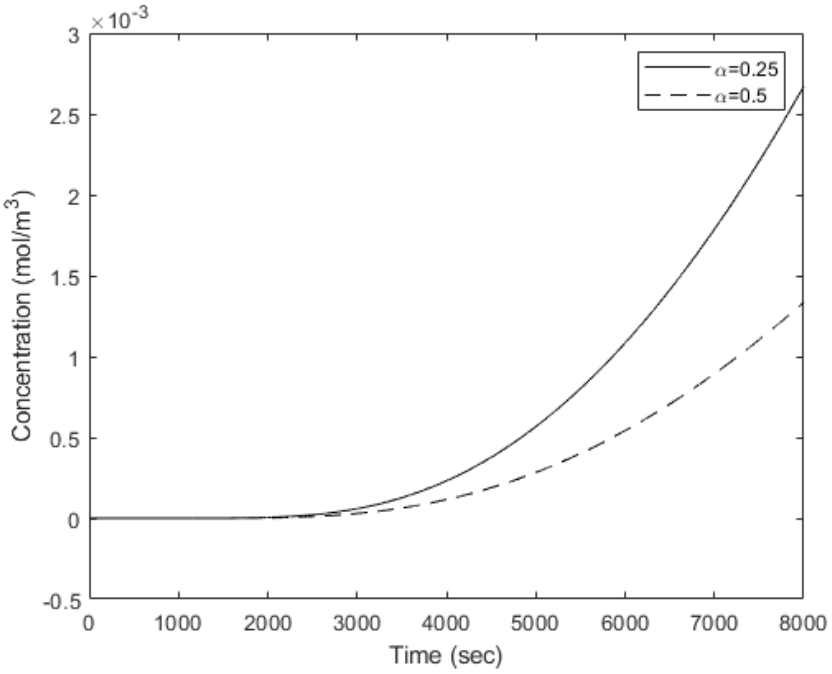


Figure 7.9: QS Concentration at BNT for varying volume fraction.

is observed that a higher tortuosity value corresponds to a lower QS concentration at the receiver.

### 7.5.4 Infection Detection Time

In previous sections, we have simulated the QS molecule concentration at the receiver, i.e., BNTs in a tissue environment. As described in Section 7.2, BNTs are equipped with QS sensors. In the literature, there are sensors specific for the QS molecules of *P. aeruginosa* reporting minimum detectable concentrations around 100 nanomolars which corresponds to $10^{-3}\ mol/m^3$ [237]. Therefore, a concentration above this level is deemed measurable by BNTs.

Even though we have bacteria in and on our body, not all of them are causing infections. However, a continuous logistic growth with concentration exceeding $10^5$ CFU/ml is considered as abnormal growth leading to infection for *P. aeruginosa*. During the simulations, we observed that this critical threshold corresponds to approximately a $2 \times 10^{-3}\ mol/m^3$

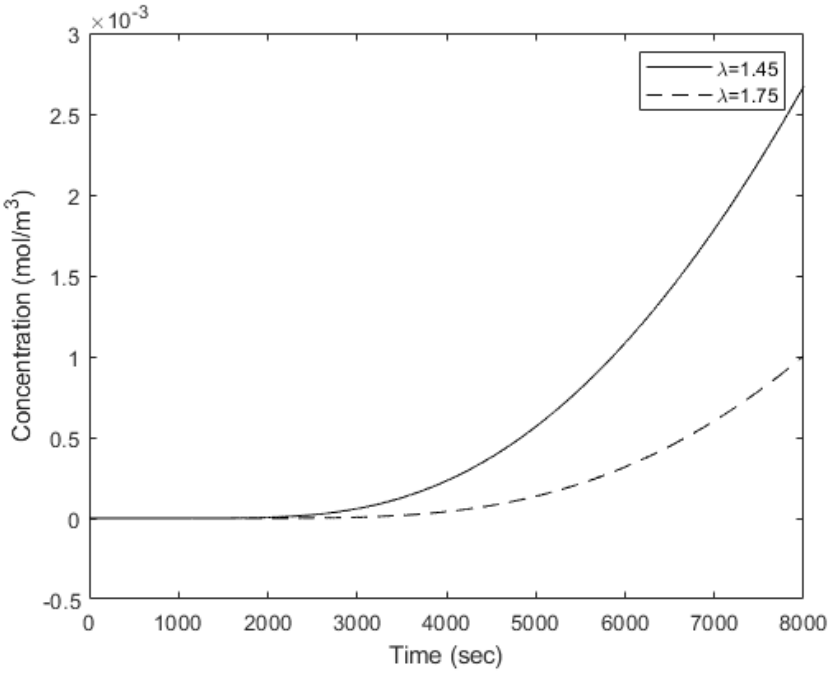


Figure 7.10: QS Concentration at BNT for varying tortuosity.

for the given BNT distance to the wound.

In both Fig. 7.9 and 7.10, it is observed that the threshold $2 \times 10^{-3}\ mol/m^3$ is reached in a time interval of [6000,7000] sec. Therefore, BNTs can detect the infection of *P. aeruginosa* in 1.5-2 hours after the start of infection. Compared to 16-24 hours required for the culture of *P. aeruginosa* for lab test. Our proposed framework can detect infections earlier than lab tests.

The detection time of 1.5-2 hours found for this scenario may vary according to infected tissue structure, the distance of BNTs to the infection site, and diffusion properties of QS molecules, and may be higher or lower for different systems. However, by utilizing the various detection techniques devised for molecular communication in the literature, it is possible to improve the detection times. Another improvement might come from the compensation of interpersonal variations since every patients body is unique. Hence, a calibration of the sensors at the time of deployment can be also used to improve the detection efficiency and speed paving the way for personalized medicine.

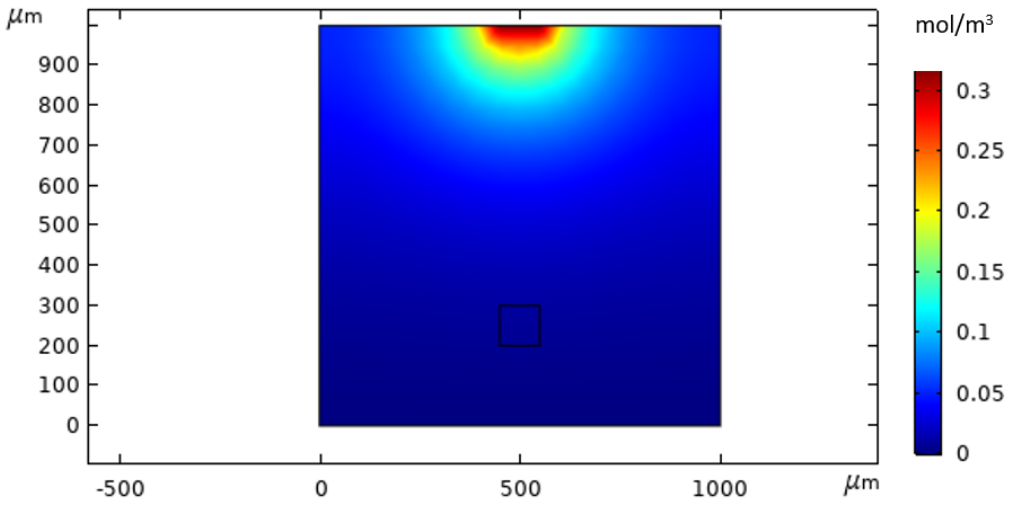


Figure 7.11: Concentration of QS molecules at time t=3 hours.

## 7.6 Conclusion

A compelling and critical stage in the realization of IoBNT concept is developing the proper BNT, able to detect the communication with molecules among biological cells, so that the "cell-to-Internet" connection will be put into practice. In this study, we carry further the discussion of IoT, IoNT, and IoBNT theory to practice by introducing a logical implementation flow for a BNT devoted to detect the communication among the infectious bacteria. As showing an example in this specific PANACEA application, the outcomes of IoBNT research will be the proof of its game-changer position in the communication society and catalyze a revolution in biomedical technologies.

# CHAPTER 8
# CONCLUSION

Molecular Communication (MC) is a novel bio-inspired paradigm for the exchange of information among autonomous nanotechnology and biotechnology enabled devices forming Internet of Bio-NanoThings (IoBNT). In MC, the transmitter sends a message encoded on the concentration, type or timing of molecules that are then propagated through the medium towards the receiver via diffusion or convection. Since MC offers a unique way of communication at nanoscale, it is not only a candidate for nanonetwork communication, but it is also a possible tool for establishing the future nanonetworks that can interact with living organisms and their biological processes. With the research conducted in this thesis, we hope to fill in the gaps in bacteria-based MC studies and to move the field one step forward towards the implementation of fully functional IoBNT for healthcare applications.

Leveraging the vast literature of microbiology enabling easy programmability and well-defined observability of bacteria, in this thesis we aim to model and analyze bacteria-based MC channels where bacteria is used either as a communication device or an information carrier. The studies with bacteria offer MC researchers many insights for the future of MC for IoBNT field that will study human cells and their communication in the more complex environment of human body. Furthermore, we provide blueprints for both biological devices based on engineered bacteria and electrical devices based on MEMS technology when implemented will constitute the first custom design bio-nanothings communicating through MC. The major contributions included in each chapter of this PhD thesis are summarized as follows.

In Chapter 3, we proposed, modeled and analyzed a genetically-engineered bacteria based biotransceiver for MC. In particular,

- We presented a biochemical model of biological circuits and studied both analog and

digital signaling.

- For the first time in the literature, we introduced a biotransceiver architecture that combines sensing, transmitting, receiving and processing blocks for MC.

- This architecture is then tailored for transmission of signals with M-ary pulse amplitude modulation.

In Chapter 4, we modeled and analyzed bacterial chemotaxis channels as travelling waves using Keller-Segel models and incorporated the impact of social interactions in this model. In particular,

- Travelling wave models for bacterial chemotaxis channels is developed and the closed form solutions for bacterial population density at the receiver, delay, and attenuation are derived.

- The models are modified to reflect the complex community structure of bacteria participating in cooperation, competition and cheating. And the effect of social behavior on the channel performance is evaluated.

In Chapter 5, modulation schemes for bacterial chemotaxis channels with plasmid diversity and distributed receivers are studied. In particular,

- We first simulated the bacteria propagation behavior in 3D to determine the probability distribution for the first passage time of bacteria which is modeled as an Inverse Gaussian Function.

- We introduced *Binary Density Modulation*, *M-ary Density Modulation*, and *Distributed Modulation* schemes and compared them by evaluating the performance metrics such as the bit error probability as well as the achievable rate, where we vary the distances between the transmitter and receivers, as well as the average transmit power which corresponds to the quantity of bacteria released from the transmitter.

- The results from our analysis show that the Distributed Modulation scheme outperforms the other two schemes due to the minimization of ISI that can result from bacteria emitted during previous time slots.

In Chapter 6, Microbiome-Gut-Brain Axis is investigated as an infrastucture for IoBNT systems to interconnect wearable and implantable devices within the body. In particular,

- We present a methodology that comprises both analytical and experimental efforts. The analytical effort builds on top of neuroscience and bioinformatics to abstract and model with reliable mathematical expressions the propagation of device-sourced information through biological tissues utilized as communication channels

- The experimental effort is based on the design of a unique integrated network probe device composed of a hub connected to an ensemble of electrical and molecular stimulation and sensing interfaces.

- As part of our work we introduce design elements, opportunities, and challenges to realize the aforementioned IoBNT network infrastructure.

In Chapter 7, an IoBNT application for early detection of infections is developed based on bacteria-based MC abstraction of infection. In particular,

- Bacterial infection is abstracted as a MC channel where our sensors are eavesdropping to quorum sensing communication of bacteria.

- A design of a bio-nanothing comprising the design of MEMS bionanosensor, ASIC interface circuits and wireless power and data transfer units is given to provide an example of a complete bio-nanothing, for the first time in literature.

- Through simulations, the feasibility of this IoBNT healthcare application for early detection of infection is demonstrated.

During the last decade, MC research has been focused on the physical characteristics of communication channels based on various molecule transport processes such as diffusion, molecular motors, microfluidic flow. Despite the advancements made in the theoretical foundations, the definition of technologies for feasible and useful applications of MC theory is still limited. The vision for this field is that the tools of communications and networking will be utilized to sense and manipulate the natural information flow in the body for biomedical applications translated by MC theory. Health monitoring through tapping into natural communications in the body, disease diagnosis via sensing the impairments in these communications, and connected healthcare via connecting implantable and wearable medical devices through the natural communication channels in the body are examples of possible applications. In line with this vision, we plan to extend our work on molecular communication for IoBNT in several directions:

- *Bacteria-based MC.* Using the previous experience in the field, we plan to study first multi-user systems for bacteria-based MC. The complex community structure of bacteria complicates the existing models for the diffusion-based and flow-induced MC channels which are already not characterized completely. By revisiting noise, channel capacity, and interference derivations, we will investigate the channel capacity limits and the probability of error. Stemming from the peculiarities of the channel, we will study novel modulation, coding, and detection algorithms to mitigate the long delays of MC and increase the data rate. Furthermore, we will also explore novel medium access schemes for bacteria in a multi-user setting where the common resources are the available carrier molecules in the medium and the nutrients necessary to keep bacteria alive compared to frequency spectrum and power in conventional communications.

- *Experimental Platform.* Genetic manipulation of bacteria is at a stage that bacteria can be programmed to act as a counter or a switch, detect & fight cancer, and sense chemicals. Collaborating with synthetic biologists, we aim to design networks of

engineered bacteria based biosensors connected via MC for both on chip and *in vivo* diagnosis. As a validation platform, we envision to develop a testbed for bacteria-based MC to validate our previous findings.

- *Modeling and analysis of intra-body communication networks.* We plan to incorporate the disruptive technology of machine learning in the modelling of not only the bacteria based molecular communication but also in the modelling of intra-body networks such as nervous, endocrine and cardiovascular networks, and the information flow on the microbiome-gut-brain axis. For example, nervous networks have been studied to identify the frequency response of electrical signals propagating through single neurons and molecular signals propagating through synapses between neurons in MC literature whereas more physiological aspects are studied by neuroscience. With the help of computational biology, its vast databases, and deep learning, we would like to explore these nervous networks to quantify the information flow through the body without necessarily identifying all physiological processes, explore patterns, identify impairments, and correlation with nervous system disorders.

# PUBLICATIONS

## Journals


1. Akyildiz, I. F., Chen, J., Ghovanloo, M., Guler, U., Ozkaya-Ahmedov, T., Pierobon, M., Sarioglu, A. F., Unluturk, B. D., "Microbiome-Gut-Brain Axis as a Biomolecular Communication Network for the Internet of Bio-NanoThings," IEEE Access, vol. 7, pp. 136161-136175, September 2019.

2. Loscri, V., Vegni, Unluturk, B. D., A. M.,"A Molecular Channel Model based on Upconversion Phenomenon," IEEE Transactions on Communications, vol. 66, no. 12, pp. 6247-6259, 2018.

3. Unluturk, B. D., Islam, S., Ivanov, S., Balasubramaniam S., "Towards Concurrent Data Transmission: Exploiting Plasmid Diversity by Bacterial Conjugation," IEEE Transactions on NanoBioscience, vol. 16, no. 4, pp. 287-298, June 2017.

4. Unluturk, B. D., Akyildiz, I. F., "An End-to-end Model of Plant Pheromone Channel for Long Range Molecular Communications," IEEE Transactions on Nanobioscience, vol. 16, no. 1, pp. 11-20, 2017.

5. Unluturk, B. D., Balasubramaniam S., Akyildiz, I. F., "The Impact of Social Behavior on the Attenuation and Delay of Bacterial Nanonetworks," IEEE Transactions on Nanobioscience, vol. 15, no.8, pp. 959-969, 2016.

6. Unluturk, B. D., Bicen, A. O., and Akyildiz, I. F., "Genetically Engineered Bacteria-based BioTransceivers for Molecular Communication," IEEE Transactions on Communications, vol. 63, no.4, pp. 1271-1281, 2015.

7. Akyildiz, I. F., Ghovanloo, M., Guler, U., Ozkaya-Ahmedov, T., Rather, P., Sarioglu, A. F., Unluturk, B. D., "PANACEA: An Internet of Bio-NanoThings Application for

Early Detection and Mitigation of Infectious Diseases," submitted to IEEE Access, 2020.

**Conferences**

1. Sakkaff, Z., Unluturk, B. D., Pierobon, M., "Applying Molecular Communication Theory to Multi-Scale Integrated Models of Biological Pathways," in Proc. ACM Nanocom 2019, Dublin, Ireland, September 2019.

2. Nieto-Chaupis, H., Unluturk, B.D., "Can the Nano Level Electrodynamics Explain the Very Early Diagnosis of Diabetoc Nephropathy in Type-2 Diabetes Patients?, in Proc. IEEE Nano 2017, Pittsburgh, Pennsylvania, USA, July 2017.

## REFERENCES


[1] I. F. Akyildiz, J. M. Jornet, and M. Pierobon, "Nanonetworks: A new frontier in communications," *Communications of the ACM*, vol. 54, no. 11, pp. 84–89, 2011.

[2] I. F. Akyildiz, M. Pierobon, S. Balasubramaniaam, and Y. Koucheryavy, "The internet of bio-nano things," *IEEE Communications Mag.*, vol. 53, no. 3, pp. 32–40, 2015.

[3] O. B. Akan, H. Ramezani, T. Khan, N. A. Abbasi, and M. Kuscu, "Fundamentals of molecular information and communication science," *Proceedings of the IEEE*, vol. 105, no. 2, pp. 306–318, 2016.

[4] I. F. Akyildiz and J. M. Jornet, "The internet of nano-things," *IEEE Wireless Communications*, vol. 17, no. 6, pp. 58–63, 2010.

[5] I. F. Akyildiz, M. Pierobon, S. Balasubramaniam, and Y Koucheryavy, "The internet of bio-nano things," *IEEE Communications Magazine*, vol. 53, no. 3, pp. 32–40, 2015.

[6] I. F. Akyildiz, J. M. Jornet, and M. Pierobon, "Nanonetworks: A new frontier in communications," *Communications of the ACM*, vol. 54, no. 11, pp. 84–89, 2011.

[7] I. F. Akyildiz, F. Brunetti, and C. Blázquez, "Nanonetworks: A new communication paradigm," *Computer Networks*, vol. 52, no. 12, pp. 2260–2279, 2008.

[8] I. F. Akyildiz, F. Fekri, R. Sivakumar, C. R. Forest, and B. K. Hammer, "Monaco: Fundamentals of molecular nano-communication networks," *IEEE Wireless Communications*, vol. 19, no. 5, pp. 12–18, 2012.

[9] M. B. Miller and B. L. Bassler, "Quorum sensing in bacteria," *Annual Reviews in Microbiology*, vol. 55, no. 1, pp. 165–199, 2001.

[10] M. Pierobon and I. F. Akyildiz, "Diffusion-based noise analysis for molecular communication in nanonetworks," *IEEE Transactions on signal processing*, vol. 59, no. 6, pp. 2532–2547, 2011.

[11] ——, "Capacity of a diffusion-based molecular communication system with channel memory and molecular noise," *IEEE Transactions on Information Theory*, vol. 59, no. 2, pp. 942–954, 2012.

[12] B. Krishnaswamy, C. M. Henegar, J. P. Bardill, D. Russakow, G. L. Holst, B. K. Hammer, C. R. Forest, and R. Sivakumar, "When bacteria talk: Time elapse communication for super-slow networks," in *2013 IEEE International Conference on Communications (ICC)*, IEEE, 2013, pp. 6348–6353.

[13] A. O. Bicen and I. F. Akyildiz, "System-theoretic analysis and least-squares design of microfluidic channels for flow-induced molecular communication," *IEEE Transactions on Signal Processing*, vol. 61, no. 20, pp. 5000–5013, 2013.

[14] Y. Chahibi and I. Balasingham, "Channel modeling and analysis for molecular motors in nano-scale communications," in *Proceedings of the Second Annual International Conference on Nanoscale Computing and Communication*, 2015, pp. 1–6.

[15] A. O. Bicen, I. F. Akyildiz, S. Balasubramaniam, and Y. Koucheryavy, "Linear channel modeling and error analysis for intra/inter-cellular ca 2+ molecular communication," *IEEE transactions on nanobioscience*, vol. 15, no. 5, pp. 488–498, 2016.

[16] M. Kuscu and O. B. Akan, "A communication theoretical analysis of fret-based mobile ad hoc molecular nanonetworks," *IEEE transactions on nanobioscience*, vol. 13, no. 3, pp. 255–266, 2014.

[17] I. F. Akyildiz, M. Pierobon, and S. Balasubramaniam, "An information theoretic framework to analyze molecular communication systems based on statistical mechanics," *Proceedings of the IEEE*, vol. 107, no. 7, pp. 1230–1255, 2019.

[18] N. Farsad, H. B. Yilmaz, A. Eckford, C.-B. Chae, and W. Guo, "A comprehensive survey of recent advancements in molecular communication," *IEEE Communications Surveys & Tutorials*, vol. 18, no. 3, pp. 1887–1919, 2016.

[19] M. Pierobon and I. F. Akyildiz, "A physical end-to-end model for molecular communication in nanonetworks," *IEEE Journal on Selected Areas in Communications*, vol. 28, no. 4, pp. 602–611, 2010.

[20] ——, "Noise analysis in ligand-binding reception for molecular communication in nanonetworks," *IEEE Transactions on Signal Processing*, vol. 59, no. 9, pp. 4168–4182, 2011.

[21] B. Atakan and O. B. Akan, "Deterministic capacity of information flow in molecular nanonetworks," *Nano Communication Networks*, vol. 1, no. 1, pp. 31–42, 2010.

[22] A. O. Bicen and I. F. Akyildiz, "End-to-end propagation noise and memory analysis for molecular communication over microfluidic channels," *IEEE Transactions on Communications*, vol. 62, no. 7, pp. 2432–2443, 2014.

[23] ——, "Interference modeling and capacity analysis for microfluidic molecular communication channels," *IEEE Transactions on Nanotechnology*, vol. 14, no. 3, pp. 570–579, 2015.

[24] L. C. Cobo and I. F. Akyildiz, "Bacteria-based communication in nanonetworks," *Nano Communication Networks*, vol. 1, no. 4, pp. 244–256, 2010.

[25] M. Gregori, I. Llatser, A. Cabellos-Aparicio, and E. Alarcón, "Physical channel characterization for medium-range nanonetworks using flagellated bacteria," *Computer Networks*, vol. 55, no. 3, pp. 779–791, 2011.

[26] T. D. Wyatt *et al.*, *Pheromones and animal behaviour: communication by smell and taste*. Cambridge university press, 2003.

[27] L. P. Giné and I. F. Akyildiz, "Molecular communication options for long range nanonetworks," *Computer Networks*, vol. 53, no. 16, pp. 2753–2766, 2009.

[28] U. Alon, *An introduction to systems biology: design principles of biological circuits*. CRC press, 2006.

[29] P. E. Purnick and R. Weiss, "The second wave of synthetic biology: From modules to systems," *Nature reviews Molecular cell biology*, vol. 10, no. 6, pp. 410–422, 2009.

[30] C. J. Myers, *Engineering genetic circuits*. Chapman and Hall/CRC, 2016.

[31] H. H. McAdams and A. Arkin, "Gene regulation: Towards a circuit engineering discipline," *Current Biology*, vol. 10, no. 8, R318–R320, 2000.

[32] T. Romeo, C. A. Vakulskas, and P. Babitzke, "Post-transcriptional regulation on a global scale: Form and function of csr/rsm systems," *Environmental microbiology*, vol. 15, no. 2, pp. 313–324, 2013.

[33] A. Tamsir, J. J. Tabor, and C. A. Voigt, "Robust multicellular computing using genetically encoded nor gates and chemical wires," *Nature*, vol. 469, no. 7329, pp. 212–215, 2011.

[34] J. R. van der Meer, "Bacterial sensors: Synthetic design and application principles," *Synthesis lectures on synthetic biology*, vol. 2, no. 1, pp. 1–167, 2010.

[35] T. S. Gardner, C. R. Cantor, and J. J. Collins, "Construction of a genetic toggle switch in escherichia coli," *Nature*, vol. 403, no. 6767, pp. 339–342, 2000.

[36] S. Basu, Y. Gerchman, C. H. Collins, F. H. Arnold, and R. Weiss, "A synthetic multicellular system for programmed pattern formation," *Nature*, vol. 434, no. 7037, pp. 1130–1134, 2005.

[37] R. Weiss, S. Basu, S. Hooshangi, A. Kalmbach, D. Karig, R. Mehreja, and I. Netravali, "Genetic circuit building blocks for cellular computation, communications, and signal processing," *Natural Computing*, vol. 2, no. 1, pp. 47–84, 2003.

[38] G. Karlebach and R. Shamir, "Modelling and analysis of gene regulatory networks," *Nature Reviews Molecular Cell Biology*, vol. 9, no. 10, pp. 770–780, 2008.

[39] C. M. Austin, W. Stoy, P. Su, M. C. Harber, J. P. Bardill, B. K. Hammer, and C. R. Forest, "Modeling and validation of autoinducer-mediated bacterial gene expression in microfluidic environments," *Biomicrofluidics*, vol. 8, no. 3, p. 034 116, 2014.

[40] C. W. Mullineaux, A. Nenninger, N. Ray, and C. Robinson, "Diffusion of green fluorescent protein in three cell environments in escherichia coli," *Journal of bacteriology*, vol. 188, no. 10, pp. 3442–3448, 2006.

[41] A. Ay and D. N. Arnosti, "Mathematical modeling of gene expression: A guide for the perplexed biologist," *Critical reviews in biochemistry and molecular biology*, vol. 46, no. 2, pp. 137–151, 2011.

[42] G. Yagil and E. Yagil, "On the relation between effector concentration and the rate of induced enzyme synthesis," *Biophysical journal*, vol. 11, no. 1, p. 11, 1971.

[43] N. Roquet and T. K. Lu, "Digital and analog gene circuits for biotechnology," *Biotechnology journal*, vol. 9, no. 5, pp. 597–608, 2014.

[44] C. Tan, F. Reza, and L. You, "Noise-limited frequency signal transmission in gene circuits," *Biophysical journal*, vol. 93, no. 11, pp. 3753–3761, 2007.

[45] M. L. Simpson, C. D. Cox, and G. S. Sayler, "Frequency domain analysis of noise in autoregulated gene circuits," *Proceedings of the National Academy of Sciences*, vol. 100, no. 8, pp. 4551–4556, 2003.

[46] R. Alur, C. Belta, V. Kumar, M. Mintz, G. J. Pappas, H. Rubin, and J. Schug, "Modeling and analyzing biomolecular networks," *Computing in Science & Engineering*, vol. 4, no. 1, pp. 20–31, 2002.

[47] P. Siuti, J. Yazbek, and T. K. Lu, "Synthetic circuits integrating logic and memory in living cells," *Nature biotechnology*, vol. 31, no. 5, p. 448, 2013.

[48] R. Weiss, S. Basu, S. Hooshangi, A. Kalmbach, D. Karig, R. Mehreja, and I. Netravali, "Genetic circuit building blocks for cellular computation, communications, and signal processing," *Natural Computing*, vol. 2, no. 1, pp. 47–84, 2003.

[49] H. Zhang, Y. Chen, and Y. Chen, "Noise propagation in gene regulation networks involving interlinked positive and negative feedback loops," *PloS one*, vol. 7, no. 12, 2012.

[50] T. S. Moon, C. Lou, A. Tamsir, B. C. Stanton, and C. A. Voigt, "Genetic programs constructed from layered logic gates in single cells," *Nature*, vol. 491, no. 7423, pp. 249–253, 2012.

[51] L. H. D. Endy T. Knight. (2010). Biobricks foundation, (visited on 09/30/2010).

[52] H. H. McAdams and L. Shapiro, "Circuit simulation of genetic networks," *Science*, vol. 269, no. 5224, pp. 650–656, 1995.

[53] J. P. Armitage, "Bacterial tactic responses," in *Advances in microbial physiology*, vol. 41, Elsevier, 1999, pp. 229–289.

[54] M. Llosa, F. X. Gomis-Rüth, M. Coll, and F. d. l. Cruz, "Bacterial conjugation: A two-step mechanism for dna transport," *Molecular microbiology*, vol. 45, no. 1, pp. 1–8, 2002.

[55] S. Balasubramaniam *et al.*, "Multi-hop conjugation based bacteria nanonetworks," *IEEE Transactions on nanobioscience*, vol. 12, no. 1, pp. 47–59, 2013.

[56] S. Balasubramaniam, N. Lyamin, D. Kleyko, M. Skurnik, A. Vinel, and Y. Koucheryavy, "Exploiting bacterial properties for multi-hop nanonetworks," *IEEE Communications Magazine*, vol. 52, no. 7, pp. 184–191, 2014.

[57] V. Petrov, S. Balasubramaniam, R. Lale, D. Moltchanov, Y. Koucheryavy, *et al.*, "Forward and reverse coding for chromosome transfer in bacterial nanonetworks," *Nano Communication Networks*, vol. 5, no. 1-2, pp. 15–24, 2014.

[58] E. B. Jacob, I. Becker, Y. Shapira, and H. Levine, "Bacterial linguistic communication and social intelligence," *TRENDS in Microbiology*, vol. 12, no. 8, pp. 366–372, 2004.

[59] E. Ben-Jacob, I. Cohen, and D. L. Gutnick, "Cooperative organization of bacterial colonies: From genotype to morphotype," *Annual review of microbiology*, vol. 52, no. 1, pp. 779–806, 1998.

[60] C. D. Nadell, J. B. Xavier, and K. R. Foster, "The sociobiology of biofilms," *FEMS microbiology reviews*, vol. 33, no. 1, pp. 206–224, 2008.

[61] G. M. Dunny, T. J. Brickman, and M. Dworkin, "Multicellular behavior in bacteria: Communication, cooperation, competition and cheating," *Bioessays*, vol. 30, no. 4, pp. 296–298, 2008.

[62] M. Hasan, E. Hossain, S. Balasubramaniam, and Y. Koucheryavy, "Social behavior in bacterial nanonetworks: Challenges and opportunities," *IEEE Network*, vol. 29, no. 1, pp. 26–34, 2015.

[63] A. Bren and M. Eisenbach, "How signals are heard during bacterial chemotaxis: Protein-protein interactions in sensory signal propagation," *Journal of bacteriology*, vol. 182, no. 24, pp. 6865–6873, 2000.

[64] M. J. Tindall, S. Porter, P. Maini, G Gaglia, and J. P. Armitage, "Overview of mathematical approaches used to model bacterial chemotaxis i: The single cell," *Bulletin of mathematical biology*, vol. 70, no. 6, pp. 1525–1569, 2008.

[65] M. J. Tindall, P. K. Maini, S. L. Porter, and J. P. Armitage, "Overview of mathematical approaches used to model bacterial chemotaxis ii: Bacterial populations," *Bulletin of mathematical biology*, vol. 70, no. 6, p. 1570, 2008.

[66] T. Hillen and K. J. Painter, "A users guide to pde models for chemotaxis," *Journal of mathematical biology*, vol. 58, no. 1-2, p. 183, 2009.

[67] E. F. Keller and L. A. Segel, "Traveling bands of chemotactic bacteria: A theoretical analysis," *Journal of theoretical biology*, vol. 30, no. 2, pp. 235–248, 1971.

[68] D. Horstmann, "From 1970 until present: The keller-segel model in chemotaxis and its consequences," 2003.

[69] L. You, R. S. Cox, R. Weiss, and F. H. Arnold, "Programmed population control by cell–cell communication and regulated killing," *Nature*, vol. 428, no. 6985, pp. 868–871, 2004.

[70] K. W. Bayles, "Bacterial programmed cell death: Making sense of a paradox," *Nature Reviews Microbiology*, vol. 12, no. 1, pp. 63–69, 2014.

[71] D. Feltham and M. A. Chaplain, "Travelling waves in a model of species migration," *Applied Mathematics Letters*, vol. 13, no. 7, pp. 67–73, 2000.

[72] A. Be'Er, H. Zhang, E.-L. Florin, S. M. Payne, E. Ben-Jacob, and H. L. Swinney, "Deadly competition between sibling bacterial colonies," *Proceedings of the National Academy of Sciences*, vol. 106, no. 2, pp. 428–433, 2009.

[73] R. Popat, S. A. Crusz, M. Messina, P. Williams, S. A. West, and S. P. Diggle, "Quorum-sensing and cheating in bacterial biofilms," *Proceedings of the Royal Society B: Biological Sciences*, vol. 279, no. 1748, pp. 4765–4771, 2012.

[74] I. Strauss, P. D. Frymier, C. M. Hahn, and R. M. Ford, "Analysis of bacterial migration: Ii. studies with multiple attractant gradients," *AIChE Journal*, vol. 41, no. 2, pp. 402–414, 1995.

[75] R. M. Ford and D. A. Lauffenburger, "Measurement of bacterial random motility and chemotaxis coefficients: Ii. application of single-cell-based mathematical model," *Biotechnology and bioengineering*, vol. 37, no. 7, pp. 661–672, 1991.

[76] M. Sitti, "Voyage of the microrobots," *Nature*, vol. 458, no. 7242, pp. 1121–1122, 2009.

[77] G. Wei, P. Bogdan, and R. Marculescu, "Bumpy rides: Modeling the dynamics of chemotactic interacting bacteria," *IEEE Journal on Selected Areas in Communications*, vol. 31, no. 12, pp. 879–890, 2013.

[78] P. Bogdan, G. Wei, and R. Marculescu, "Modeling populations of micro-robots for biological applications," in *2012 IEEE International Conference on Communications (ICC)*, IEEE, 2012, pp. 6188–6192.

[79] M. T. Barros, S. Balasubramaniam, B. Jennings, and Y. Koucheryavy, "Transmission protocols for calcium-signaling-based molecular communications in deformable cellular tissue," *IEEE Transactions on Nanotechnology*, vol. 13, no. 4, pp. 779–788, 2014.

[80] Y. Okaie, T. Nakano, T. Hara, T. Obuchi, K. Hosoda, Y. Hiraoka, and S. Nishio, "Cooperative target tracking by a mobile bionanosensor network," *IEEE transactions on nanobioscience*, vol. 13, no. 3, pp. 267–277, 2014.

[81] V. Petrov, D. Moltchanov, S. Balasubramaniam, and Y. Koucheryavy, "Incorporating bacterial properties for plasmid delivery in nano sensor networks," *IEEE Transactions on Nanotechnology*, vol. 14, no. 4, pp. 751–760, 2015.

[82] G. Wei, P. Bogdan, and R. Marculescu, "Efficient modeling and simulation of bacteria-based nanonetworks with bnsim," *IEEE Journal on Selected Areas in Communications*, vol. 31, no. 12, pp. 868–878, 2013.

[83] N. A. Ruhi and P. Bogdan, "Multiscale modeling of biological communication," in *2015 IEEE International Conference on Communications (ICC)*, IEEE, 2015, pp. 1140–1145.

[84] G. Castorina, L. Galluccio, and S. Palazzo, "On modeling information spreading in bacterial nano-networks based on plasmid conjugation," *IEEE transactions on nanobioscience*, vol. 15, no. 6, pp. 567–575, 2016.

[85] M. S. Kuran, H. B. Yilmaz, T. Tugcu, and I. F. Akyildiz, "Modulation techniques for communication via diffusion in nanonetworks," in *2011 IEEE international conference on communications (ICC)*, IEEE, 2011, pp. 1–5.

[86] M. U. Mahfuz, D. Makrakis, and H. T. Mouftah, "On the characterization of binary concentration-encoded molecular communication in nanonetworks," *Nano Communication Networks*, vol. 1, no. 4, pp. 289–300, 2010.

[87] P.-C. Yeh, K.-C. Chen, Y.-C. Lee, L.-S. Meng, P.-J. Shih, P.-Y. Ko, W.-A. Lin, and C.-H. Lee, "A new frontier of wireless communication theory: Diffusion-based molecular communications," *IEEE Wireless Communications*, vol. 19, no. 5, pp. 28–35, 2012.

[88] L. Cong, F. A. Ran, D. Cox, S. Lin, R. Barretto, N. Habib, P. D. Hsu, X. Wu, W. Jiang, L. A. Marraffini, *et al.*, "Multiplex genome engineering using crispr/cas systems," *Science*, vol. 339, no. 6121, pp. 819–823, 2013.

[89] M. K. Winson, S. Swift, L. Fish, J. P. Throup, F. Jørgensen, S. R. Chhabra, B. W. Bycroft, P. Williams, and G. S. Stewart, "Construction and analysis of luxcdabe-based plasmid sensors for investigating n-acyl homoserine lactone-mediated quorum sensing," *FEMS microbiology letters*, vol. 163, no. 2, pp. 185–192, 1998.

[90] E. A. Meighen, "Bacterial bioluminescence: Organization, regulation, and application of the lux genes.," *The FASEB journal*, vol. 7, no. 11, pp. 1016–1022, 1993.

[91] ——, "Genetics of bacterial bioluminescence," *Annual review of genetics*, vol. 28, no. 1, pp. 117–139, 1994.

[92] K. M. Passino, "Biomimicry of bacterial foraging for distributed optimization and control," *IEEE control systems magazine*, vol. 22, no. 3, pp. 52–67, 2002.

[93] F. Bonhoeffer, "Dna transfer and dna synthesis during bacterial conjugation," *Zeitschrift für Vererbungslehre*, vol. 98, no. 2, pp. 141–149, 1966.

[94] D. B. Clewell, *Bacterial conjugation*. Springer Science & Business Media, 2013.

[95] S. J. Sørensen, M. Bailey, L. H. Hansen, N. Kroer, and S. Wuertz, "Studying plasmid horizontal transfer in situ: A critical review," *Nature Reviews Microbiology*, vol. 3, no. 9, pp. 700–710, 2005.

[96] L. Simonsen, D. Gordon, F. Stewart, and B. R. Levin, "Estimating the rate of plasmid transfer: An end-point method," *Microbiology*, vol. 136, no. 11, pp. 2319–2325, 1990.

[97] D. M. Gordon, "Rate of plasmid transfer among escherichia coli strains isolated from natural populations," *Microbiology*, vol. 138, no. 1, pp. 17–21, 1992.

[98] S. Abadal and I. F. Akyildiz, "Bio-inspired synchronization for nanocommunication networks," in *2011 IEEE Global Telecommunications Conference-GLOBECOM 2011*, IEEE, 2011, pp. 1–5.

[99] T. Zhou, L. Chen, and K. Aihara, "Molecular communication through stochastic synchronization induced by extracellular fluctuations," *Physical review letters*, vol. 95, no. 17, p. 178 103, 2005.

[100] H. Shahmohammadian, G. G. Messier, and S. Magierowski, "Blind synchronization in diffusion-based molecular communication channels," *IEEE communications letters*, vol. 17, no. 11, pp. 2156–2159, 2013.

[101] A. Guney, B. Atakan, and O. B. Akan, "Mobile ad hoc nanonetworks with collision-based molecular communication," *IEEE Transactions on Mobile Computing*, vol. 11, no. 3, pp. 353–366, 2011.

[102] T. E. Gorochowski, A. Matyjaszkiewicz, T. Todd, N. Oak, K. Kowalska, S. Reid, K. T. Tsaneva-Atanasova, N. J. Savery, C. S. Grierson, and M. Di Bernardo, "Bsim: An agent-based tool for modeling bacterial populations in systems and synthetic biology," *PloS one*, vol. 7, no. 8, 2012.

[103] J. L. Folks and R. S. Chhikara, "The inverse gaussian distribution and its statistical applicationa review," *Journal of the Royal Statistical Society: Series B (Methodological)*, vol. 40, no. 3, pp. 263–275, 1978.

[104] T. Nakano, Y. Okaie, and J.-Q. Liu, "Channel model and capacity analysis of molecular communication with brownian motion," *IEEE communications letters*, vol. 16, no. 6, pp. 797–800, 2012.

[105] P. Trieu-Cuot, C Carlier, P. Martin, and P Courvalin, "Plasmid transfer by conjugation from escherichia coli to gram-positive bacteria," *FEMS Microbiology Letters*, vol. 48, no. 1-2, pp. 289–294, 1987.

[106] J. Müller, C. Kuttler, and B. A. Hense, "Sensitivity of the quorum sensing system is achieved by low pass filtering," *Biosystems*, vol. 92, no. 1, pp. 76–81, 2008.

[107] M. Carabotti, A. Scirocco, M. A. Maselli, and C. Severi, "The gut-brain axis: Interactions between enteric microbiota, central and enteric nervous systems," *Annals*

*of gastroenterology: quarterly publication of the Hellenic Society of Gastroenterology*, vol. 28, no. 2, p. 203, 2015.

[108] G. Sharon, T. R. Sampson, D. H. Geschwind, and S. K. Mazmanian, "The central nervous system and the gut microbiome," *Cell*, vol. 167, no. 4, pp. 915–932, 2016.

[109] J. F. Cryan and T. G. Dinan, "Mind-altering microorganisms: The impact of the gut microbiota on brain and behaviour," *Nature reviews neuroscience*, vol. 13, no. 10, p. 701, 2012.

[110] Y. Wang and L. H. Kasper, "The role of microbiome in central nervous system disorders," *Brain, behavior, and immunity*, vol. 38, pp. 1–12, 2014.

[111] M. Lyte and J. F. Cryan, *Microbial endocrinology: the microbiota-gut-brain axis in health and disease*. Springer, 2014, vol. 817.

[112] M. Pierobon and I. F. Akyildiz, "A physical end-to-end model for molecular communication in nanonetworks," *IEEE Journal on Selected Areas in Communications*, vol. 28, no. 4, pp. 602–611, 2010.

[113] Y. Chahibi, M. Pierobon, S. O. Song, and I. F. Akyildiz, "A molecular communication system model for particulate drug delivery systems," *IEEE Transactions on Biomedical Engineering*, vol. 60, no. 12, pp. 3468–3483, 2013.

[114] M. Pierobon, Z. Sakkaff, J. L. Catlett, and N. R. Buan, "Mutual information upper bound of molecular communication based on cell metabolism," in *Signal Processing Advances in Wireless Communications (SPAWC), 2016 IEEE 17th International Workshop on*, IEEE, 2016, pp. 1–6.

[115] Z. Sakkaff, J. L. Catlett, M. Cashman, M. Pierobon, N. R. Buan, M. B. Cohen, and C. A. Kelley, "End-to-end molecular communication channels in cell metabolism: An information theoretic study," in *Proceedings of the 4th ACM International Conference on Nanoscale Computing and Communication*, ACM, 2017, p. 21.

[116] A. Khodaei and M. Pierobon, "An intra-body linear channel model based on neuronal subthreshold stimulation," in *Communications (ICC), 2016 IEEE International Conference on*, IEEE, 2016, pp. 1–7.

[117] D. Purves, G. J. Augustine, D. Fitzpatrick, W. Hall, A.-S. Lamantia, J. O. McNamara, and L. White, "Neuroscience. ed," *Glutamate. Sunderland (MA): Sinauer Associates*, 2001.

[118] E. Balevi and O. B. Akan, "A physical channel model for nanoscale neuro-spike communications," *IEEE Transactions on Communications*, vol. 61, no. 3, pp. 1178–1187, 2013.

[119] M. Veletić, F. Mesiti, P. A. Floor, and I. Balasingham, "Communication theory aspects of synaptic transmission," in *Communications (ICC), 2015 IEEE International Conference on*, IEEE, 2015, pp. 1116–1121.

[120] D. Malak and O. B. Akan, "A communication theoretical analysis of synaptic multiple-access channel in hippocampal-cortical neurons," *IEEE Transactions on communications*, vol. 61, no. 6, pp. 2457–2467, 2013.

[121] D. Malak, M. Kocaoglu, and O. B. Akan, "Communication theoretic analysis of the synaptic channel for cortical neurons," *Nano Communication Networks*, vol. 4, no. 3, pp. 131–141, 2013.

[122] M. Veletić, P. A. Floor, Z. Babić, and I. Balasingham, "Peer-to-peer communication in neuronal nano-network," *IEEE Transactions on Communications*, vol. 64, no. 3, pp. 1153–1166, 2016.

[123] A. Khodaei and M. Pierobon, "Subthreshold linear modeling of dendritic trees: A computational approach," in *Engineering in Medicine and Biology Society (EMBC), 2016 IEEE 38th Annual International Conference of the*, IEEE, 2016, pp. 235–238.

[124] C. Koch, "Cable theory in neurons with active, linearized membranes," *Biological cybernetics*, vol. 50, no. 1, pp. 15–33, 1984.

[125] R. Miftahof, H. G. Nam, and D. L. Wingate, *Mathematical modeling and simulation in enteric neurobiology*. World Scientific, 2009.

[126] J. Yin and J. D. Chen, "Electrogastrography: Methodology, validation and applications," *Journal of neurogastroenterology and motility*, vol. 19, no. 1, p. 5, 2013.

[127] J. D. Chambers, E. A. Thomas, and J. C. Bornstein, "Mathematical modelling of enteric neural motor patterns," *Clinical and Experimental Pharmacology and Physiology*, vol. 41, no. 3, pp. 155–164, 2014.

[128] E. Thomas, P. Bertrand, and J. Bornstein, "A computer simulation of recurrent, excitatory networks of sensory neurons of the gut in guinea-pig," *Neuroscience letters*, vol. 287, no. 2, pp. 137–140, 2000.

[129] G. Drion, T. OLeary, and E. Marder, "Ion channel degeneracy enables robust and tunable neuronal firing rates," *Proceedings of the National Academy of Sciences*, vol. 112, no. 38, E5361–E5370, 2015.

[130] P. Bertrand, E. Thomas, W. Kunze, and J. Bornstein, "A simple mathematical model of second-messenger mediated slow excitatory postsynaptic potentials," *Journal of computational neuroscience*, vol. 8, no. 2, pp. 127–142, 2000.

[131] X. Bian, P. P. Bertrand, and J. C. Bornstein, "Descending inhibitory reflexes involve p2x receptor-mediated transmission from interneurons to motor neurons in guinea-pig ileum," *The Journal of physiology*, vol. 528, no. 3, pp. 551–560, 2000.

[132] B. B. Barth, C. S. Henriquez, W. M. Grill, and X. Shen, "Electrical stimulation of gut motility guided by an in silico model," *Journal of neural engineering*, vol. 14, no. 6, p. 066 010, 2017.

[133] K. Diba, H. A. Lester, and C. Koch, "Intrinsic noise in cultured hippocampal neurons: Experiment and modeling," *Journal of Neuroscience*, vol. 24, no. 43, pp. 9723–9733, 2004.

[134] P. N. Steinmetz, A. Manwani, C. Koch, M. London, and I. Segev, "Subthreshold voltage noise due to channel fluctuations in active neuronal membranes," *Journal of computational neuroscience*, vol. 9, no. 2, pp. 133–148, 2000.

[135] W.-L. Wang, S.-Y. Xu, Z.-G. Ren, L. Tao, J.-W. Jiang, and S.-S. Zheng, "Application of metagenomics in the human gut microbiome," *World journal of gastroenterology: WJG*, vol. 21, no. 3, p. 803, 2015.

[136] J. D. Orth, I. Thiele, and B. Ø. Palsson, "What is flux balance analysis?" *Nature biotechnology*, vol. 28, no. 3, p. 245, 2010.

[137] T. J. McGenity, K. N. Timmis, and B. N. Fernández, *Hydrocarbon and lipid microbiology protocols*. Springer, 2016.

[138] S. Shoaie, F. Karlsson, A. Mardinoglu, I. Nookaew, S. Bordel, and J. Nielsen, "Understanding the interactions between bacteria in the human gut through metabolic modeling," *Scientific reports*, vol. 3, p. 2532, 2013.

[139] R. R. Stein, V. Bucci, N. C. Toussaint, C. G. Buffie, G. Rätsch, E. G. Pamer, C. Sander, and J. B. Xavier, "Ecological modeling from time-series inference: Insight into dynamics and stability of intestinal microbiota," *PLoS computational biology*, vol. 9, no. 12, e1003388, 2013.

[140] M. A. Henson and T. J. Hanly, "Dynamic flux balance analysis for synthetic microbial communities," *IET systems biology*, vol. 8, no. 5, pp. 214–229, 2014.

[141] Y. Cu and W. M. Saltzman, "Mathematical modeling of molecular diffusion through mucus," *Advanced drug delivery reviews*, vol. 61, no. 2, pp. 101–114, 2009.

[142] D. Liao, D. Lelic, F. Gao, A. M. Drewes, and H. Gregersen, "Biomechanical functional and sensory modelling of the gastrointestinal tract," *Philosophical Transactions of the Royal Society of London A: Mathematical, Physical and Engineering Sciences*, vol. 366, no. 1879, pp. 3281–3299, 2008.

[143] M. A. Swartz and M. E. Fleury, "Interstitial flow and its effects in soft tissues," *Annu. Rev. Biomed. Eng.*, vol. 9, pp. 229–256, 2007.

[144] H. J. Kim, D. Huh, G. Hamilton, and D. E. Ingber, "Human gut-on-a-chip inhabited by microbial flora that experiences intestinal peristalsis-like motions and flow," *Lab on a Chip*, vol. 12, no. 12, pp. 2165–2174, 2012.

[145] B. J. Kane, M. J. Zinner, M. L. Yarmush, and M. Toner, "Liver-specific functional studies in a microfluidic array of primary mammalian hepatocytes," *Analytical Chemistry*, vol. 78, no. 13, pp. 4291–4298, 2006.

[146] A. Agarwal, J. A. Goss, A. Cho, M. L. McCain, and K. K. Parker, "Microfluidic heart on a chip for higher throughput pharmacological studies," *Lab on a Chip*, vol. 13, no. 18, pp. 3599–3608, 2013.

[147] D. Huh, H. Fujioka, Y.-C. Tung, N. Futai, R. Paine, J. B. Grotberg, and S. Takayama, "Acoustically detectable cellular-level lung injury induced by fluid mechanical stresses in microfluidic airway systems," *Proceedings of the National Academy of Sciences*, vol. 104, no. 48, pp. 18 886–18 891, 2007.

[148] M. B. Esch, J. H. Sung, J. Yang, C. Yu, J. Yu, J. C. March, and M. L. Shuler, "On chip porous polymer membranes for integration of gastrointestinal tract epithelium with microfluidic body-on-a-chipdevices," *Biomedical microdevices*, vol. 14, no. 5, pp. 895–906, 2012.

[149] A. Grosberg, A. P. Nesmith, J. A. Goss, M. D. Brigham, M. L. McCain, and K. K. Parker, "Muscle on a chip: In vitro contractility assays for smooth and striated muscle," *Journal of pharmacological and toxicological methods*, vol. 65, no. 3, pp. 126–135, 2012.

[150] E. L. Jackson and H. Lu, "Three-dimensional models for studying development and disease: Moving on from organisms to organs-on-a-chip and organoids," *Integrative Biology*, vol. 8, no. 6, pp. 672–683, 2016.

[151] D. Huh, B. D. Matthews, A. Mammoto, M. Montoya-Zavala, H. Y. Hsin, and D. E. Ingber, "Reconstituting organ-level lung functions on a chip," *Science*, vol. 328, no. 5986, pp. 1662–1668, 2010.

[152] S. B. Lee, B. Lee, M. Kiani, B. Mahmoudi, R. Gross, and M. Ghovanloo, "An inductively-powered wireless neural recording system with a charge sampling analog front-end," *IEEE sensors journal*, vol. 16, no. 2, pp. 475–484, 2016.

[153] E. G. Kilinc, G. Conus, C. Weber, B. Kawkabani, F. Maloberti, and C. Dehollain, "A system for wireless power transfer of micro-systems in-vivo implantable

in freely moving animals," *IEEE Sensors Journal*, vol. 14, no. 2, pp. 522–531, 2014.

[154] C. T. Wentz, J. G. Bernstein, P. Monahan, A. Guerra, A. Rodriguez, and E. S. Boyden, "A wirelessly powered and controlled device for optical neural control of freely-behaving animals," *Journal of neural engineering*, vol. 8, no. 4, p. 046 021, 2011.

[155] Y. Jia, S. A. Mirbozorgi, Z. Wang, C.-C. Hsu, T. E. Madsen, D. Rainnie, and M. Ghovanloo, "Position and orientation insensitive wireless power transmission for enercage-homecage system," *IEEE Trans. Biomed. Eng*, vol. 10, 2017.

[156] *Alternative design manufacturing supply. rat plastic cage.* 2016.

[157] D. Seo, R. M. Neely, K. Shen, U. Singhal, E. Alon, J. M. Rabaey, J. M. Carmena, and M. M. Maharbiz, "Wireless recording in the peripheral nervous system with ultrasonic neural dust," *Neuron*, vol. 91, no. 3, pp. 529–539, 2016.

[158] P. Nadeau, M. Mimee, S. Carim, T. K. Lu, and A. P. Chandrakasan, "21.1 nanowatt circuit interface to whole-cell bacterial sensors," in *Solid-State Circuits Conference (ISSCC), 2017 IEEE International*, IEEE, 2017, pp. 352–353.

[159] S. B. Lee, H.-M. Lee, M. Kiani, U.-M. Jow, and M. Ghovanloo, "An inductively powered scalable 32-channel wireless neural recording system-on-a-chip for neuroscience applications," in *Solid-State Circuits Conference Digest of Technical Papers (ISSCC), 2010 IEEE International*, IEEE, 2010, pp. 120–121.

[160] A. M. Kuncel and W. M. Grill, "Selection of stimulus parameters for deep brain stimulation," *Clinical neurophysiology*, vol. 115, no. 11, pp. 2431–2441, 2004.

[161] D. R. Merrill, M. Bikson, and J. G. Jefferys, "Electrical stimulation of excitable tissue: Design of efficacious and safe protocols," *Journal of neuroscience methods*, vol. 141, no. 2, pp. 171–198, 2005.

[162] A. Munge, V. Sankar, M. S. E. Sendi, M. Ghovanloo, and U. Guler, "A bio-impedance measurement ic for neural interface applications," in *2018 IEEE Biomedical Circuits and Systems Conference (BioCAS)*, 2018, pp. 1–4.

[163] J. Vidal and M. Ghovanloo, "Towards a switched-capacitor based stimulator for efficient deep-brain stimulation," in *Engineering in Medicine and Biology Society (EMBC), 2010 Annual International Conference of the IEEE*, IEEE, 2010, pp. 2927–2930.

[164] J. Simpson and M. Ghovanloo, "An experimental study of voltage, current, and charge controlled stimulation front-end circuitry," in *ISCAS*, 2007, pp. 325–328.

[165] K. Chen, Z. Yang, L. Hoang, J. Weiland, M. Humayun, and W. Liu, "An integrated 256-channel epiretinal prosthesis," *IEEE Journal of Solid-State Circuits*, vol. 45, no. 9, pp. 1946–1956, 2010.

[166] S. K. Arfin and R. Sarpeshkar, "An energy-efficient, adiabatic electrode stimulator with inductive energy recycling and feedback current regulation," *IEEE transactions on biomedical circuits and systems*, vol. 6, no. 1, pp. 1–14, 2012.

[167] M. Ghovanloo, "Switched-capacitor based implantable low-power wireless microstimulating systems," in *Circuits and Systems, 2006. ISCAS 2006. Proceedings. 2006 IEEE International Symposium on*, IEEE, 2006, 4–pp.

[168] H.-M. Lee, K. Y. Kwon, W. Li, and M. Ghovanloo, "A power-efficient switched-capacitor stimulating system for electrical/optical deep brain stimulation," *IEEE Journal of Solid-State Circuits*, vol. 50, no. 1, pp. 360–374, 2015.

[169] R. R. Harrison, R. J. Kier, C. A. Chestek, V. Gilja, P. Nuyujukian, S. Ryu, B. Greger, F. Solzbacher, and K. V. Shenoy, "Wireless neural recording with single low-power integrated circuit," *IEEE Transactions on Neural Systems and Rehabilitation Engineering*, vol. 17, no. 4, pp. 322–329, 2009.

[170] U. Guler and M. Ghovanloo, "Power management in wireless power-sipping devices: A survey," *IEEE Circuits and Systems Magazine*, vol. 17, no. 4, pp. 64–82, 2017.

[171] J. Zhang, N. Trombly, and A. Mason, "A low noise readout circuit for integrated electrochemical biosensor arrays," in *Sensors, 2004. Proceedings of IEEE*, IEEE, 2004, pp. 36–39.

[172] J. P. Villagrasa, J. Colomer-Farrarons, and P. L. Miribel, "Bioelectronics for amperometric biosensors," in *State of the Art in Biosensors-General Aspects*, Intech, 2013.

[173] S. K. Islam, R. Vijayaraghavan, M. Zhang, S. Ripp, S. D. Caylor, B. Weathers, S. Moser, S. Terry, B. J. Blalock, and G. S. Sayler, "Integrated circuit biosensors using living whole-cell bioreporters," *IEEE Transactions on Circuits and Systems I: Regular Papers*, vol. 54, no. 1, pp. 89–98, 2007.

[174] M. Kiani, B. Lee, P. Yeon, and M. Ghovanloo, "12.7 a power-management asic with q-modulation capability for efficient inductive power transmission," in *Solid-State Circuits Conference-(ISSCC), 2015 IEEE International*, IEEE, 2015, pp. 1–3.

[175] U. Guler, Y. Jia, and M. Ghovanloo, "A reconfigurable passive rf-to-dc converter for wireless iot applications," *IEEE Transactions on Circuits and Systems II: Express Briefs*, pp. 1–1, 2019.

[176] P. K. Campbell, K. E. Jones, R. J. Huber, K. W. Horch, and R. A. Normann, "A silicon-based, three-dimensional neural interface: Manufacturing processes for an intracortical electrode array," *IEEE Transactions on Biomedical Engineering*, vol. 38, no. 8, pp. 758–768, 1991.

[177] K. Najafi, K. Wise, and T. Mochizuki, "A high-yield ic-compatible multichannel recording array," *IEEE Transactions on Electron Devices*, vol. 32, no. 7, pp. 1206–1211, 1985.

[178] E. G. Hawkins, W. L. Dewey, M. Anitha, S. Srinivasan, J. R. Grider, and H. I. Akbarali, "Electrophysiological characteristics of enteric neurons isolated from the immortomouse," *Digestive diseases and sciences*, vol. 58, no. 6, pp. 1516–1527, 2013.

[179] G. Clarke, R. M. Stilling, P. J. Kennedy, C. Stanton, J. F. Cryan, and T. G. Dinan, "Minireview: Gut microbiota: The neglected endocrine organ," *Molecular endocrinology*, vol. 28, no. 8, pp. 1221–1238, 2014.

[180] I. A. Ges, R. L. Brindley, K. P. Currie, and F. J. Baudenbacher, "A microfluidic platform for chemical stimulation and real time analysis of catecholamine secretion from neuroendocrine cells," *Lab on a Chip*, vol. 13, no. 23, pp. 4663–4673, 2013.

[181] A. R. Perestrelo, A. C. Águas, A. Rainer, and G. Forte, "Microfluidic organ/body-on-a-chip devices at the convergence of biology and microengineering," *Sensors*, vol. 15, no. 12, pp. 31 142–31 170, 2015.

[182] L. Jin, Z. Han, J. Platisa, J. R. Wooltorton, L. B. Cohen, and V. A. Pieribone, "Single action potentials and subthreshold electrical events imaged in neurons with a fluorescent protein voltage probe," *Neuron*, vol. 75, no. 5, pp. 779–785, 2012.

[183] E. A. Thomas, "Mathematical and computer modelling of the enteric nervous system," PhD thesis, 2001.

[184] M. Joossens, G. Huys, M. Cnockaert, V. De Preter, K. Verbeke, P. Rutgeerts, P. Vandamme, and S. Vermeire, "Dysbiosis of the faecal microbiota in patients with crohn's disease and their unaffected relatives," *Gut*, gut–2010, 2011.

[185] G. F. Riley and T. R. Henderson, "The ns-3 network simulator," in *Modeling and tools for network simulation*, Springer, 2010, pp. 15–34.

[186] S. L. Weiss, J. C. Fitzgerald, F. Balamuth, E. R. Alpern, J. Lavelle, M. Chilutti, R. Grundmeier, V. M. Nadkarni, and N. J. Thomas, "Delayed antimicrobial therapy increases mortality and organ dysfunction duration in pediatric sepsis," *Critical care medicine*, vol. 42, no. 11, p. 2409, 2014.

[187] A. Kumar, P. Ellis, Y. Arabi, D. Roberts, B. Light, J. E. Parrillo, P. Dodek, G. Wood, A. Kumar, D. Simon, *et al.*, "Initiation of inappropriate antimicrobial therapy results in a fivefold reduction of survival in human septic shock," *Chest*, vol. 136, no. 5, pp. 1237–1248, 2009.

[188] V. Brown and E. Lowbury, "Use of an improved cetrimide agar medium and other culture methods for pseudomonas aeruginosa," *Journal of Clinical Pathology*, vol. 18, no. 6, pp. 752–756, 1965.

[189] C. M. Waters and B. L. Bassler, "Quorum sensing: Cell-to-cell communication in bacteria," *Annu. Rev. Cell Dev. Biol.*, vol. 21, pp. 319–346, 2005.

[190] S. Palliyil, C. Downham, I. Broadbent, K. Charlton, and A. J. Porter, "High-sensitivity monoclonal antibodies specific for homoserine lactones protect mice from lethal pseudomonas aeruginosa infections," *Applied and environmental microbiology*, vol. 80, no. 2, pp. 462–469, 2014.

[191] E. Baldrich, F. X. Munoz, and C. García-Aljaro, "Electrochemical detection of quorum sensing signaling molecules by dual signal confirmation at microelectrode arrays," *Analytical chemistry*, vol. 83, no. 6, pp. 2097–2103, 2011.

[192] Y. Lei, W. Chen, and A. Mulchandani, "Microbial biosensors," *Analytica chimica acta*, vol. 568, no. 1-2, pp. 200–210, 2006.

[193] F. Si, B. Li, W. Margolin, and S. X. Sun, "Bacterial growth and form under mechanical compression," *Scientific reports*, vol. 5, p. 11 367, 2015.

[194] J. Lee and G. Kaletunç, "Evaluation of the heat inactivation of escherichia coli and lactobacillus plantarum by differential scanning calorimetry," *Applied and Environmental Microbiology*, vol. 68, no. 11, pp. 5379–5386, 2002.

[195] J. C. Chang, S. F. Ossoff, D. C. Lobe, M. H. Dorfman, C. M. Dumais, R. G. Qualls, and J. D. Johnson, "Uv inactivation of pathogenic and indicator microorganisms.," *Applied and environmental microbiology*, vol. 49, no. 6, pp. 1361–1365, 1985.

[196] D. C. Klonoff, *Overview of fluorescence glucose sensing: A technology with a bright future*, 2012.

[197] Y. Jia, U. Guler, Y. Lai, Y. Gong, A. Weber, W. Li, and M. Ghovanloo, "26.8 a trimodal wireless implantable neural interface system-on-chip," in *2020 IEEE International Solid- State Circuits Conference - (ISSCC)*, 2020, pp. 414–416.

[198] I. Costanzo, D. Sen, and U. Guler, "A prototype towards a transcutaneous oxygen sensing wearable," in *2019 IEEE Biomedical Circuits and Systems Conference (BioCAS)*, 2019, pp. 1–4.

[199] ——, "An integrated readout circuit for a transcutaneous oxygen sensing wearable device," in *2020 IEEE Custom Integrated Circuits Conference (CICC)*, 2020, pp. 1–4.

[200] M. Roham, J. M. Halpern, H. B. Martin, H. J. Chiel, and P. Mohseni, "Wireless amperometric neurochemical monitoring using an integrated telemetry circuit," *IEEE Transactions on Biomedical Engineering*, vol. 55, no. 11, pp. 2628–2634, 2008.

[201] "IEEE standard for safety levels with respect to human exposure to radio frequency electromagnetic fields, 3 kHz to 300 GHz," *IEEE Std C95.1-2005 (Revision of IEEE Std C95.1-1991)*, pp. 1–238, 2006.

[202] V. Talla, B. Kellogg, B. Ransford, S. Naderiparizi, J. R. Smith, and S. Gollakota, "Powering the next billion devices with wi-fi," *Communications of the ACM*, vol. 60, no. 3, pp. 83–91, 2017.

[203] P. Harpe, H. Gao, R. van Dommele, E. Cantatore, and A. van Roermund, "21.2 a 3nw signal-acquisition ic integrating an amplifier with 2.1 nef and a 1.5 fj/conv-step adc," in *Solid-State Circuits Conference-(ISSCC), 2015 IEEE International*, IEEE, 2015, pp. 1–3.

[204] B Murmann, *Adc performance survey 1997-2016, accessed on mar. 2017*.

[205] M. Bolatkale, L. J. Breems, R. Rutten, and K. A. Makinwa, "A 4ghz ct $\Delta\Sigma$ adc with 70db dr and- 74dbfs thd in 125mhz bw," in *Solid-State Circuits Conference Digest of Technical Papers (ISSCC), 2011 IEEE International*, IEEE, 2011, pp. 470–472.

[206] U.-M. Jow and M. Ghovanloo, "Design and optimization of printed spiral coils for efficient transcutaneous inductive power transmission," *IEEE Transactions on biomedical circuits and systems*, vol. 1, no. 3, pp. 193–202, 2007.

[207] U. Guler and M. Ghovanloo, "Power management in wireless power-sipping devices: A survey," *IEEE Circuits and Systems Magazine*, vol. 17, no. 4, pp. 64–82, 2017.

[208] J. Lim, B. Lee, and M. Ghovanloo, "Optimal design of a resonance-based voltage boosting rectifier for wireless power transmission," *IEEE Transactions on Industrial Electronics*, vol. 65, no. 2, pp. 1645–1654, 2018.

[209] H. S. Gougheri and M. Kiani, "Self-regulated reconfigurable voltage/current-mode inductive power management," *IEEE Journal of Solid-State Circuits*, vol. 52, no. 11, pp. 3056–3070, 2017.

[210] J. S. Ho, A. J. Yeh, E. Neofytou, S. Kim, Y. Tanabe, B. Patlolla, R. E. Beygui, and A. S. Poon, "Wireless power transfer to deep-tissue microimplants," *Proceedings of the National Academy of Sciences*, vol. 111, no. 22, pp. 7974–7979, 2014.

[211] K. L. Montgomery, A. J. Yeh, J. S. Ho, V. Tsao, S. M. Iyer, L. Grosenick, E. A. Ferenczi, Y. Tanabe, K. Deisseroth, S. L. Delp, *et al.*, "Wirelessly powered, fully internal optogenetics for brain, spinal and peripheral circuits in mice," *Nature methods*, vol. 12, no. 10, pp. 969–974, 2015.

[212] B. Lee, D. Ahn, and M. Ghovanloo, "Three-phase time-multiplexed planar power transmission to distributed implants," *IEEE journal of emerging and selected topics in power electronics*, vol. 4, no. 1, pp. 263–272, 2016.

[213] U. Guler, Y. Jia, and M. Ghovanloo, "A reconfigurable passive voltage multiplier for wireless mobile iot applications," *IEEE Transactions on Circuits and Systems II: Express Briefs*, vol. 67, no. 4, pp. 615–619, 2020.

[214] ——, "A reconfigurable passive rf-to-dc converter for wireless iot applications," *IEEE Transactions on Circuits and Systems II: Express Briefs*, vol. 66, no. 11, pp. 1800–1804, 2019.

[215] C. M. Waters and B. L. Bassler, "Quorum sensing: Cell-to-cell communication in bacteria," *Annu. Rev. Cell Dev. Biol.*, vol. 21, pp. 319–346, 2005.

[216] M. Pierobon and I. F. Akyildiz, "Capacity of a diffusion-based molecular communication system with channel memory and molecular noise," *IEEE Transactions on Information Theory*, vol. 59, no. 2, pp. 942–954, 2013.

[217] A. O. Bicen and I. F. Akyildiz, "System-theoretic analysis and least-squares design of microfluidic channels for flow-induced molecular communication," *IEEE Transactions on Signal Processing*, vol. 61, no. 20, pp. 5000–5013, 2013.

[218] Y. Chahibi and I. F. Akyildiz, "Molecular communication noise and capacity analysis for particulate drug delivery systems," *IEEE Transactions on Communications*, vol. 62, no. 11, pp. 3891–3903, 2014.

[219] B. D. Unluturk, A. O. Bicen, and I. F. Akyildiz, "Genetically engineered bacteria-based biotransceivers for molecular communication," *IEEE Transactions on Communications*, vol. 63, no. 4, pp. 1271–1281, 2015.

[220] B. D. Unluturk, S. Balasubramaniam, and I. F. Akyildiz, "The impact of social behavior on the attenuation and delay of bacterial nanonetworks," *IEEE transactions on nanobioscience*, vol. 15, no. 8, pp. 959–969, 2016.

[221] B. D. Unluturk, M. S. Islam, S. Balasubramaniam, and S. Ivanov, "Towards concurrent data transmission: Exploiting plasmid diversity by bacterial conjugation," *IEEE transactions on nanobioscience*, vol. 16, no. 4, pp. 287–298, 2017.

[222] J. Pérez-Velázquez, M. Gölgeli, and R. García-Contreras, "Mathematical modelling of bacterial quorum sensing: A review," *Bulletin of mathematical biology*, vol. 78, no. 8, pp. 1585–1639, 2016.

[223] C. Grandclément, M. Tannières, S. Moréra, Y. Dessaux, and D. Faure, "Quorum quenching: Role in nature and applied developments," *FEMS microbiology reviews*, vol. 40, no. 1, pp. 86–116, 2015.

[224] Y. Chahibi, I. F. Akyildiz, S. Balasubramaniam, and Y. Koucheryavy, "Molecular communication modeling of antibody-mediated drug delivery systems," *IEEE Transactions on Biomedical Engineering*, vol. 62, no. 7, pp. 1683–1695, 2015.

[225] Y. Chahibi, M. Pierobon, and I. F. Akyildiz, "Pharmacokinetic modeling and biodistribution estimation through the molecular communication paradigm," *IEEE Transactions on Biomedical Engineering*, vol. 62, no. 10, pp. 2410–2420, 2015.

[226] N. Høiby, O. Ciofu, and T. Bjarnsholt, "Pseudomonas aeruginosa biofilms in cystic fibrosis," *Future microbiology*, vol. 5, no. 11, pp. 1663–1674, 2010.

[227] E. B. Hirsch and V. H. Tam, "Impact of multidrug-resistant pseudomonas aeruginosa infection on patient outcomes," *Expert review of pharmacoeconomics & outcomes research*, vol. 10, no. 4, pp. 441–451, 2010.

[228] M. D. Williams, L. A. Braun, L. M. Cooper, J. Johnston, R. V. Weiss, R. L. Qualy, and W. Linde-Zwirble, "Hospitalized cancer patients with severe sepsis: Analysis of incidence, mortality, and associated costs of care," *Critical Care*, vol. 8, no. 5, R291, 2004.

[229] G. M. Nixon, D. S. Armstrong, R. Carzino, J. B. Carlin, A. Olinsky, C. F. Robertson, and K. Grimwood, "Clinical outcome after early pseudomonas aeruginosa infection in cystic fibrosis," *The Journal of pediatrics*, vol. 138, no. 5, pp. 699–704, 2001.

[230] A. E. LaBauve and M. J. Wargo, "Growth and laboratory maintenance of pseudomonas aeruginosa," *Current protocols in microbiology*, vol. 25, no. 1, 6E–1, 2012.

[231] L. Sherwood, J. M. Willey, and C. Woolverton, *Prescott's microbiology*. McGraw-Hill, 2011.

[232] C. S. Curran, T. Bolig, and P. Torabi-Parizi, "Mechanisms and targeted therapies for pseudomonas aeruginosa lung infection," *American journal of respiratory and critical care medicine*, vol. 197, no. 6, pp. 708–727, 2018.

[233] A. Koerber, J. King, J. Ward, P Williams, J. Croft, and R. Sockett, "A mathematical model of partial-thickness burn-wound infection by pseudomonas aeruginosa: Quorum sensing and the build-up to invasion," *Bulletin of mathematical biology*, vol. 64, no. 2, pp. 239–259, 2002.

[234] J. P. Ward, J. R. King, A. Koerber, P Williams, J. Croft, and R. Sockett, "Mathematical modelling of quorum sensing in bacteria," *Mathematical Medicine and Biology*, vol. 18, no. 3, pp. 263–292, 2001.

[235] K Khanafer and K Vafai, "The role of porous media in biomedical engineering as related to magnetic resonance imaging and drug delivery," *Heat and mass transfer*, vol. 42, no. 10, p. 939, 2006.

[236] S. Ramanujan, A. Pluen, T. D. McKee, E. B. Brown, Y. Boucher, and R. K. Jain, "Diffusion and convection in collagen gels: Implications for transport in the tumor interstitium," *Biophysical journal*, vol. 83, no. 3, pp. 1650–1660, 2002.

[237] K. Y. Wen, L. Cameron, J. Chappell, K. Jensen, D. J. Bell, R. Kelwick, M. Kopniczky, J. C. Davies, A. Filloux, and P. S. Freemont, "A cell-free biosensor for detecting quorum sensing molecules in p. aeruginosa-infected respiratory samples," *ACS synthetic biology*, vol. 6, no. 12, pp. 2293–2301, 2017.

# VITA

Bige Deniz Unluturk was born on February 14, 1989, in Ankara, Turkey. She received the B.Sc. degree in Electrical and Electronics Engineering from Middle East Technical University, Ankara, Turkey, in 2011 as valedictorian. She received the M.Sc. degrees in Electrical and Computer Engineering from Koc University, Istanbul, Turkey in 2013, under the supervision of Dr. Ozgur Baris Akan. She attended the doctoral program at the School of Electrical and Computer Engineering of Georgia Institute of Technology, Atlanta, GA, from August 2013 to July 2020, where she was a research and teaching assistant in the Broadband and Wireless Networking Laboratory (BWN-LAB). She also worked as a graduate instructor for ECE 3710 Circuits class. She is the recipient of the Outstanding Graduate Instructor of the Year Award within the School of ECE, Georgia Tech, Spring 2018. She was selected as one of the Rising Stars in Electrical Engineering and Computer Science in 2019. In July 2020, she received her Ph.D. in Electrical and Computer Engineering from Georgia Institute of Technology, under the supervision of Dr. Ian F. Akyildiz.